8-9-2006

Analysis of a Turbopiston Pump

Kiranmayi Venkata Sristy
University of New Orleans

ANALYSIS OF A TURBOPISTON PUMP

A Thesis

Submitted to the Graduate Faculty of the
University of New Orleans
in partial fulfillment of the
requirements for the degree of

Master of Science
in
Department of Mechanical Engineering

by

Kiranmayi Venkata Sristy

Bachelors of Technology, JNTU, 1998

August 2006

ACKNOWLEDGEMENT

I take this opportunity to thank my principal advisor, Dr. Ting Wang, for his valuable suggestions on simulations and the authenticity of the simulated data with basic principles of engineering, supervising my work and for guiding me through the correct path. I would also like to thank Dr. Xianchang Li, for his patience, valuable suggestions, and advising me to try different new techniques, and Dr. Paul Schilling and Dr. Martin Guillot for being a part of my thesis committee.

I would like to thank Mr. Patrick Rousset of the Power Engineering, Inc for giving me an opportunity to work under this project. My special thanks to the Murphy Oil and Exploration Company, New Orleans for providing me an opportunity to work on my thesis even after being employed as a mechanical engineering intern for their company. I would also like to extend my thanks to the Department of Physics, UNO and to the technical support from Fluent Inc.

Finally I would like to thank my family and friends for their constant support and help in dealing with difficult times. My heartfelt thanks go to my dad, Mr. Narayana Rao Sristy, who is a constant source of inspiration in my life, and also for his extended support throughout my career. I am also indebted to my Mom, Mrs. Hemalatha Sristy, for instilling confidence in me always and my sister, Ms. Ujwala Sristy, for her understanding, and to my very close friend, Sandeep Nallagula, for his support through out my program.

TABLE OF CONTENTS

LIST OF FIGURES

LIST OF TABLES

NOMENCLATURE

c_p	heat capacity at constant pressure (J/kg-K)
c_v	heat capacity at constant volume (J/kg-K)
D_H	hydraulic diameter (m)
D_{ij}	mass diffusion coefficient (m^2/s)
D_t	turbulent diffusivity (m^2/s)
E	total energy (J)
g	gravitational acceleration (m/s^2)
G	incident radiation
Gr	Grashof number ($L^3.\rho^2.g.\beta.\Delta T/\mu^2$)
J	mass flux; diffusion flux (kg/m^2-s)
k	turbulence kinetic energy (m^2/s^2)
m	mass (kg)
M_W	molecular weight (kg/kgmol)
M	Mach number
p	pressure (atm)
Pr	Prandtl number (ν/α)
S	source term
t	time (s)
T	temperature (K)
U	mean velocity (m/s)
x, y, z	coordinates

Greek letter

β	coefficient of thermal expansion (K^{-1})
ε	turbulence dissipation (m^2/s^3)
ε_w	wall emissivity

κ	von Karman constant
μ	dynamics viscosity (kg/m-s)
μ_k	turbulent viscosity (kg/m-s)
v	kinematic viscosity (m^2/s)
ρ	density (kg/m^3)
σ	Stefan-Boltzmann constant
τ	stress tensor ($kg/m\text{-}s^2$)

Subscript

i	reactant i
j	product j

ABSTRACT

An innovative pump, TurboPiston Pump, has been invented to incorporate the merits of centrifugal, axial, and positive displacement pumps. The TurboPiston pump is designed to deliver large flow rates at very high pressure of up to 1000 psia. To improve the original design, an understanding of flow behavior inside the pump is needed. Therefore, this thesis focuses on simulating the flow field inside the pump and studying its performance. This study includes modeling the pump using a commercial CAD package, GAMBIT and a 3-D computational fluid dynamic (CFD) solver, FLUENT. The calculation employs both the simplified steady moving frame and the complicated transient sliding mesh schemes. The flow pattern, static pressure distribution, and total pressure losses are calculated and analyzed. The regions of high total pressure losses and potential creation of cavitation are identified. Design changes are recommended to minimize cavitation and total pressure losses to improve the pump performance.

CHAPTER ONE

INTRODUCTION AND LITERATURE REVIEW

1.0 Introduction

For thousands of years, pumping devices have been an important way to move fluids. The Ancient Egyptians invented water wheels with buckets mounted on them to move water for irrigation. In the 200's B.C. Ctesibius, a Greek inventor, made a reciprocating pump for pumping water. At about the same time, Archimedes, a Greek mathematician, invented a screw pump made of a screw rotating in a cylinder. The centrifugal pump, one of the forms of the several pump classifications, was invented by Denis Papin (1674-1712). Times have changed, but pumps still operate in the same basic way.

1.1 Literature Search

The literature search concentrates on the definition and classification of the pumps, performance characteristics, and factors affecting performance.

1.1.1 Pump

One of the most important technologies that affect our daily life is the science and engineering of moving fluids with pumps. They are an integral part of the world economy, widely used in agriculture, manufacturing, and transportation. Most mechanical pumps consist of three major types: centrifugal, axial, and positive displacement (reciprocating, screw or rotor

devices). A pump is a device used for continuously raising, forcing, compressing or exhausting fluid by mechanical or other means.

1.1.2 Classification of Pumps

Pumps are basically divided into two categories

1. Positive displacement pumps (PDP)
2. Dynamic pumps

A. Positive displacement pumps

This type of pump forces fluid from one chamber to the other by reducing the volume of the first chamber while increasing the volume of the other. This pump produces a constant flow regardless of the intake pressure or the outlet pressure, unless the intake pressure drops below a certain limit causing cavitations, or the outlet pressure exceeds the capacity of the pump causing pump failure. Their great advantage is the delivery of any fluid regardless of viscosity.

Positive displacement pumps are again divided into

- Reciprocating positive displacement pump
- Rotary positive displacement pump.

Reciprocating positive displacement pumps are further categorized into

- Piston or Plunger
- Diaphragm

Rotary pumps are rotary positive displacement pumps in which the main pumping action is caused by the relative movement between the rotating and stationary elements of the pump. The rotary motion of these pumps distinguishes them from the reciprocating positive displacement pumps because the motion of the moving element is reciprocating. The

characteristic of the rotary pumps is that the amount of liquid displaced by each revolution is independent of speed.

a. Single rotor
    - Sliding vane
    - Flexible impeller pumps
    - Screw
b. Multiple rotors
    - Gear pumps
    - Lobe
    - Circumferential piston pump
    - Axial piston pump
    - Radial piston pump

Sliding vane pumps, or vane pumps as they are normally called, are suitable for low and medium pressure duties. The pump itself consists of a circular rotor with radial slots mounted eccentrically in a substantially circular casing. Each rotor slot carries a rigid vane, free to slide in a radial direction. Rotation throws the vanes outwards so the tips always rub against the inner surface of the casing providing the seal. The shape of the casing and the eccentric location of the rotor produce pockets between the adjacent vanes that alternately expand and contract in volume. An inlet port communicates with the casing on the expanding volume side (or suction side), and an outlet port connects on the contracting valve side (or pressure side). Fluid is thus sucked in through the inlet port and squeezed out under pressure through the outlet port.

Flexible impeller pump has similar characteristics to that of a sliding vane pump; however, it is limited in the amount of maximum head pressure it can develop because of the flexible nature of the elastomeric impeller. It is also more limited in terms of practical sizes in which it can be produced, but it is very useful for handling a wide variety of non-viscous and low viscosity fluids. A flexible elastomeric impeller is mounted centrally in the circular casing incorporating an eccentric section. Intake and outlet ports are positioned at the ends of this eccentric section. On rotation, when the impeller leaves the eccentric section of the pump body, the flexible impeller blades extend to create a partial vacuum, and as a result, the liquid is sucked into the pump. As the impeller rotates, the fluid accompanies it from the suction to the feed side, while the blade sucks in more fluid. Flexible vane pumps are normally self-priming since sufficient residual fluid is usually present in the casing to wet the vane tips after single revolution.

Screw rotary pumps are a special type of positive displacement pumps in which the flow through the pumping element is truly axial. The liquid is carried between the screw threads on one or more rotors and is displaced axially as the screws rotate and mesh. It is capable of handling liquids in a pressure range of 50 to 50,000lb/in^2 and flows up to 5,000gal/min. Screw pumps are capable of operating at higher speeds than other rotary or reciprocating pumps of comparable displacement. The advantages of screw pumps are low mechanical vibration, pulsation free flow, quiet operation, and high tolerance to contamination.

Gear pumps (Figure 1) are rotary pumps in which two or more gears mesh to provide the pumping action. One of them is the driving, and the other is the driven gear. The mechanical contacts between the gears form a part of the moving fluid seal between the inlet and the outlet

port. The outer radial tips and the sides of the gears form a part of the moving fluid seal between the inlet and outlet ports.

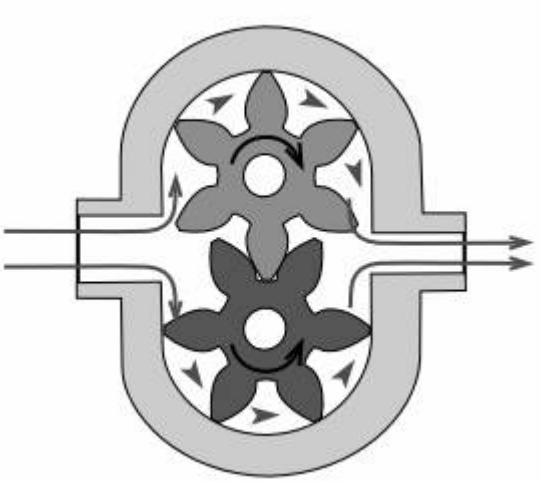

Figure 1.1 Gear Pump.

The lobe pump (Figure 1.2) derives its name from the rounded shape of the rotor radial surfaces, which permits the rotors to be continuously in contact with each other as they rotate. Unlike the gear pumps, neither the number of lobes nor their shape permits one rotor to drive the other. They require the timing gears.

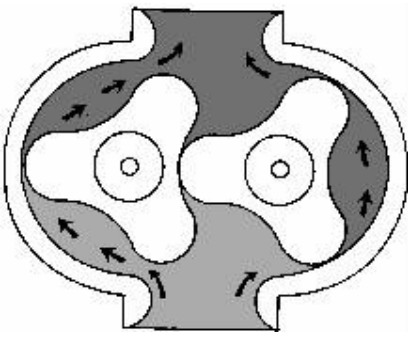

Figure 1.2 Lobe Pump.

Circumferential piston pump (Figure 1.3) has piston like rotor elements supported from cylindrical hubs inset into pump endplate and traveling in circular paths in mating body bores. The rotors do not mesh or touch. Fluid seals exist only between the rotor and stator surfaces and not between rotors. With no pumping torque transfer from rotor to rotor, timing gears are usually not needed even for a pump handling non-lubricating fluids.

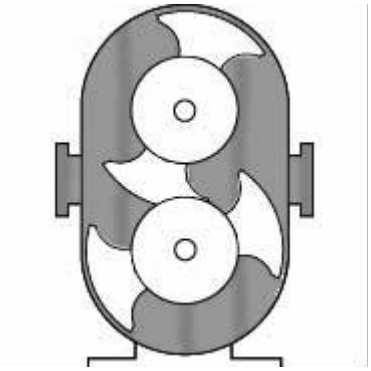

Figure 1.3 Circumferential Piston Pump.

Advantages of the circumferential piston pump:

a. Flow largely independent of changes in fluid viscosity
b. Self priming and with minimal pulsation
c. Flow direction can be reversed and has minimum shear

In axial piston pumps (Figure 1.4a) the cylinders and the drive shaft are parallel. The reciprocating motion is created by a cam plate, also known as a wobble plate, tilting plate, or swash plate. This plate lies in a plane that cuts across the centerline of the drive shaft and cylinder barrel. The plate does not rotate. In a fixed-displacement pump, the cam plate will be rigidly mounted in a position that intersects the centerline of the cylinder barrel at an angle

approximately 25 degrees from perpendicular. Variable-delivery axial piston pumps are designed so the angle the cam plate makes will be perpendicular to the centerline of the cylinder barrel and may vary from zero to 20 or 25 degrees to one or both sides. One end of each piston rod is held in contact with the cam plate as the cylinder block. The piston assembly rotates with the drive shaft. This causes the pistons to reciprocate within the cylinders. The length of the piston stroke is proportional to the angle that the cam plate is set from the perpendicular line to the centerline of the cylinder barrel.

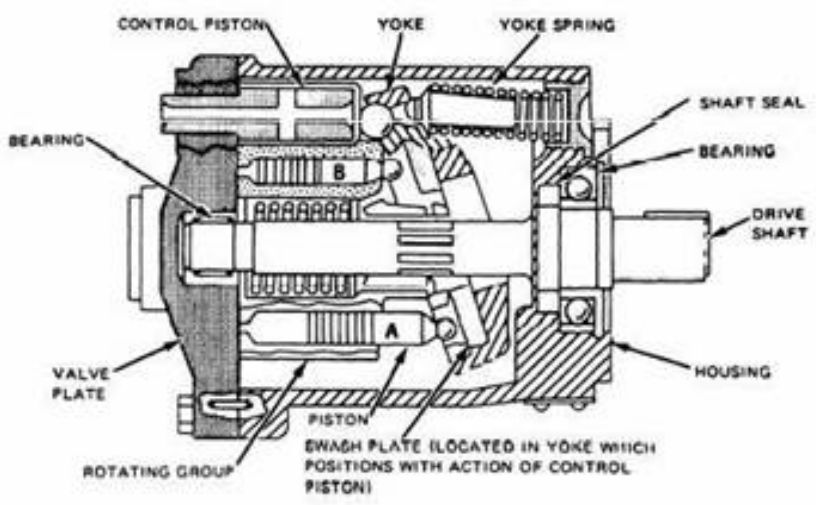

Figure 1.4a Axial piston pump.

A variation of axial piston pump is the bent-axis type shown in Figure 1.4b. This type does not have a tilting cam plate as the in-line pump does. Instead, the cylinder block axis is varied from the drive shaft axis. The ends of the connecting rods are retained in sockets on a disc that turns with the drive shaft. The cylinder block is turned with the drive shaft by a universal joint assembly at the intersection of the drive shaft and the cylinder block shaft. To vary the pump displacement, the cylinder block and valve plate are mounted in a yoke,

and the entire assembly is swung in an arc around a pair of mounting pintles attached to the pump housing.

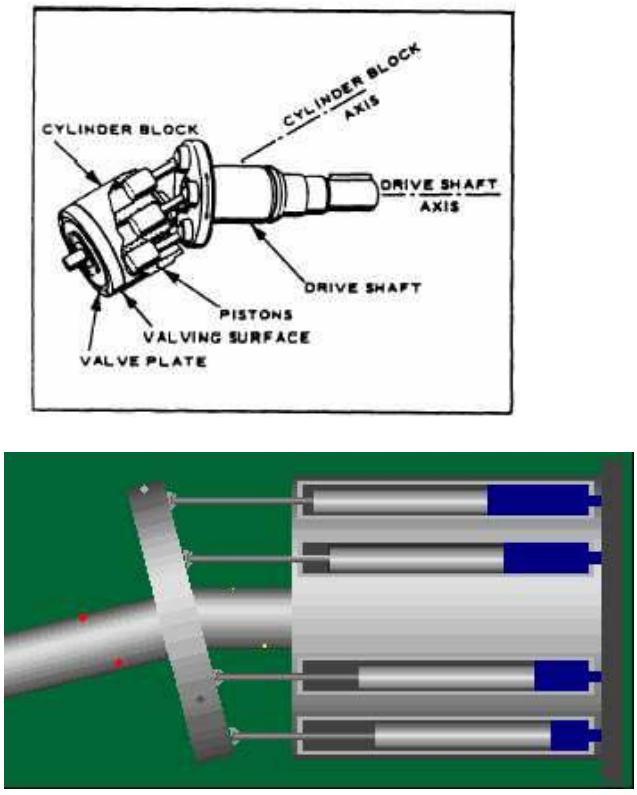

Figure 1.4b Bent Axis PistonPump.

Radial piston pump is another design using rotating displacement cylinder as shown in Figure 1.5. The inner rotating block is installed eccentrically from the center of the fixed ring on which cylinders are attached. The stroke of the piston is twice the eccentricity.

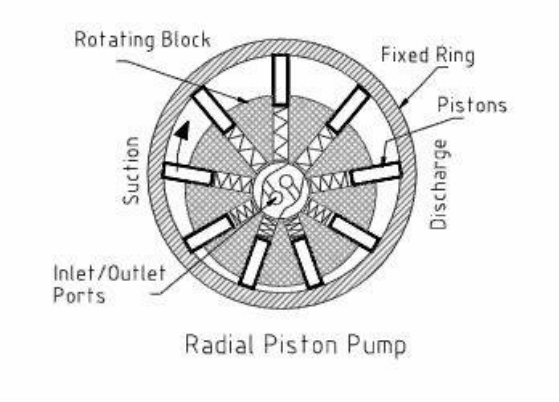

Figure 1.5 Radial piston pump.

B. Dynamic pump

This kind of pump causes the fluid to move from inlet to outlet under its own momentum. Fluid motion can be rotary as in centrifugal pumps or linear as in reciprocating dynamic pumps.

Dynamic pumps can be classified as follows

a. Rotary
    - Centrifugal or radial exit flow
    - Axial flow
    - Mixed flow (between radial and axial)

b. Special designs
    - Jet pump or ejector
    - Electromagnetic pumps for liquid metals
    - Fluid –actuated: gas-lift or hydraulic ram

Dynamic pumps generally provide a higher flow rate than positive displacement pumps and a much steadier discharge but are ineffective in handling high-viscosity liquids. Dynamic pumps also generally need priming i.e., if they are filled with gas, they cannot suck up a liquid from below into their inlet. The positive displacement pump (PDP), on the other hand, is self-priming for almost any application.

A centrifugal pump consists of a set of rotating vanes that are enclosed within housing. These vanes are utilized to impart energy to a liquid through centrifugal force. The rotating element of the pump, which is motivated by the prime mover, is the impeller. The liquid being pumped surrounds the impeller, and as the impeller rotates, the rotating motion of the impeller imparts a rotating motion to the liquid. As the liquid leaves the impeller, it tends to move in a direction tangential to the outside diameter of the impeller.

Figure 1.6 Centrifugal Pump

In an axial flow pump, the impeller pushes the liquid in a direction parallel to the pump shaft. Axial flow pumps are sometimes called propeller pumps. These pumps develop most of their pressure by the propelling action of the vanes on the liquid. In general, vertical single-stage axial and mixed-flow pumps are used; however, sometimes two-stage axial-flow pumps are economically more practical.

A mixed flow pump is a pump in which the head is developed partly by centrifugal force and partly by the lift of the vanes on the liquid. This pump has a single inlet impeller with the flow entering axially and discharging in an axial/radial direction.

The flow chart below gives a brief classification of the available pumps in the market. Figure 1.7 shows a general performance of various pumps in terms of pumping volume flow rate versus pressure heads.

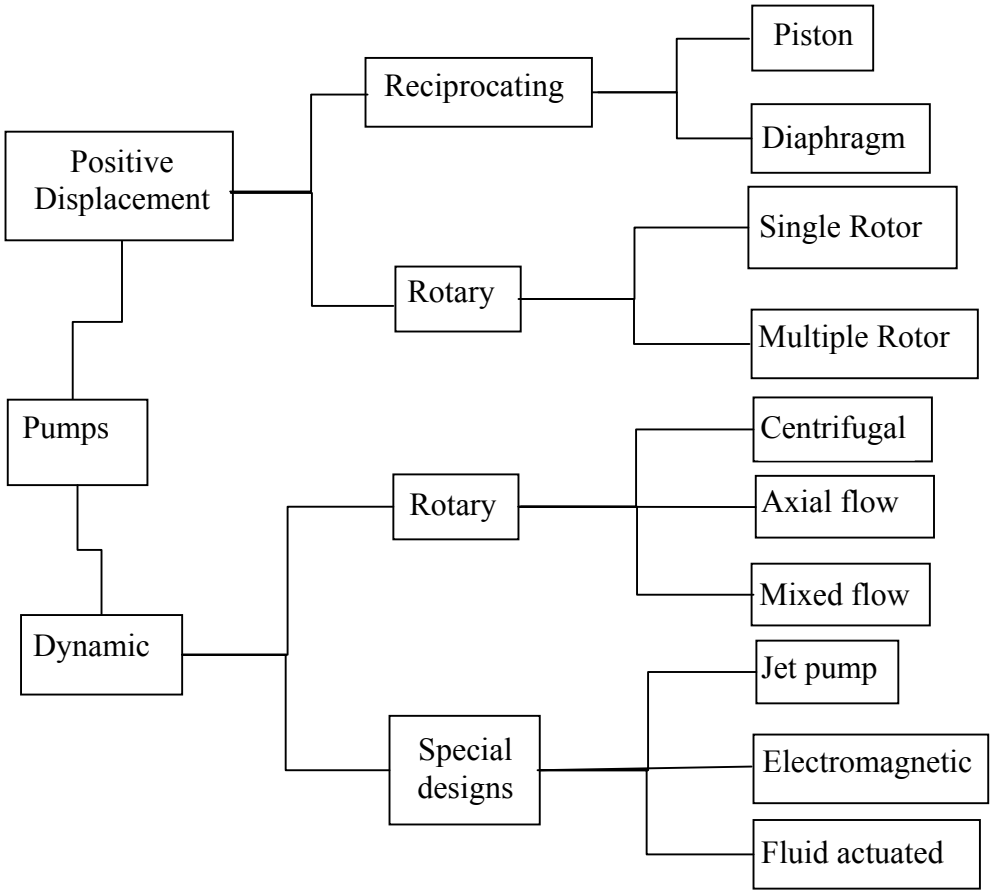

Figure 1.7 Classifications of Pumps

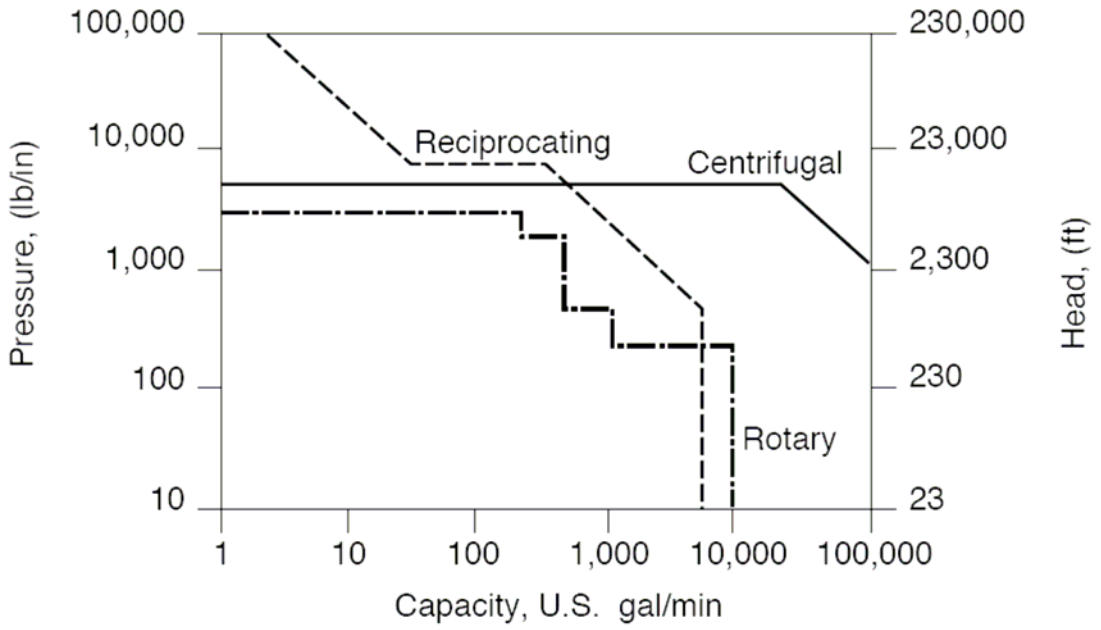

Figure 1.8 Performance characteristics of various pumps

1.1.3 Factors affecting the performance of the pump

The following are the factors that would cause a decrease in the pump efficiency:

a. Friction and minor losses

b. Factors affecting the performance are most effected by viscosity, pressure, material of stator, rotor RPM.

The actual design and construction of the pumps requires considerable effort and insight while the operating principles remain easy. Each of the above-mentioned pumps has its own advantages and disadvantages. The various hydraulic and mechanical pump problems of displacement pumps, which affect the performance, are pump pulsations, piping vibrations etc.

Pulsations are caused due to the intermittent flow of a liquid through the internal valves of the pump. The mechanical resonances when excited by these pulsations cause vibrations in the pipes. The performance of the centrifugal pump is affected by factors like cavitation, suction, and discharge recirculations. Progress has already been made to deal with these problems in the past; however, continuous improvements are needed to achieve better pump performance for more challenging tasks.

1.1.4 Pump performance curves

Pump design is complicated. Due to the general complexity of flow through a pump, the performance of a pump is difficult to be predicted purely based on theoretical calculations. Actual performance of the pump is determined by conducting performance tests. Based on these tests, pump characteristics are determined and presented as pump performance curves. An example pump performance curves is shown in Figure 1.9.

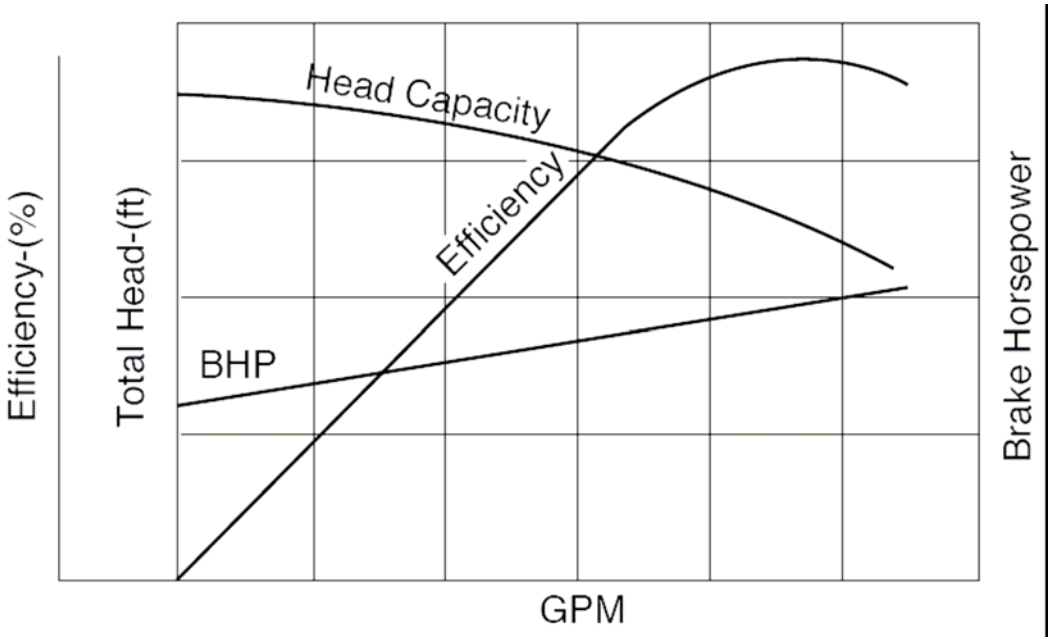

Figure 1.9 A typical pump performance curves

1.1.5 Cavitation

Cavitation is a major cause of piping and pump vibrations, and mechanical failures. Cavitation occurs in liquids when the local static pressure falls below the liquid vapor pressure. The extent of cavitation depends upon many factors including nuclei concentration. The nuclei serve as seeds for formation of the cavitation bubbles. Abundant nuclei are usually available in the form of dissolved gas, liquid impurities, and surface imperfections. The subsequent collapse of vapor pockets as the fluid is swept into the higher-pressure regions of the pump may cause damage of pump parts, generate sound and vibration, and produce flow and pressure pulsations in piping. The dynamic valve effects like lift, valve mass, spring rate, preload, valve lip area, flow areas etc., can greatly influence local cavitation at the valve. The static pressure in the suction system must be adequate to compensate for frictional pressure drop losses, the required acceleration head, and the pulsations present in the system. The pulsations consist of positive and negative peaks of pressure, of which the positive peak will be added to the static pressure and negative peak subtracted from the static pressure. When the static pressure, after subtracting the negative peak, reaches the vapor pressure, fluid cavitates and results in high-pressure spikes as the liquid vaporizes and then collapses as the pressure increases above the vapor pressure. Experimental conclusions made by J.C. Wachel, F.R. Szenasi, and S.C. Denison [1989] show that high pulsations cause the static pressure to drop below the vapor pressure and hence causing cavitation.

Significant amounts of vapor lead to a reduction in pump performance due primarily to the alteration of the passage flow field by the presence of vapor filled regions. As a result, proper operation of a pump requires an inlet pressure above a specific threshold to avoid cavitation. The

other important effect of cavitation is the erosion of the impeller blades and adjacent structures due to the collapse of the vapor bubbles. This damage impacts the life of the pump as well as affects its operation. Furthermore, the collapse of the vapor bubbles produce noise, which can be undesirable in noise-sensitive applications like submarines and related naval craft.

1.2 TurboPiston Pump (TPP)

A revolutionary new pump, " TurboPiston Pump" (TPP), was invented by Patrick Rousset, PE (U.S. Patent #7029241). He is president of Power Engineering, Inc. and a mechanical engineer who graduated from UNO in 1982. This new pump combines the merits of each existing type of pump (i.e. centrifugal pump, reciprocating piston pump, and rotary screw pump) while discarding the problems relating to each. It is positive displacement and capable of high discharge and pressure flow rates in a smaller space and weight than the existing pumps. (See UNO Press Release, December 16, 2005 in Appendix G)

1.2.1 Working principle of the TPP

The pump is divided into three sections namely suction section, compression cylinders, and discharge section (see Figures 1.10 - 1.14). The pump combines the attributes of centrifugal and positive displacement pumps into a device that uses the rotary motion of two opposing rotors with multiple positive displacement piston receiver pairs for pressure addition to the stream. The suction end of the pump has an inlet pipe through which the water enters and a rotating impeller inside characterizes centrifugal pump. Fluid enters the impeller at the center and is accelerated through the blades to the outside of the impeller and into the case. The stream pressure is achieved by the centrifugal force of the water being accelerated to the outside of the impeller.

Unlike the centrifugal pumps the TurboPiston pump has a positive displacement and hence the ability to produce high pressure. A shaft runs through the entire volume incorporating the axial flow. The TPP consists of two opposing rotating disks with the suction side disk being mounted with a slightly inclined angle, so these two disks are separated with a wedge of volume. Eight pistons are built on the inclined suction disk and eight corresponding cylinders are built on the vertical discharging disk. Each chamber has both suction and a discharge valve associated with it and rotating as an integral part of each rotor. The rotating motion will drive a continuous piston motion of compressing and expanding as the pistons and cylinders combine on the circumference of a circle and glide in and out of each other. The rotating motion harnesses the feature of a high volume flow rate of the centrifugal pump (Turbo-motion). The piston motion achieves the positive displacement feature of high compression ratio of a piston pump, and the wedge volume simulates the energy saving feature of the extended surface of a rotary screw pump.

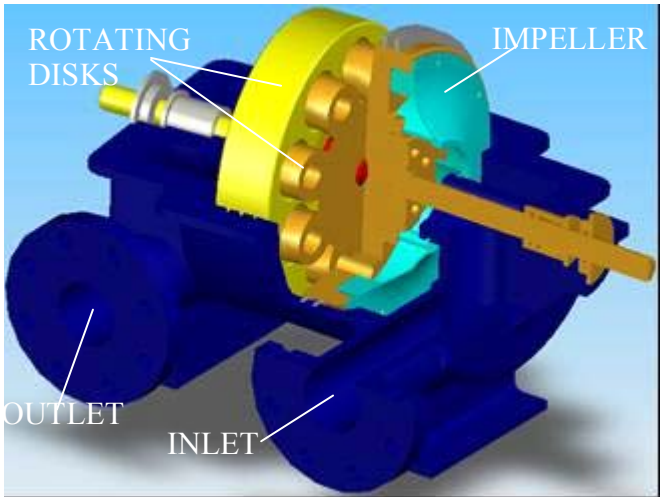

Figure 1.10 A cut-away view of the TurboPiston Pump.

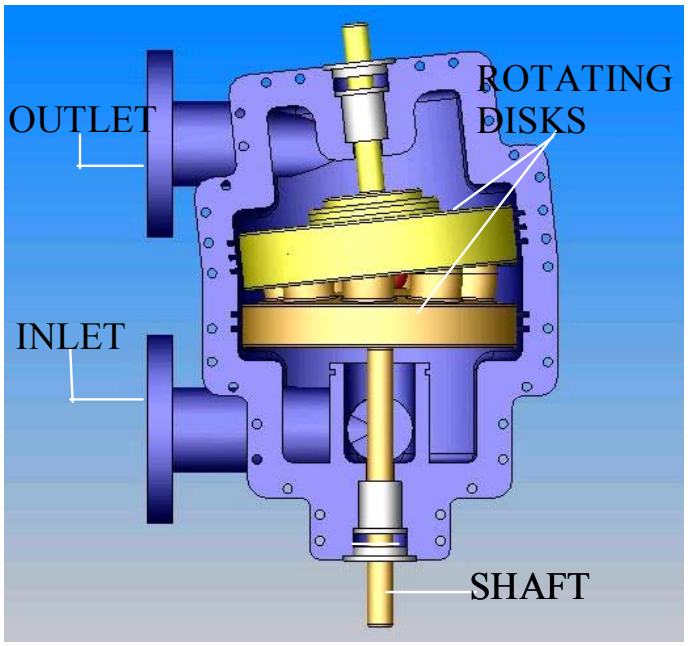

Figure 1.11 Top View of the TurboPiston Pump.

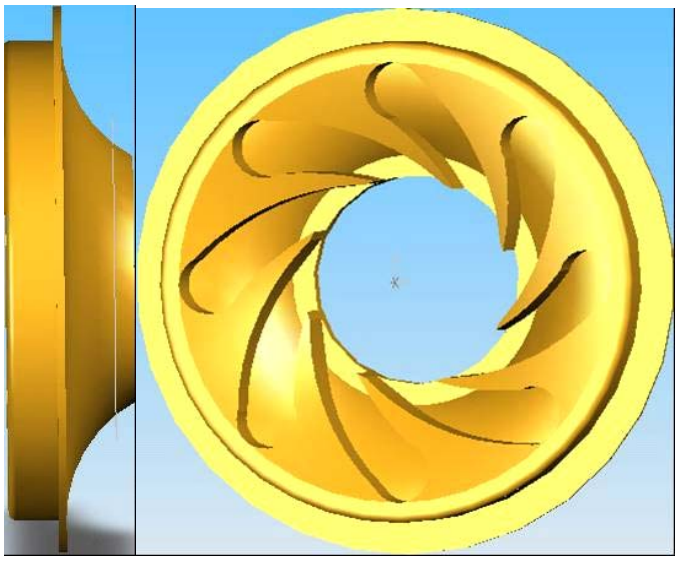

Figure 1.12 Front and side views of the impeller.

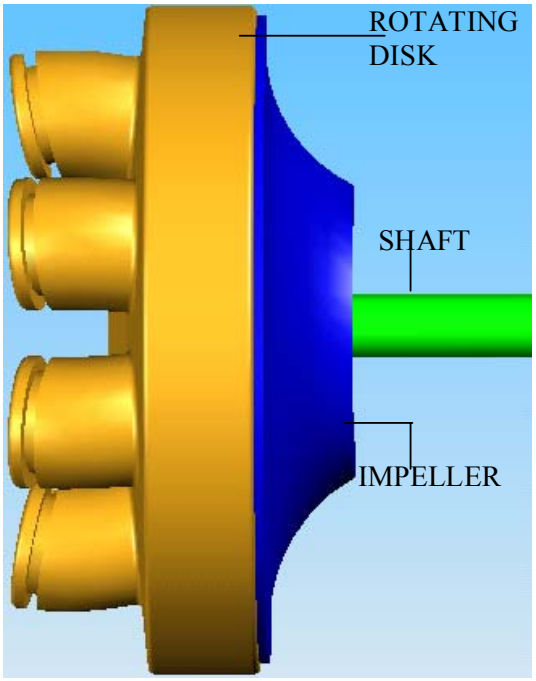

Figure 1.13 Impeller and the rotor at the suction side of the TurboPiston pump.

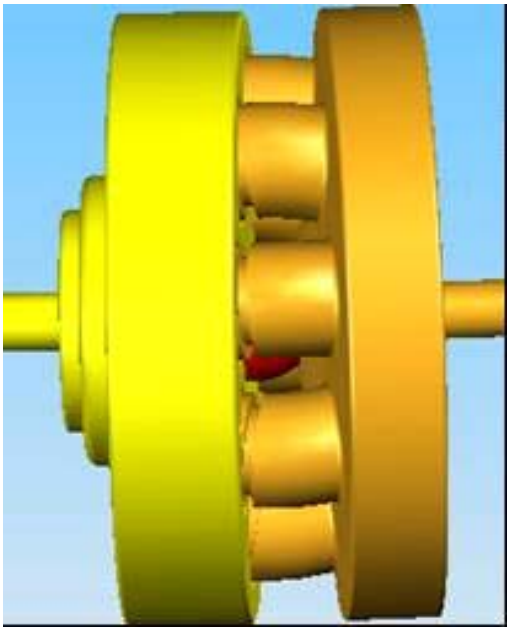

Figure 1.14 Rotary section of the TurboPiston pump.

The capacity and flow rates of various sizes of TurboPiston pumps are calculated in Appendix B and listed in Table 1.2

Piston circle (in)	Bore (in)	Stroke (in)	Flow Rate(USGPM)			Flow Rate(ft^3/s)		
			900 rpm	1800 rpm	3600 rpm	900 rpm	1800 rpm	3600 rpm
72	22.125	7.50	90,358	180,716	361,431	201	403	805
96	29.500	10.00	214,182	428,363	858,726	477	954	1,909
120	36.875	12.50	418,323	836,647	1,673,294	932	1,864	3,728
144	44.250	15.00	722,863	1,445,726	2,891,452	1,610	3,221	6,442
180	55.375	18.75	1,415,304	2,830,068	5,660,136	3,163	6,305	12,610
240	73.750	25.00	3,346,588	6,693,175	13,386,351	7,456	14,911	29,823
300	92.250	31.25	6,645,170	13,090,340	26,180,679	14,582	29,164	58,327

Table 1.2 Flow rates of various sizes of TurboPiston pumps. See Appendix-II for detailed calculations.

1.2.2 Comparison of existing pumps

Table 1.3 gives a comparison of the characteristics of various commercial pumps (including multistage pumps) available in the market and the single-stage turbo piston pump (TPP).

Parameter	Centrifugal Pumps	Reciprocating Pumps	Rotary Pumps	Turbo piston pump(TPP)
Optimum Flow and Pressure Applications	Medium/High Capacity, Low/Medium Pressure	Low Capacity, High Pressure	Low/Medium Capacity, Low/Medium Pressure	High capacity/High pressure
Maximum Flow Rate	100,000+ GPM	10,000+ GPM	10,000+ GPM	100,000GPM
Low Flow Rate Capability	No	Yes	Yes	Yes
Maximum pressure (single stage)	600PSI	9000PSI	250PSI	1000 PSI
Maximum Pressure (multiple stages)	6,000+ PSI	100,000+ PSI	4,000+ PSI	NA
Requires Relief Valve	No	Yes	Yes	
Smooth or Pulsating Flow	Smooth	Pulsating	Smooth	Pulsating
Variable or Constant Flow	Variable	Constant	Constant	Variable
Self-priming	No	Yes	Yes	Yes
Space Considerations	Requires Less Space	Requires More Space	Requires Less Space	Requires Less Space
Costs	Lower Initial Lower Maintenance Higher Power	Higher Initial Higher Maintenance Lower Power	Lower Initial Lower Maintenance Lower Power	Lower Initial Lower Maintenance High Power

Table 1.3 Comparison of single -stage TPP with available single and multistage pumps in the market.

1.3 Objectives of This Study

Since the TPP has not been fully demonstrated or commercialized, the objectives of this study are:

(a) Use computational fluid dynamics (CFD) to calculate the flow field and understand the flow behavior inside the pump.

(b) Estimate the total pressure losses and overall efficiency.

(c) Examine the potential cavitation locations under various rotation speeds.

(d) Identify potential means to improve the pump performance.

CHAPTER TWO

COMPUTATIONAL ANALYSIS

This chapter describes the steps involved in building the computational flow volume and the methodologies used to simulate the flow field in the TurboPiston pump. The three-dimensional domain of the flow volume is created in GAMBIT. The dimensions for this geometry are obtained from the AutoCAD drawings given by the designer of the TurboPiston Pump. The following sections of this chapter explain the procedures in simulating the problem.

2.1 Physical Characteristics and Assumptions Made

The following are the physical characteristics of the problem.

1. Three dimensional flow
2. Varying fluid properties

2.2 Governing Equations

The governing equations include the conservation of mass, conservation of momentum and conservation of energy as shown below. The continuity is described as

$$\frac{\partial \rho}{\partial t} + \nabla .\left(\rho \bar{\mathrm{v}}\right) = S_m \qquad (2.1)$$

This equation is the general form of the mass conservation equation and is valid for incompressible as well as compressible flows. The source S_m is the mass added to the continuous phase.

The momentum equation is presented in the Navier-Stokes form,

$$\frac{\partial}{\partial t}(\rho\vec{v}) + \nabla.(\rho\vec{v}\vec{v}) = -\nabla p + \nabla.\left(\overline{\overline{\tau}}\right) + \rho\vec{g} + \vec{F} \tag{2.2}$$

Where p is the static pressure, $\overline{\overline{\tau}}$ is the stress tensor; $\rho\vec{g}$ and $\vec{F}$ are the gravitational body force and external body forces. In this study, the rotational motion is added as the body force. No buoyancy force is considered.

The stress tensor $\overline{\overline{\tau}}$ is given by

$$\overline{\overline{\tau}} = \mu\left[\left(\nabla\vec{v} + \nabla\vec{v}^{T}\right) - \frac{2}{3}\nabla.v.I\right] \tag{2.3}$$

Where μ is the molecular viscosity, I is the unit tensor, and the second term on the right hand side is the effect of volume dilatation.

2.3 Computational Model

The simulation is conducted by separating the pump into three separated computational domains: the suction section, the discharging section, and the cylinder. The suction and discharging sections are simulated by using the computational fluid dynamics (CFD), whereas the compression process in the cylinder is not simulated computationally. The total pressure loss in the cylinder is calculated by engineering approach as a pipe flow. The geometry of the entire pump is provided by the designer and shown as the AutoCAD drawings in Figure 2.1 below. The total dimension is approximately 26 inches $\times$ 17 inches $\times$19 inches.

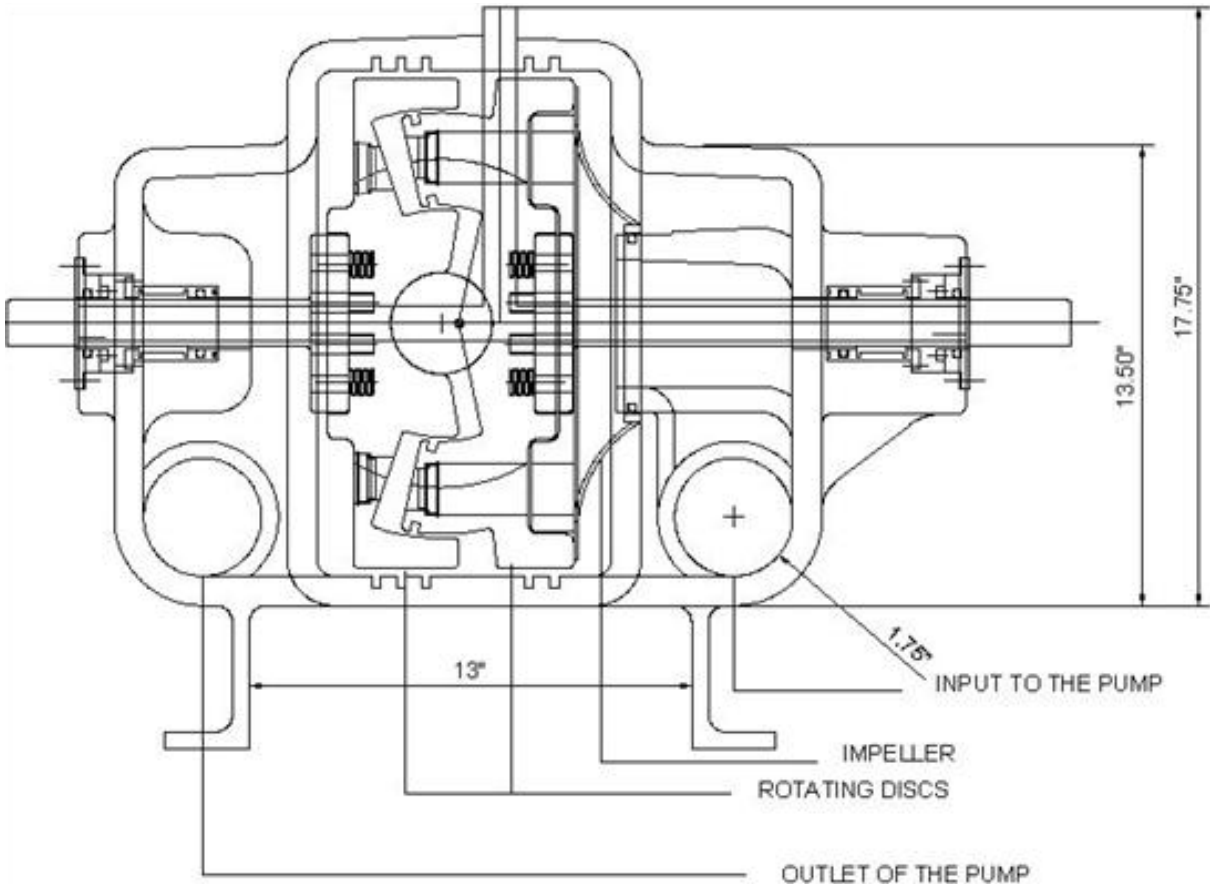

Figure 2.1 Elevation view of the TurboPiston pump

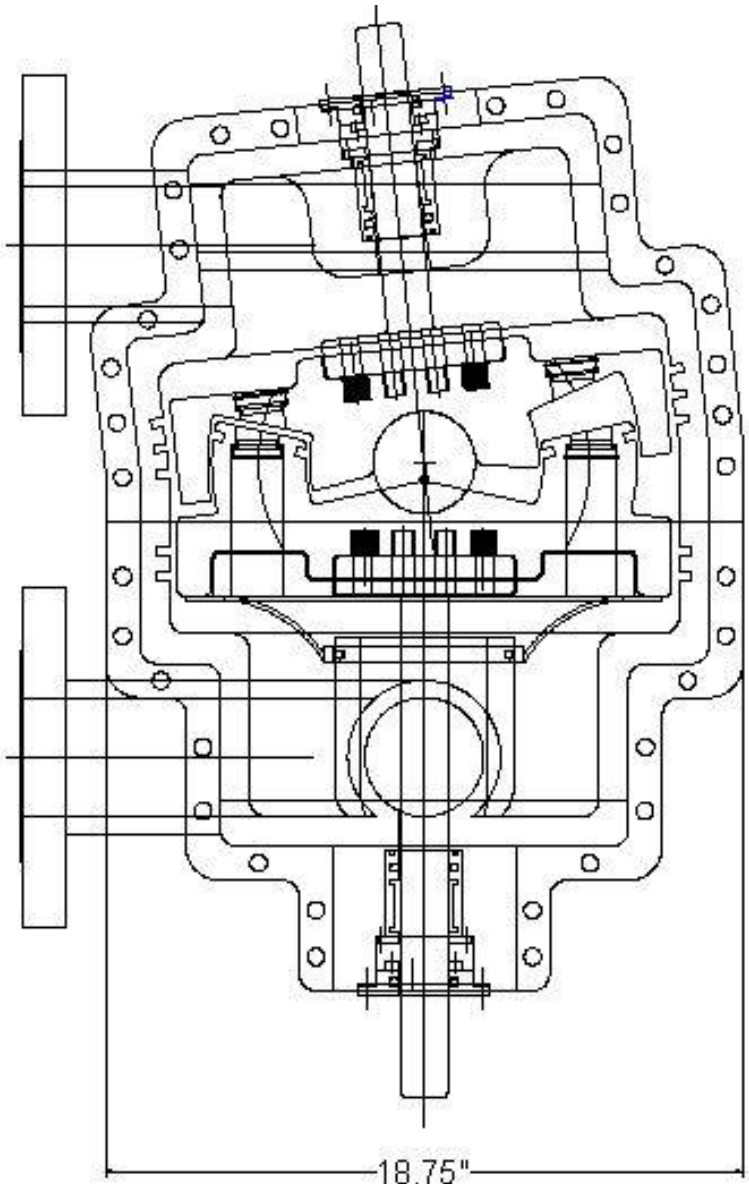

Figure 2.2 Plan view of the TurboPiston pump (TPP)

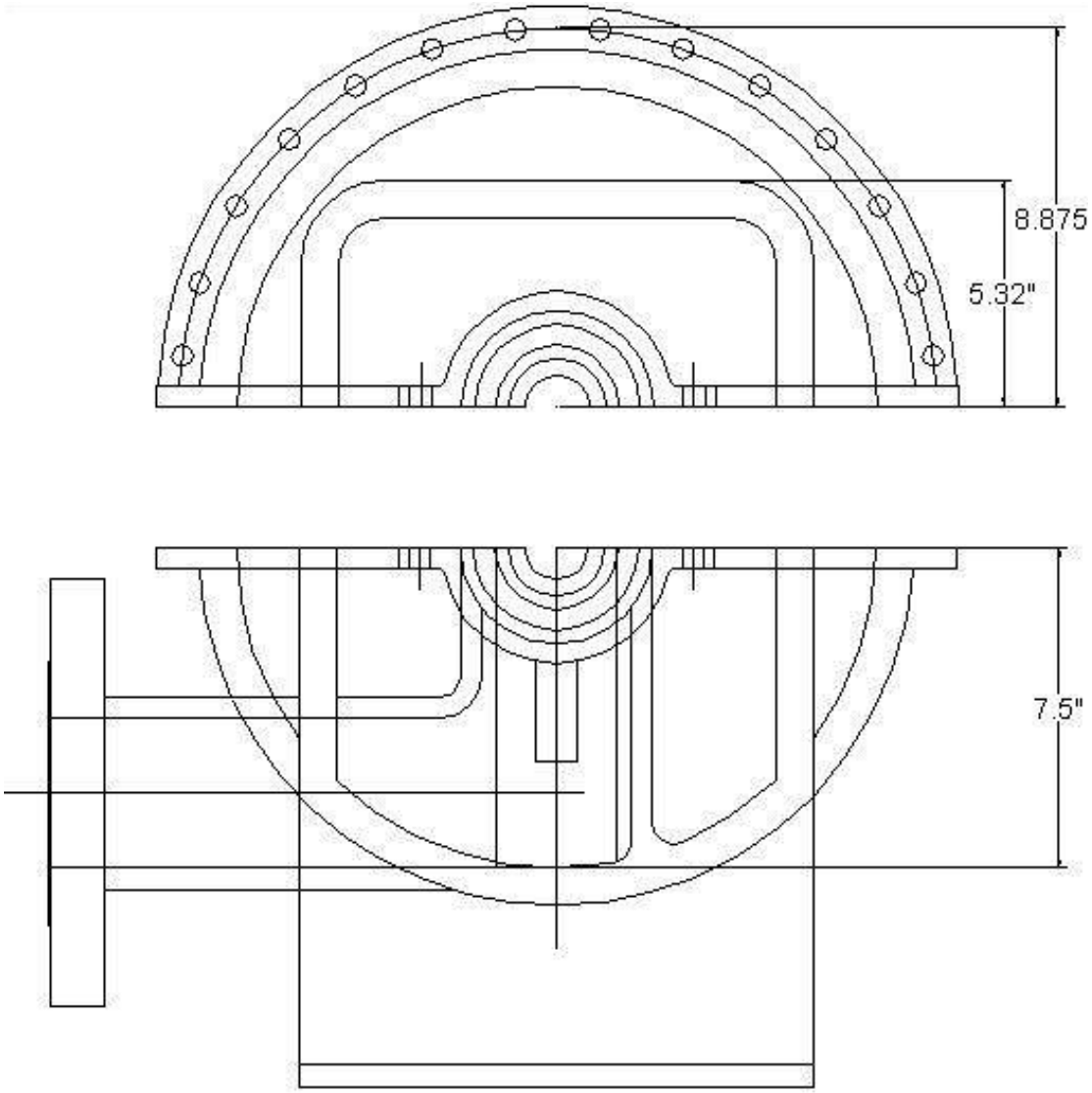

Figure 2.3 End view of the suction side.

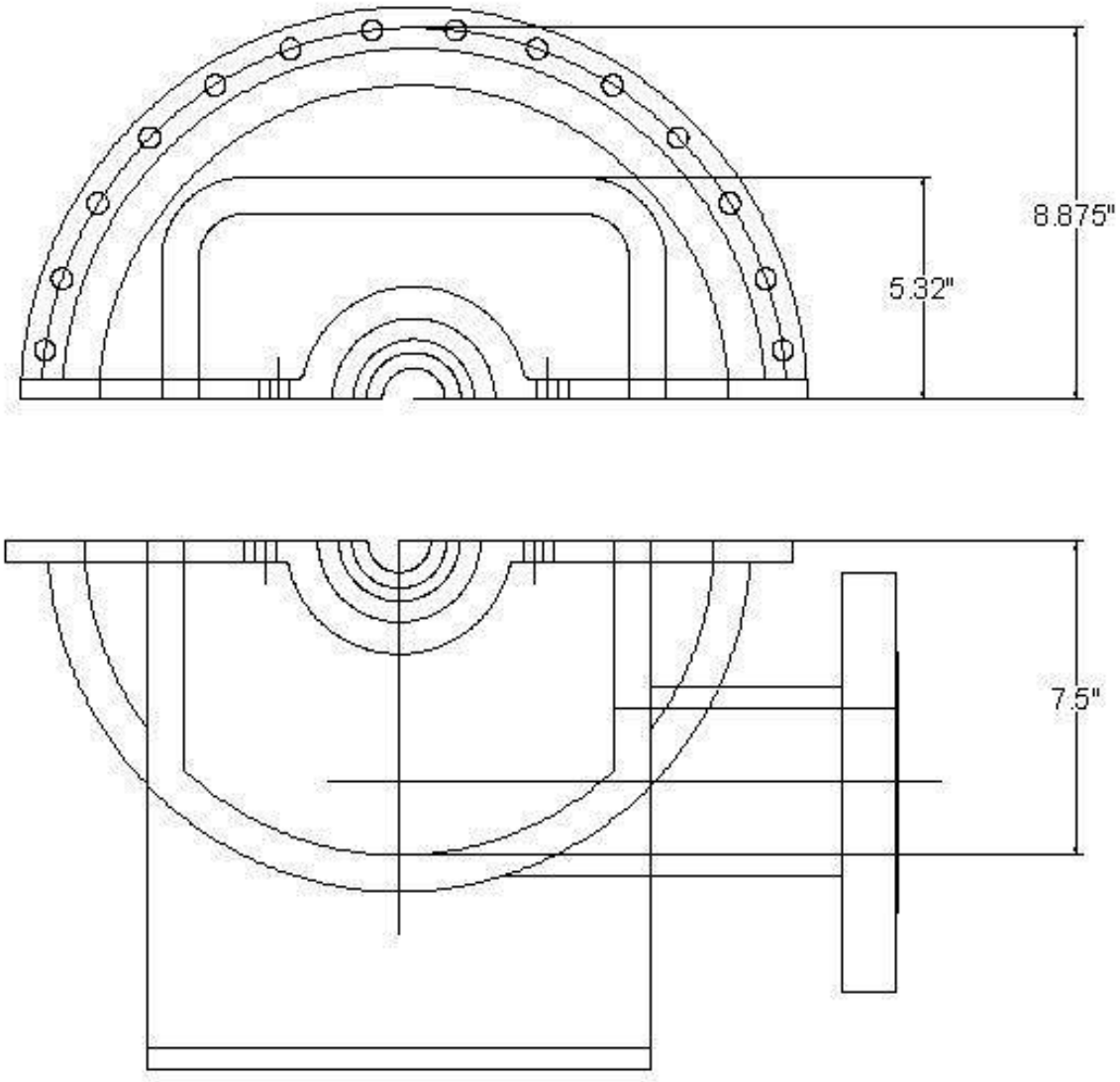

Figure 2.4 End view of the discharge side.

The above figures are the actual pump casings and components. In the computational domains, only the flow path needs to be considered. Figure 2.5 shows the computational domain of the suction section, and Figure 2.6 shows the 3-D model of the suction section.

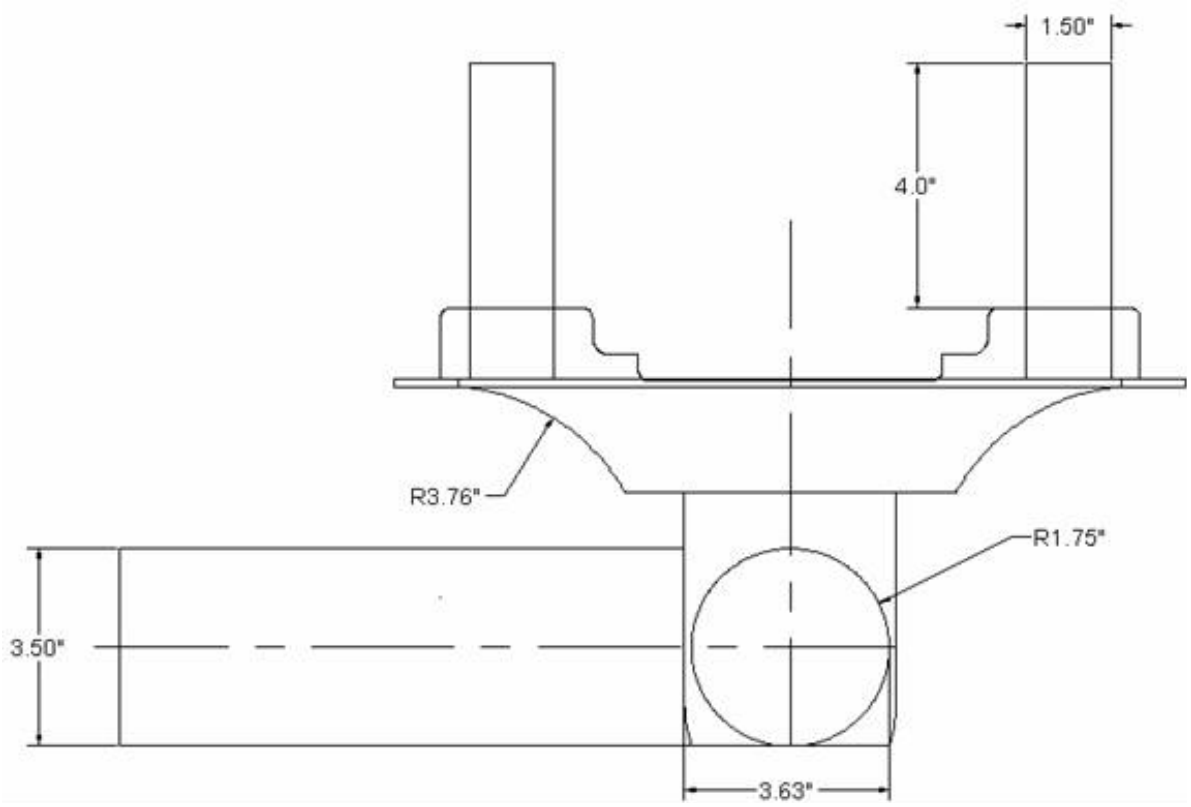

Figure 2.5 2-D Computational domain of the suction section.

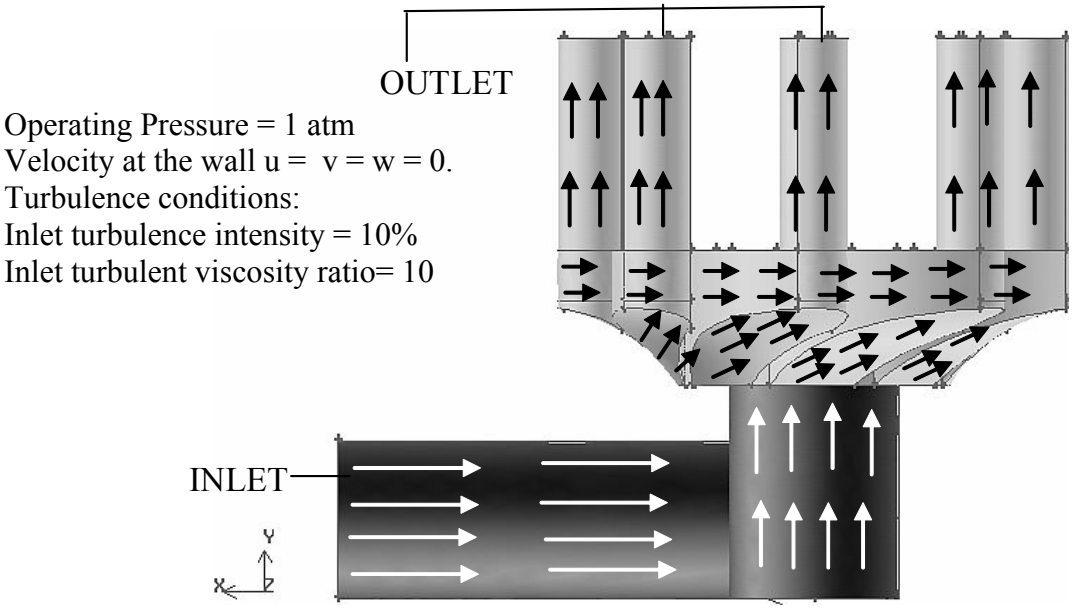

Figure2.6(a) 3-D model of the suction section showing the flow direction

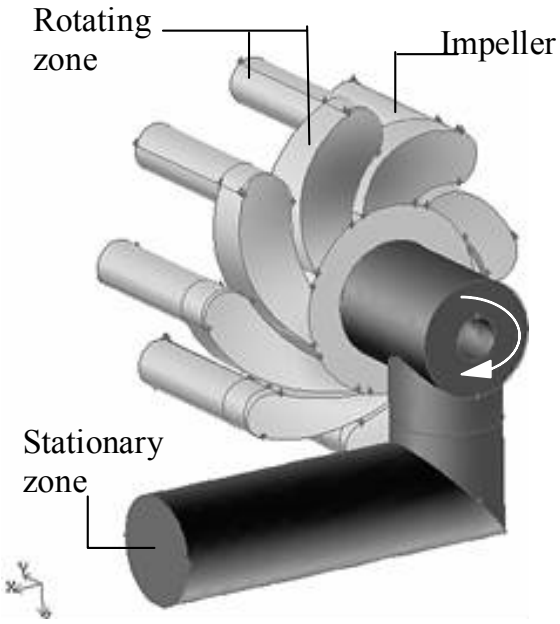

Figure 2.6 3-D model of the suction section showing the flow direction.

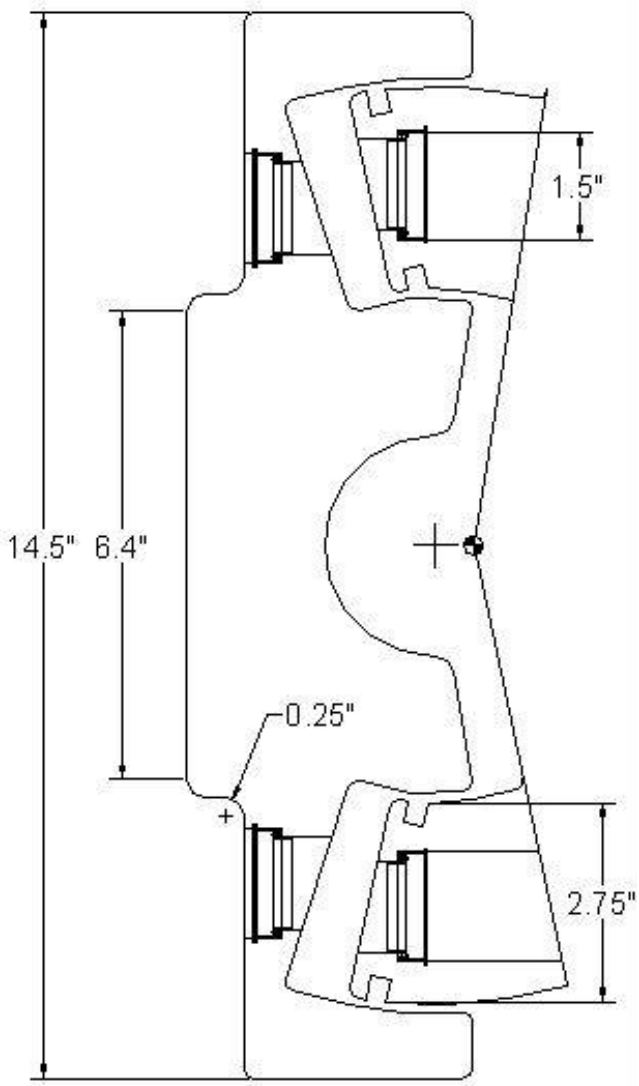

Figure 2.7 AutoCAD drawing of the rotating discs.

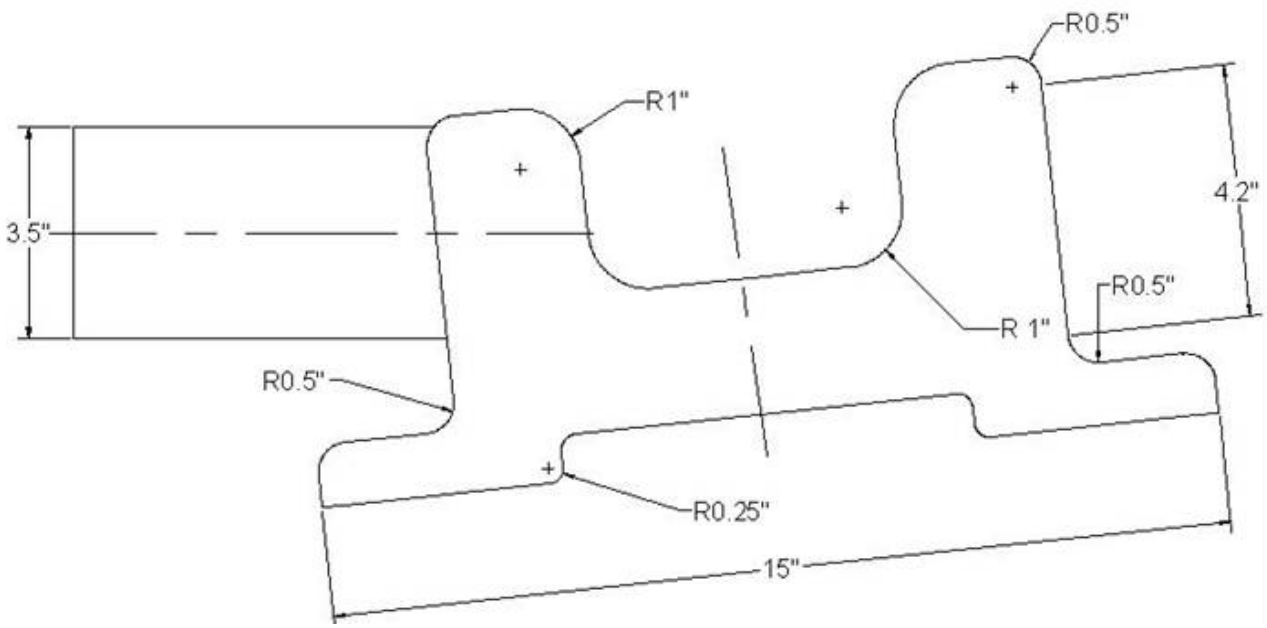

Figure 2.8 2-D computational domain for the discharge section.

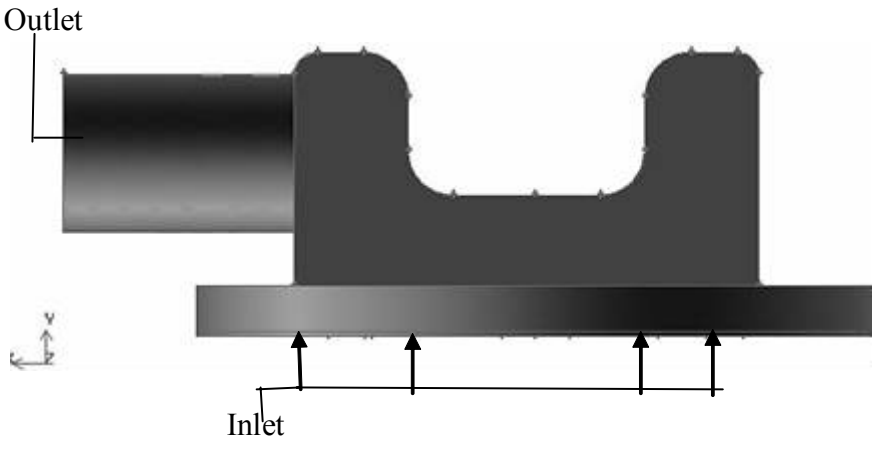

Figure 2.9 Top view of the 3-D model of the discharge section.

Operating Pressure = 34 atm (500 psig)
Velocity at the wall u = v = w = 0.
Turbulence conditions:
Inlet turbulence intensity = 10%
Inlet Turbulent viscosity ratio = 10

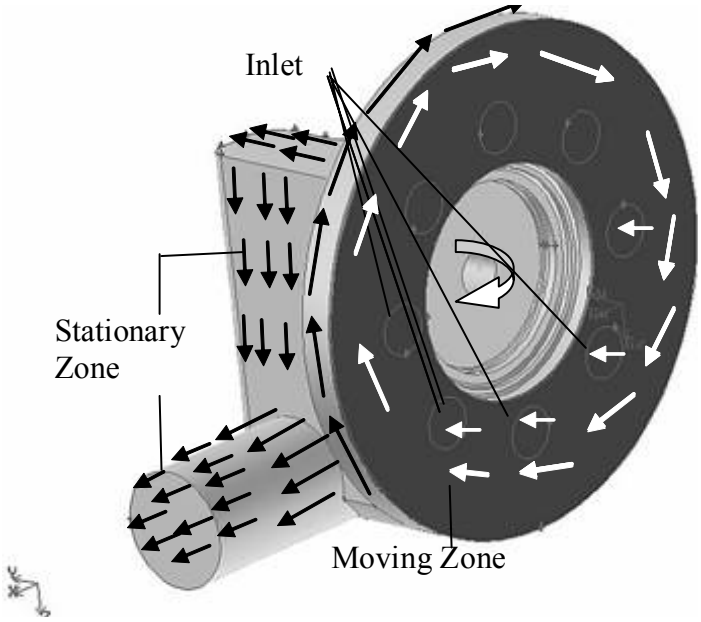

Figure 2.10 3-D model of the discharge section showing the flow direction.

2.4 Assumptions

- No cavitation
- No buoyancy force
- No viscous dissipation as heat

2.5 Boundary Conditions

The following are the boundary conditions considered for each computational domain.

(a) Boundary conditions in the suction section:

- The speed of the shaft equals 0 and 100 rpm. This condition is imposed on the shaft wall as $2\pi r$ (rpm), where r = 1.37 inches is the shaft radius.
- Mass flow rate at the inlet =1.337 Kg/s corresponding to the shaft speed 100 rpm.

- No slip condition at the stationary walls: u = v = w = 0
- Pressure at the outlet varies with the location:
  - In the upper half of the circle ($270^o \rightarrow 0^o \rightarrow 90^o$), valves open.
  - P = -0.999999atm gauge (or 0.000001atm absolute) and a loss coefficient of 1.0
  - In the lower half of the circle ($90^o \rightarrow 180^o \rightarrow 270^o$), valves close; the outlets are treated as walls.
- Inlet turbulent intensity = 10 percent
- Inlet turbulent viscosity = 10 kg/m-s
- Operating pressure = 1atm

(b) Boundary conditions at the discharge section

- Inlet condition:
  - In the upper half of the circle ($270^o \rightarrow 0^o \rightarrow 90^o$), valves close. The inlets are treated as the wall.
  - In the lower half of the circle ($90^o \rightarrow 180^o \rightarrow 270^o$), valves open. The mass flow rate at the inlet is1.337 Kg/s corresponding to the shaft speed 100 rpm
- Outlet boundary condition: pressure at 500 psig (34atm)

2.6 Turbulence Model

Turbulent flows are characterized by fluctuating velocity fields. These fluctuations mix transported quantities such as momentum, energy and species concentration and cause the transported quantities to fluctuate as well. Because these fluctuations are small, they are

computationally expensive to simulate directly in engineering calculations. Hence, the governing equations are time averaged to remove the fluctuating scales that result in equations that are computationally less expensive to solve. However, time average of the governing equations results in unknown quantities called the Reynolds Stresses. Many different turbulence models have been developed to determine these unknown quantities. The following are the turbulence models widely available,

i.Spalart- Allmaras model

ii.k-ε models

- Standard *k*-ε model
- Renormalization-group(RNG) *k*-ε model
- Realizable *k*-ε model

iii.k- ω models

- Standard *k*- ω model
- Shear-stress transport (SST) *k*- ω model

*iv.*Reynolds stress model

The choice of turbulence model depends on such considerations as the physics of the flow, level of accuracy required, available computational resources, and the time available for simulation. It is understood that different turbulence models may render different results. In this study, the standard k-ε model is employed because it is robust. The standard *k*-ε model, which is a two-equation model, uses the solution of two separate transport equations and allows the turbulent velocity and length scales to be independently determined. It is a semi-empirical model based on model transport equations for the turbulence kinetic energy (*k*) and the dissipation rate

(ε). The model transport equation for (*k)* is derived from the exact equation, while the model transport equation for (ε) is obtained using physical reasoning and bears little resemblance to its mathematically exact counterpart. The turbulence kinetic energy, *k*, and its rate of dissipation, ε, are obtained from the following transport equations:

$$\frac{\partial}{\partial t}(\rho k)+\frac{\partial}{\partial x_i}(\rho k u_i)=\frac{\partial}{\partial x_j}\left[\left(\mu+\frac{\mu_t}{\sigma_k}\right)\frac{\partial k}{\partial x_j}\right]+G_k+G_b-\sigma\varepsilon-Y_M+S_k \tag{2.4}$$

$$\frac{\partial}{\partial t}(\rho\varepsilon)+\frac{\partial}{\partial x_i}(\rho\varepsilon u_i)=\frac{\partial}{\partial x_j}\left[\left(\mu+\frac{\mu_t}{\sigma_\varepsilon}\right)\frac{\partial \varepsilon}{\partial x_j}\right]+C_{1\varepsilon}\frac{\varepsilon}{k}(G_k+G_{3\varepsilon}G_b)-C_{2\varepsilon}\rho\frac{\varepsilon^2}{k}+S_\varepsilon \tag{2.5}$$

In the above equations, G_k represents the generation of turbulence kinetic energy due to the mean velocity gradients and is defined as,

$$G_k=-\rho\overline{u_i'u_j'}\frac{\partial u_j}{\partial x_i}$$
$$G_k=-\mu_t S^2 \tag{2.6}$$

G_b is the generation of turbulence kinetic energy due to buoyancy and is defined as,

$$G_b=\beta g_i\frac{\mu_t}{\mathrm{Pr}_t}\frac{\partial T}{\partial x_i} \tag{2.7}$$

Pr_t is the turbulent Prandtl number and g_i is the component of gravitational vector in the *i*-th directon. For the standard *k*-ε model the value for Prandtl number is set to 1 in this study.

The coefficient of thermal expansion, β, is given by

$$\beta=\frac{1}{\rho}\left(\frac{\partial\rho}{\partial T}\right)_p \tag{2.8}$$

Y_M represents the contribution of the fluctuating dilatation in compressible turbulence to the overall dissipation rate, and is given by

$$Y_M = 2\rho\varepsilon M_t^2 \qquad (2.9)$$

where M_t is the turbulent Mach number which is given by

$$M_t = \sqrt{\frac{k}{a^2}} \qquad (2.10)$$

where a = $\sqrt{\gamma RT}$ gives the speed of the sound.

In this study, no buoyancy is considered and the flow is incompressible, so both G_b and Y_M are not considered.

The turbulent viscosity, μ_k, is calculated from the following equation

$$\mu_k = \rho C_\mu \frac{k^2}{\varepsilon} \qquad (2.11)$$

The model constants $C_{1\varepsilon}$, $C_{2\varepsilon}$, C_μ, σ_k, and σ_ε have the following values

$C_{1\varepsilon}$=1.44 , $C_{2\varepsilon}$=1.9,σ_k=1.0, σ_ε=1.2

Turbulent flows are significantly affected by the presence of the walls. The mean velocity is affected through the no-slip condition that must be satisfied at the wall. Presence of walls causes a significant change in the turbulence. The tangential velocity fluctuations are reduced by the viscous damping, and the kinematic blocking reduces the normal fluctuations. Toward the outer part of the near-wall region, the turbulence is augmented due to the production of turbulence kinetic energy generated by large mean velocity gradients. In flows that are driven by wall rotation, the motion of the wall tends to impart a forced vortex motion to the fluid by imposing a constant angular velocity. An important characteristic of such flows is the tendency

of fluid with high angular momentum, which is flow near the wall, to be flung radially outward. This is often referred to as "radial pumping", since the rotating wall is pumping the fluid radially outward. The solution in the near-wall region could be very important since the solution variables have large gradients in this region. The momentum and other scalar transports occur most vigorously. The representation of the flow in the near-wall region plays a vital role in determining the successful predictions of wall bounded turbulent flows. Due to the complex geometry in this study, fine meshes near the wall demand large computational power. Therefore, wall functions are adopted in the near-wall region. The wall functions approach employs a collection of semi-empirical formulae and functions to connect the viscosity-affected region between the wall and the fully turbulent region. In this approach, the viscous sub-layer where the solution variables change most rapidly is not resolved by the computational method. Because of its accuracy and economy, the wall function approach is a practical option for the near-wall treatments for industrial flow simulations.. The wall functions consist of:

- Laws-of –the-wall for mean velocity and temperature (or other scalars)
- Formulas for near-wall turbulent quantities.

The standard wall function approach adopts the law of the wall for the mean velocity as

$$U^* = \frac{1}{\kappa}\ln\left(\mathrm{Ey}^*\right) \tag{2.12}$$

Where U^* and y^* are given by the following equations

$$U^* \equiv \frac{U_p C_\mu^{1/4} k_p^{1/2}}{\tau_\omega / \rho} \tag{2.13}$$

$$y^* \equiv \frac{\rho C_\mu^{1/4} k_p^{1/2} y_p}{\mu} \tag{2.14}$$

Where,

κ =Von Karman constant (=0.4187)

E= empirical constant (=9.793)

U_p= mean velocity of the fluid at point P

k_p = turbulence kinetic energy at point P

y_p = distance from point P to the wall

μ = dynamic viscosity of the fluid

2.7 Flow In The Moving And Deforming Zones

In the rotational domain, the continuity and the momentum equations are solved in the rotating frame of reference. Here the acceleration of the fluid is augmented by additional terms that appear in the momentum equations. The rotating frame problems are solved either using the relative velocities or the absolute velocities. The two velocities are related by the following expression,

$$\vec{v}_r = \vec{v} - (\vec{\Omega} \times \vec{r}) \tag{2.16}$$

Where, $\vec{\Omega}$ is the angular velocity vector and $\vec{r}$ is the position vector in the rotating reference frame. In an inertial frame of reference, the left hand side of the momentum equation is given as

$$\frac{\partial}{\partial t}(\rho\vec{v}) + \nabla.(\rho\vec{v}\vec{v}) \tag{2.17}$$

For a rotating reference frame, the left hand side written in terms of the absolute velocities becomes

$$\frac{\partial}{\partial t}(\rho\vec{v}) + \nabla.(\rho\vec{v}_r\vec{v}) + \rho(\vec{\Omega} \times \vec{v}) \tag{2.18}$$

In terms of relative velocities the left hand side equation is given by

$$\frac{\partial}{\partial t}(\rho\vec{v}) + \nabla.(\rho\vec{v}_r\vec{v}_r) + \rho\left(2\vec{\Omega}\times\vec{v}_r + \vec{\Omega}\times\vec{\Omega}\times\vec{r}\right) + \rho\frac{\partial\vec{\Omega}}{\partial t}\times\vec{r} \tag{2.19}$$

In rotating flow domains, equation of conservation of mass can be written as the following for both relative and absolute velocity formulations

$$\frac{\partial\rho}{\partial t} + \nabla.(\rho\vec{v}_r) = S_m \tag{2.20}$$

In this study, the flow in the rotating frame of reference is rotating with the speed of the shaft. The absolute velocity is more efficient to use here. The calculation of the domain is divided into several sub-domains with each rotating or translating. The governing equations in each domain are written with respect to that domain's reference. The stationary flow domain is governed by equations (2.1) and the flow, in the rotating sub-domains, is governed by equations (2.20).

CHAPTER THREE

COMPUTATIONAL SCHEME

The commercial software package FLUENT (version 6.2.16) from FLUENT, Inc. is adopted for this study. The governing equations are discretizied using the control-volume method. The simulation uses the segregated solver, which employs an implicit pressure-correction scheme. The SIMPLE algorithm is used to couple the pressure and velocity. Second order upwind scheme is selected for spatial discretization of the convective terms and species. The detailed computational scheme is explained below.

3.1 Computational Scheme

The following are the procedures involved in the computational scheme of solving a CFD problem.

Step 0: Identifying the physical problems to be solved.

- Identify the physical problem and the associated computational domain
- Determine how to model the real problem by making appropriate assumptions and simplifications, and imposing the boundary conditions
- Identify the physical models to be used for turbulence, combustion, multiphase, etc
- Determine convergence criteria
- Import the geometry from another CAD (computational aided design) package if possible

Completing the above involves establishing the geometry, choosing the fluid properties, understanding the boundary conditions, making modeling assumptions, and establishing convergence conditions for acceptance of the results.

Step 1:Pre-processing

Pre-processing refers to the creation of the geometry, grids, and the flow boundaries. In this study, the commercial CAD package GAMBIT is used to

- Create geometry and import geometry from other CAD packages
- Construct the grids

For simple geometries, quad/hex (rectangular/hexadron) meshes provide high quality solutions with fewer cells than comparable tri/tet (triangle/tetrahedral) mesh. For complex geometries, quad/hex meshes are difficult and take time to construct; so usually tri/tet meshes are employed for complex geometries to significantly reduce effort and time. Hybrid meshes (different domains are meshed with different types) can be both efficient and accurate when compared to uniform meshes.

Step 2: Processing

In CFD, "processing" is identified as obtaining the solution of the transport equations (in this study FLUENT is used for processing). FLUENT is a finite-volume based CFD solver written in 'C' language. Processing involves running the calculations to solve the governing equations after setting up the numerical model - which includes choosing the fluid properties, establishing the flow physics, creating the computational domain and meshes, implementing the

boundary conditions, setting the convergence criteria, and selecting the numerical schemes, etc. Processing involves the following steps:

- Import the grid into the solver (i.e., FLUENT in this study)
- Select the appropriate physical models
- Prescribe operating conditions
- Define starting solution (i.e. initial guessed values) for iterations
- Set up controls for the Fluent solver
- Set up convergence criteria.
- Compute the solution

The solution will be obtained via iterations until the convergence criteria are satisfied. Residuals are used to monitor the convergence progress. The residuals are the imbalanced errors in the governing and associated equations, over all the cells in the computational domain. Conservations of mass and energy balance are achieved within the specified margins once the convergence criteria are satisfied.

Step 3: Post -processing (after the converged solution is obtained)

Post-processing involves employing different charts, graphics and visualization schemes to examine the results such as:

i. Contour and vector plots

ii. Pathlines and particle trajectory plots

iii. XY plots

iv. Animation is also used to further calculate physical factors from the converged solutions to help understand the physics of the results such as:

- Lift and drag
- Heat transfer coefficients
- Average surface temperature
- Total pressure changes
- Emissions of NO_x and CO
- Streamlines and Pathlines

Step 4: Verification

Verification of the results involves examining all the factors that could affect those results such as turbulence models, turbulence length scales, inlet and outlet conditions, boundary conditions, mesh density near the wall, grid independence, satisfaction of physical laws, comparison with experimental data, etc.

3.2 General Solution Procedure In FLUENT

- Solution parameters
  - Choosing the solver
  - Choosing discretization schemes
- Initialization (providing guessed initial values)
- Convergence
  - Monitoring convergence
  - Stability

a) Setting under- or over-relaxation factors

b) Setting Courant number (for unsteady flow)

- Accelerating convergence

➢ Accuracy

- Grid independence
- Sensitivity of near-wall grid (Y+ of the first grid)

Solution Parameters:

FLUENT offers two solution methods:

1. Segregated solution method
2. Coupled solution method

The governing equations are solved sequentially in the segregated solution method, while they are solved simultaneously in the coupled solution method. The present study uses segregated solution method. The non-linear governing equations can be linearized implicitly or explicitly with respect to the dependant variables. If linearized implicitly, the unknown values in each cell are computed using a relation that includes both existing and unknown values (to be calculated) from neighboring cells. If linearized explicitly, the unknown values in each cell are computed using a relation that includes only existing values. In segregated method, the linearization is implicit. Hence, each unknown will appear in more than one equations in the linear system produced, and these equations must be solved simultaneously to obtain the unknown quantities.

Discretization schemes:

In this scheme a control-volume-based method [Patankar 1980] is used to convert the governing equations to algebraic equations, which are then solved mathematically. This method yields discrete equations that conserve each quantity on a control-volume basis irrespective of the mesh densities.

The second order discretization scheme is applied for the following equations: momentum, turbulence kinetic energy, turbulence dissipation energy, and all the species. The SIMPLE pressure-velocity prediction and correction method [Patankar 1980] is employed.

Turbulence Model:

As discussed in chapter two, the standard k-ε model is used, and model constants used are $C_\mu = 0.09$,$C_{1\varepsilon} = 1.44$, $C_{2\varepsilon} = 1.92$, $\sigma_k = 1.0$, $\sigma_{k\varepsilon} = 1.3$.

Defining Materials:

The medium of flow in the present study is water. Water is selected from the FLUENT database for this study. FLUENT selects the properties of water automatically from its database.

Defining Boundary Conditions:

The boundary conditions are assigned in the GAMBIT. Mass flow rate condition is assigned at the inlet face. The outlet is defined as the vent outlet to include the pressure drop caused by the piston valves in the actual device. The suction condition at the outlet is assigned as an almost absolute zero, -0.999999 atm. In the actual operating condition, this outlet pressure continues to change and increase as the water fill in the cylinder. However, since the transient

condition inside the cylinder is not simulated in this study, the initial suction value (a constant value) is used for simplification during the entire simulation. After the solution is obtained, a static pressure difference is added back to the entire computational domain to compensate for the increased outlet pressure value. This pressure difference is calculated by assuming the total pressure at the inlet is 1 atm, which cannot be doubly assigned in the FLUENT when mass flow rate is already assigned as the inlet condition. This practice is justified because the computational process only involves the pressure difference, and the actual pressure values are not important for incompressible flow such as water in this study. The loss coefficient is assigned as "1.0" for the vent condition at the outlets. All the outer surfaces are defined as walls with no-slip condition on the surface.

Initialize Solution:

This is the initial guess provided for solving the governing equations. In FLUENT, the initial value is calculated from the inlet velocity of the domain. The initial condition used is the inlet velocity -0.2187462 m/s, which is opposite to the X-direction. Once the solution is initialized, the convergence criterion is fixed, and the solution is obtained by iterations.

The flow chart below briefly describes the architecture of FLUENT:

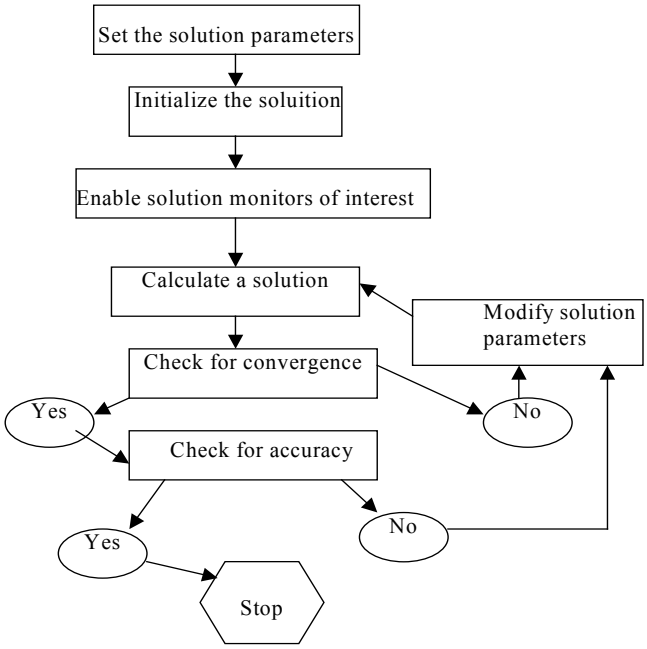

Figure 3.1 Flow chart showing the basic sequence of steps in FLUENT.

3.3 Solution Methodology

To qualify the computational results, the flow is first simulated as a steady-state case. This serves as the baseline case for qualifying the fundamental computational setup and for examining the adequacy of the flow physics. Then a steady-state “Moving Frame of Reference” scheme is adopted as an intermediate case to examine the flow physics under the influence of the rotation by assigning a rotational speed (or tangential velocity) of the rotation frame. In this method, the frame is not actually rotating but is under the influence of rotation. The results can be used to further examine the flow behavior under the effect of a steady rotational motion. Finally the unsteady case is conducted using the “Moving Mesh” or "Sliding Mesh" scheme to correctly simulate the rotating flow behavior in a transient manner.

3.3.1 Moving reference frame

The present study involves moving fluid domains in the computational domain and hence FLUENT's moving cell zone model is found to be most suitable.

The moving cell zone capability in FLUENT provides a set of features for solving problems in which the domain or parts pf the domain are in motion including:

- flow in a (single) rotating frame
- flow in multiple rotating and/or translating reference frames.

The single rotating frame option is usually used to model flows in turbomachinery, mixing tanks, and related devices. In each of these cases, the flow is unsteady in an inertial frame (i.e., a domain fixed on a non-moving frame) because the rotor/impeller blades sweep the domain periodically. However, in the absence of stators or baffles, it is possible to perform steady calculations in a domain that moves with the rotating part because there is no reference to distinguish the position of the moving part from one instant to another. In this case, the flow is steady relative to the rotating (non-inertial) frame. Only a rotational speed (or a tangential velocity) is assigned to the moving domain while the domain is actually held stationary. This approach significantly simplifies the analysis, and the results could be useful if they are carefully interpreted.

3.3.2 Moving mesh scheme

If stators or baffles are present in addition to a rotor or impeller, then it is not possible to render the computational problem steady because the stators can serve as the inertial reference, which can be used to clearly distinguish the position of the rotating frame instant by instant, i.e.,

a transient condition within each cycle. This situation occurs, for example, in turbomachinery applications where rotor and stator blades are in close proximity (and hence rotor-stator interaction is important). **FLUENT** provides three approaches to address this class of problems.

- the multiple reference frame (MRF) model
- the mixing plane model
- the sliding mesh model

Both the MRF and mixing plane models assume that the flow field is steady. Approximate means are accounting for the rotor-stator or impeller-baffle effects. These can be acceptable models in cases where the rotor-stator interaction is weak, or an approximate solution for the system is desired.

The sliding mesh model assumes that the flow is unsteady and is computationally more demanding than the other two models. Time accurate solutions for unsteady problems are computed using sliding mesh model. Unsteady solution in a sliding mesh simulation is periodic with the solution repeating within a period depending on the speed. The sliding mesh technique uses two more cell zones. Each cell zone is bounded by at least one "interface zone" where it meets the opposing cell zone. The interface zones of adjacent cell zones are associated with one another to form a "grid interface." The two cell zones will move relative to each other along the grid interface. For each moving or solid zone, moving mesh type is selected, and either a rotational or translational speed is assigned to it. The grid interface should always be positioned in such a way that it has zones on either side.

The following should be checked before simulating a case with sliding mesh in FLUENT.

1. Different cell zones are defined for different portions of the domain moving with different speeds.

2. Grid interface is located in such a way so there is no motion acting normal to it.

3. Grid interfaces could be of any shape provided that the two interfaces have the same geometry.

4. Each cell zone in a multiple cell zone domain should have a distinct face zone on the sliding boundary. The face zones for two adjacent cell zones will have the same position and shape, but one will correspond to one cell zone and one to the other.

5. The periodic angle of the mesh around the rotor blade(s) must be the same as that of the mesh around the stationary vane(s) when modeling a rotor/stator geometry using periodicity. Periodic angle is the angle at which the geometry repeats itself.

6. Periodic zones must be correctly oriented before creating the grid interface.

3.4 Modeling Transient Flow

As explained in Chapter 1, all eight vanes at the outlet of the impeller are further connected to eight different piston cylinders. For each rotation of the impeller, discharge occurs 50% of the time through only four cylinders because of the unique design of the rotating disks. Each cylinder will experience compression (discharge) and suction (charge) alternatively each at 50% of the cycle. This feature of the pump could be accurately simulated only in the transient model of FLUENT by incorporating a specific program via the avenue of User Defined Function (UDF) as shown below:

Pressure at the outlet varies with the location:

- In the upper half of the circle ($270^o \rightarrow 0^o \rightarrow 90^o$), valves open--

  P = -0.999999 atm gauge (or 0.000001 atm absolute) and a loss coefficient of 1.0.

- In the lower half of the circle ($90^o \rightarrow 180^o \rightarrow 270^o$), valves close-- the outlets are treated as walls.

However, it is time consuming to incorporate this UDF. An alternative approach is then adopted to simplify the process by approximating the actual process with a stationary "shadow domain" being assigned as a volume to receive the flow coming out from the four cylindrical outlets. This shadow domain consists of a semi-circular section with the height equaling to the diameter of the exit cylinder passage and a thin thickness of 0.28 inches that is 10% of the piston cylinder passage length. The semi-circular section is aligned with the upper half circle (270^o-0^o-90^o) with four discharge piston cylinders creating an interface between the moving cylinders and the discharge pressure outlet condition. The semi-circular section is assigned as a fluid zone but stationary. The inlet surface of the semi-circular section forms an interface with the moving domain, and the opposite surface (the outlet surface) is assigned as the constant pressure outlet. The other four faces of the domain act as walls. The results of the simulation using this method are justified in Chapter 4 by showing the strength of the pressure diffusion and the magnitude of the lateral velocity components is small.

The domain is simulated for a transient flow, and suitable time-step is assigned based on the stability criterion by examining the Courant number. To avoid instabilities the Courant number should be less than 1. The instability condition for this study is calculated below:

Courant number = $\Delta t / (\Delta x_{cell} / U_{fluid})$

Δt = time step,

Δx_{cell} = minimum cell distance (m)

U_{fluid} = Velocity of the fluid (m/s)

In the case with a rotation speed of 100 rpm in this study,

Δx_{cell} = 0.001762026 m

U_{fluid} = 0.2187462 m/s (at the inlet)

To satisfy the requirement that Courant number must be less than 1, the maximum allowable time step to avoid instability is 0.008 seconds for the 100 rpm case in this study. One cycle time period is calculated as 0.6 seconds for 100 rpm. The initial time step is taken as 0.001 seconds. Simulations are carried out using 600 time steps with 50 iterations per time step.

The meshed models of this transient model are shown below.

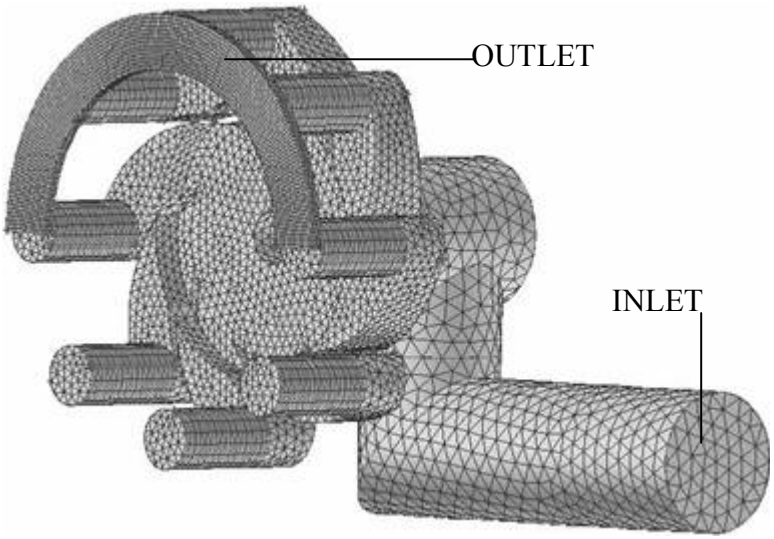

Figure 3.2 Solid mesh model for the transient model.

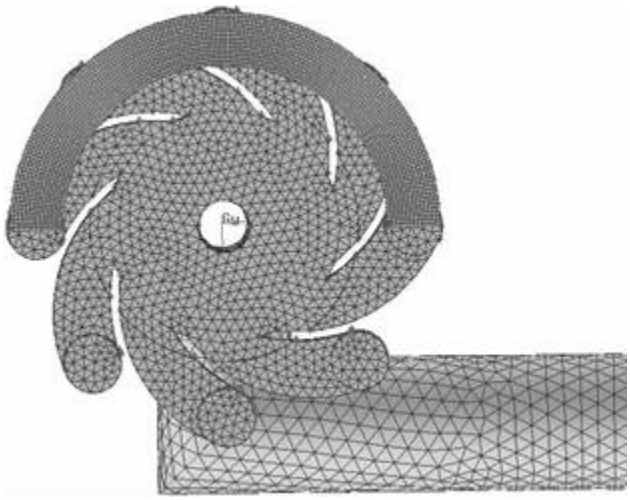

Figure 3.3 Solid meshed model of the transient model showing the alignment of the outlet face.

3.5 Creation Of Computational Flow Volume

Creation of the computational flow volume is not trivial. The details for the extraction of computational domain of the section end are explained below.

3.5.1 Creating the "L" shaped pipe:

A cylinder 12 inches in length and 3.5 inches in diameter is created, which represents the horizontal pipe as shown in Figure 3.4. It is split with a face of diameter 3.5 inches and inclined at an angle of 45^{o}. A vertical cylinder of 7.5 inches long and 3.5 inches in diameter is created. It is then split with a face of diameter of 3.5 inches and inclined at an angle of 45^{o}. Both the pipes are joined using the "unite" command. Figure 3.4 shows the solid model of the "L" shaped pipe.

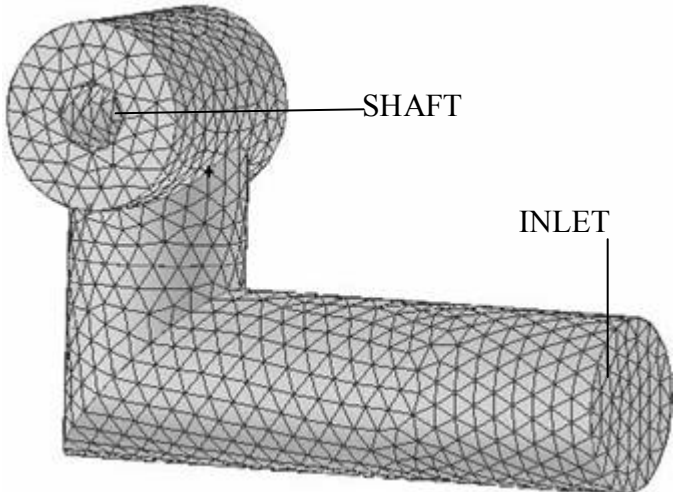

Figure 3.4 3-D model of the "L" shape section showing inlet and shaft.

3.5.2 Meshing the domain:

Because of the complexity of the geometry, the above domain is meshed using tetrahedral meshing. It consists of 9,790 meshed elements.

3.5.3 Creating the flow domain passing through the impeller:

The 2-D face of the impeller profile is created in GAMBIT using the vertices obtained from AutoCAD drawings. Edges are created using these vertices followed by faces. The solid model of the impeller hub is created using the "revolve" option in GAMBIT. The 2-D blade profile is properly aligned on the vane geometry, and the solid geometry of the blade is created using the command "sweep faces". The 3-D blade geometry is extended beyond the actual height and then use the "split geometry" command to split the extended blade geometry from the impeller hub. The computational domain of the flow passage between the impeller blades is thus created. This computational domain is then aligned with the "L" pipe using split command. The

details of the process are explained in Appendix D. The impeller section is also meshed using tetrahedral meshing scheme with the total number of 37,430 elements, as shown in Figure 3.5.

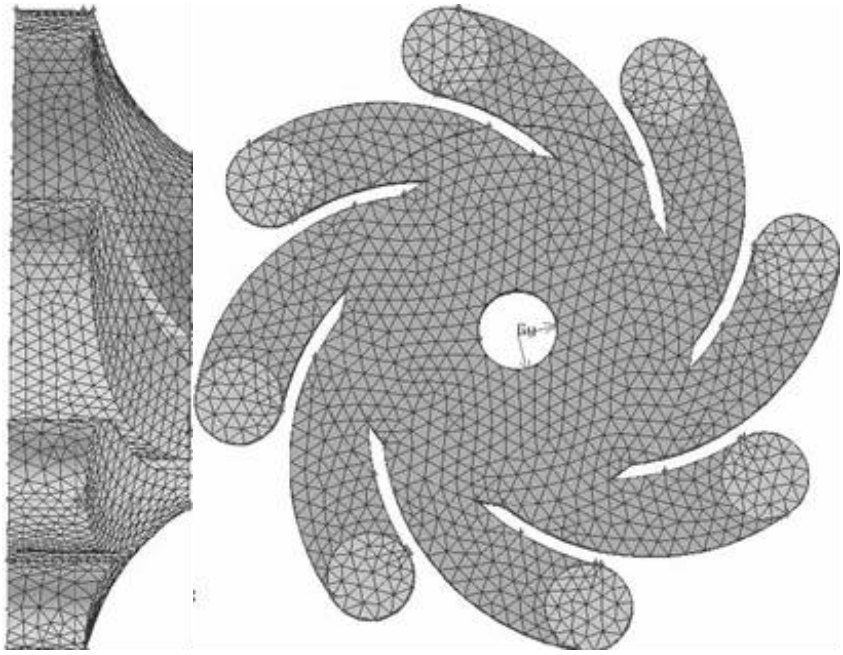

Figure 3.5 Tetrahedral mesh of the 3-D flow volume passing through the impeller.

3.5.4 Outlet domain:

The outlet section consists of eight cylindrical passages through which water flows into the piston cylinder cavity. The dimensions of the cylinders are obtained from the AutoCAD drawings. A total of eight cylindrical passages are created and joined with the vane flow volume. All the eight cylinders are meshed using the "cooper mesh scheme" as shown in Figure 3.6. Cooper meshing scheme is a structured mesh in which the volume meshing is done by first meshing the edges and then the faces. The meshing for the whole volume is then done by selecting these sources and sweeping these surface meshes through the entire volume. The total

number of meshed elements is 21,808 in the outlet passages. The total number of the meshed elements for the entire suction section is 60,220.

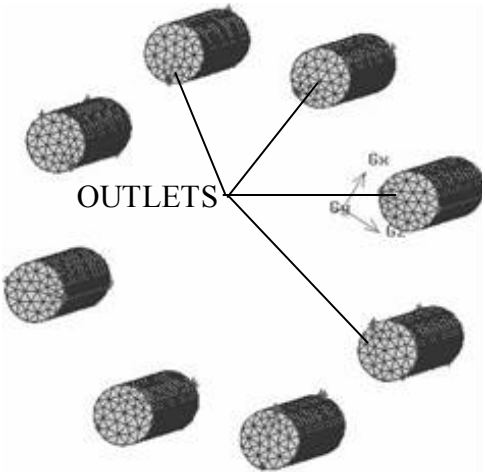

Figure 3.6 Tetrahedral meshes of the 3-D solid model of the outlet cylindrical passages.

3.5.5 Compressing cylinder:

The reciprocating flow motion inside the compressing cylinder is not modeled in this study. The total pressure loses in the compressing cylinder are computed using engineering internal flow correlations as shown in Section 4.9.

3.5.6 Discharge section:

The vertices, which form the edges of the discharge section, are obtained from AutoCAD. Vertices are then created in GAMBIT and then edges are built based on these vertices, and faces are created out of those edges. The face is revolved about an axis to obtain the solid model. The casing is formed using sweep option, and the two solid models are united using the "split option". The rotating disc, which has the inlets, is also created using the revolve face command and split with the created volume. The 3-D solid model and the meshed volume are shown in Figures 3.7 - 3.10. Figure 3.7 shows the 3-D solid model for the transient case. The same

technique of using a stationary "shadow zone" to interface the rotating domain for transient inlet condition is applied here as explained in the section 3.4. The tetrahedral meshing scheme is adopted for this flow volume. The total number of the meshed elements is 67,956.

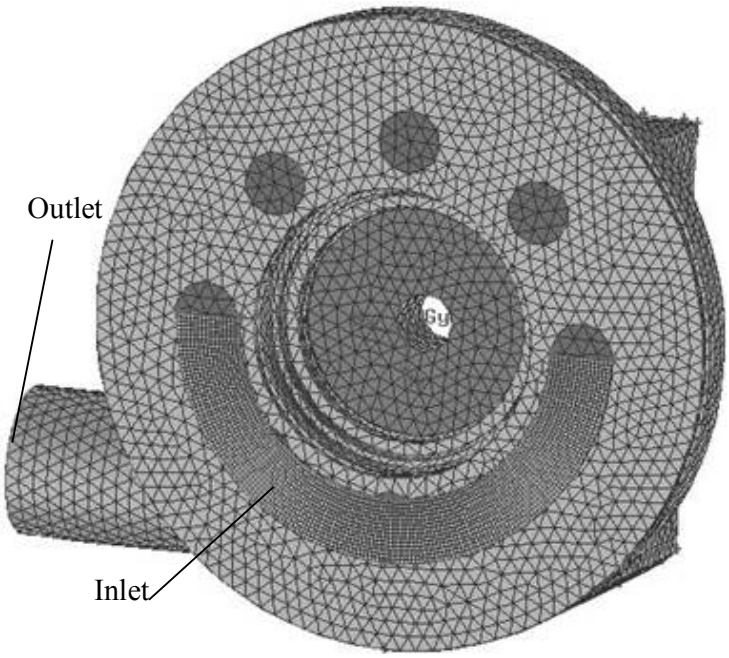

Figure 3.7 Tetrahedral meshes of the 3-D solid model of the rotating domain in the discharge section.

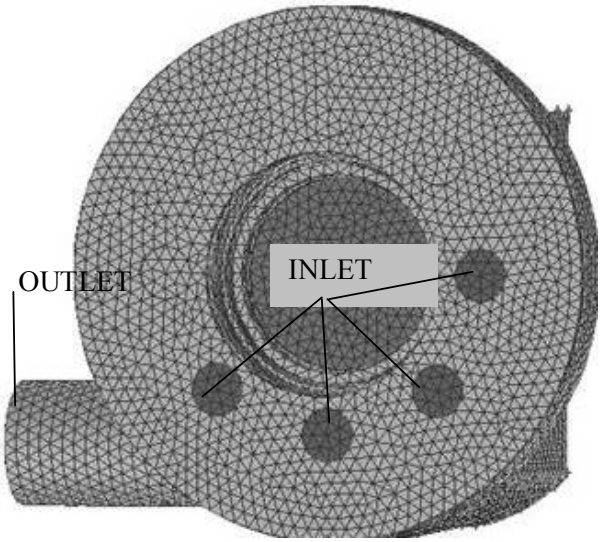

Figure 3.8 Meshed 3-D model of the stationary domain of the discharge section.

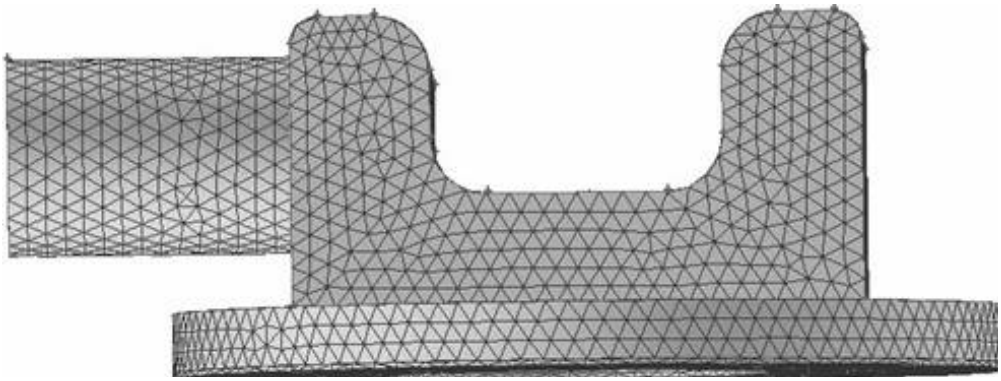

Figure 3.9 Meshed 3-D model of the stationary discharge section from the top view.

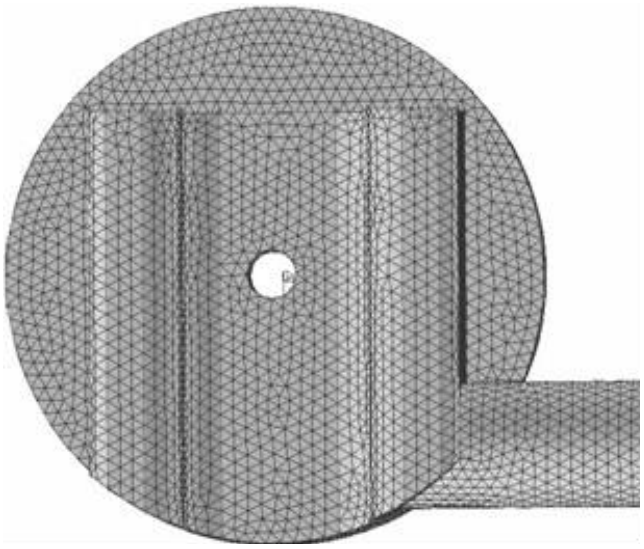

Figure 3.10 Meshed 3-D model of the stationary discharge end looking in the opposite direction of the flow.

3.6 Convergence Criterion

There are no universal metrics for judging convergence. Residual definitions, which are useful for one class of problems, are sometimes misleading for other classes of problems. Therefore, it is a good practice to judge convergence not only by examining the residual levels but also by monitoring relevant physical quantities such as drag or heat transfer coefficient. Convergence can be hindered by a number of factors including numbers of computational cells, under-relaxation factors, and complex flow physics. In this study, the convergence criterion of 10^{-3} for the residuals of continuity i.e. x-velocity, y-velocity, z- velocity, turbulence kinetic energy "κ" and dissipation rate "ε" is chosen for the stationary and moving reference frame, and 10^{-5} is chosen for the transient case.

3.6.1 Residual plots

The residual plots for the stationary case, moving reference frame case and the transient case at the suction end are as shown below. Figure 3.11 shows some crests and troughs in the initial stages of iterations. This is due to a reverse flow at the outlet, which gradually subsides as the iterations continue. The same explanation holds true for the other figures as well. Figure 3.12 shows the residuals for the moving reference frame case (MRF) and Figure 3.13 shows the residuals for the transient case at the suction section. For the transient case, 50 iterations are taken at each time step of 0.001 sec. The fluctuations in Figure 3.13 indicate the convergence trend of 50 iterations within each time step. The fluctuations are averaged out before iteration 112,500 and are not shown in the figure. Figure 3.14 shows the residual plot for the stationary case at the discharge section where 50 psi is initially used as the boundary condition until 1250th iterations when it is changed to 500 psi.

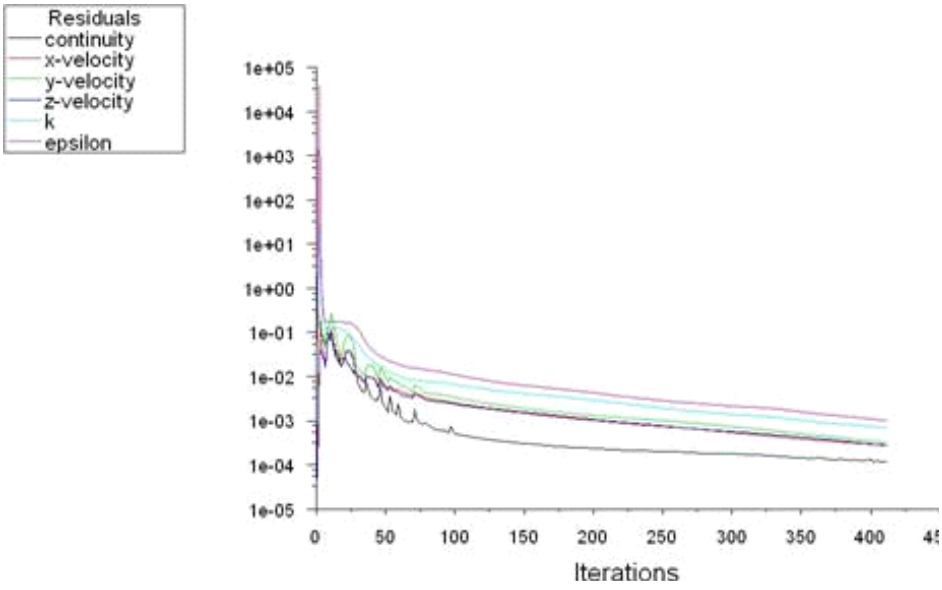

Figure 3.11 Residuals for the stationary case at the suction section.

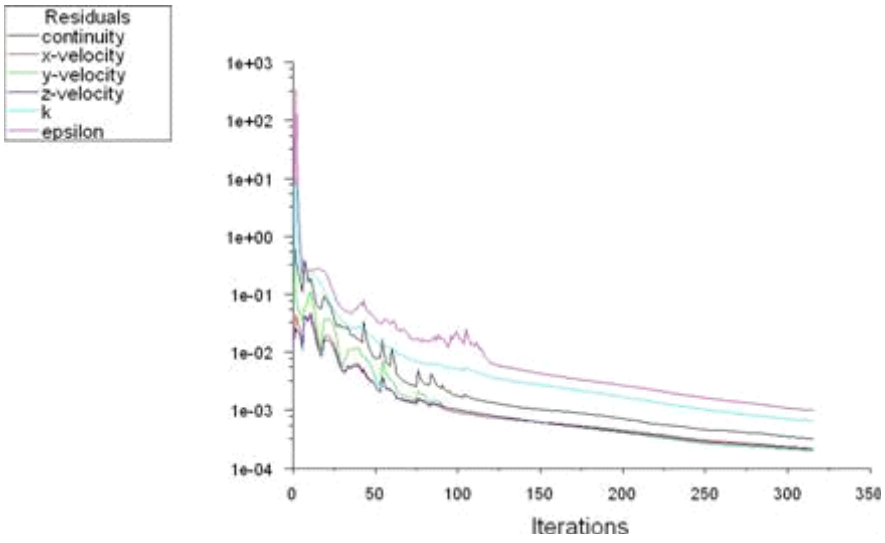

Figure 3.12 Residuals for the moving reference frame (MRF) case at the suction section.

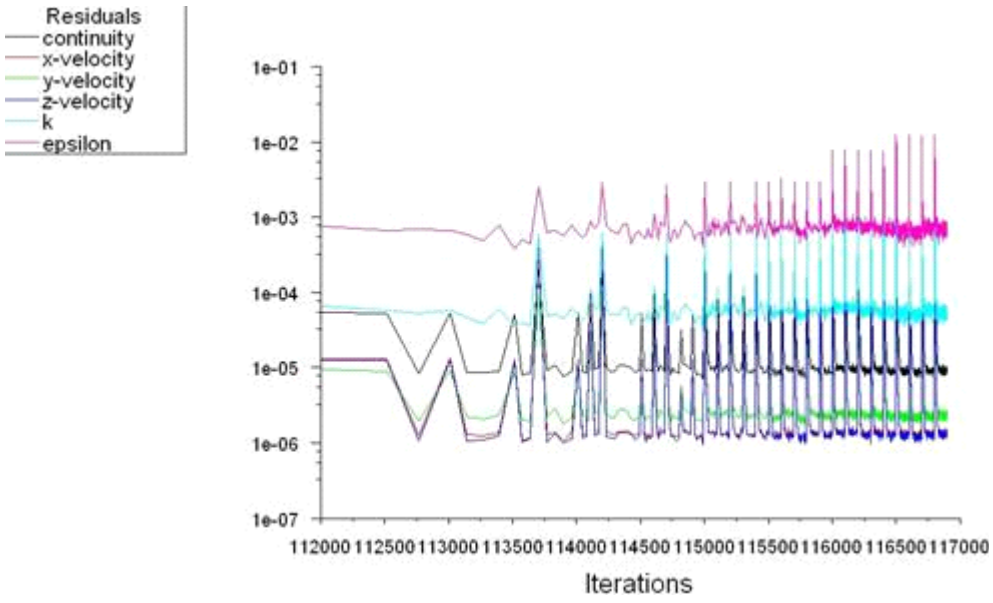

Figure 3.13 Residuals for the transient case at the suction section. The fluctuations indicate the convergence trend or 50 iterations within each time step of 0.001 sec. The fluctuations are averaged out before the 112,500th iteration and are not shown here.

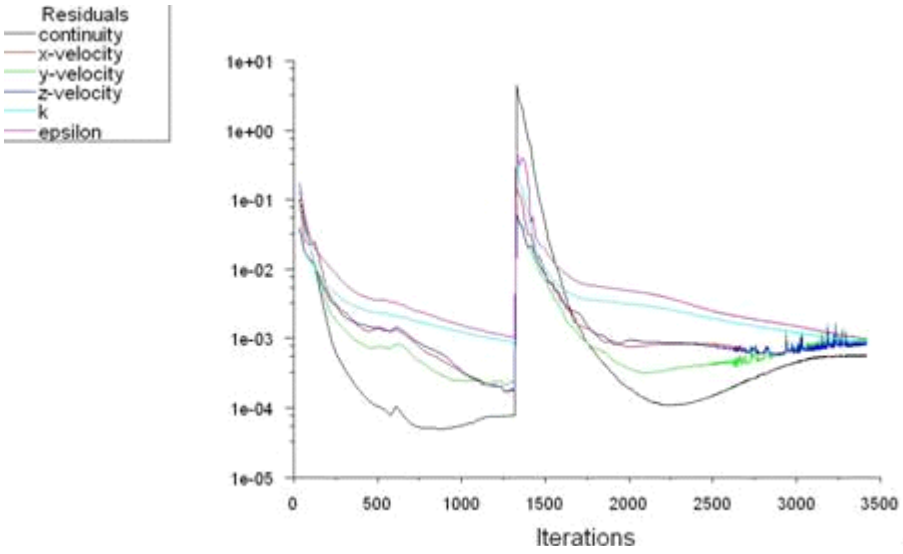

Figure 3.14 Residuals for the stationary case at the discharge section.

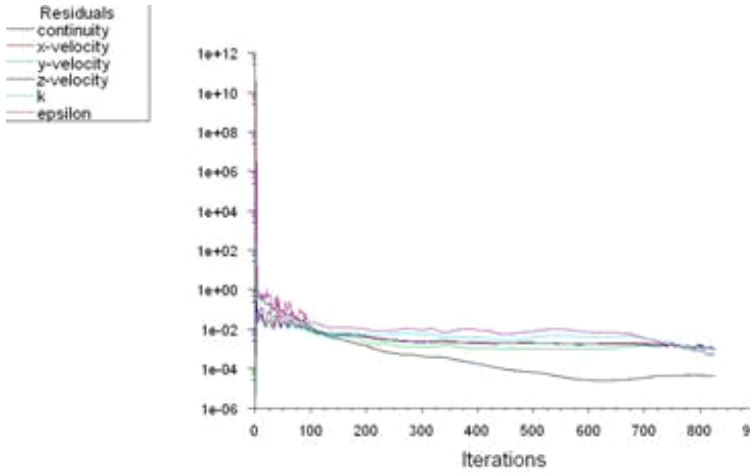

Figure 3.15 Residuals for the moving reference frame case at the discharge section.

3.7 Grid Sensitive Study

Grid sensitivity is investigated by obtaining solutions with number of elements equal to 60,220 elements against 183,735 elements at the suction end and 67,956 elements against 108,159 at the discharge end. The comparison from the table 3.1 shows the difference of the total pressure losses could be as high as 100%. This implies that the mesh numbers set in this study are not sufficient to resolve the total pressure losses. However, due to the nature of this study as a first step toward providing a preliminary view of the complex flow inside a new pump, the results of the coarse mesh is acceptable to the present study. Finer mesh simulation will be used for future studies.

Domain	Case	Meshed Elements	Ptot,1 at inlet (atm)	Ptot,2 at outlet (atm)	ΔPtot 1-2 (atm)	ΔPtot 1-2 difference (%)
Suction	Stationary	60,220	-0.9973215	-0.9990247	0.0017032	5.61
		183,735	-0.9972345	-0.99903886	0.0018044	
	MRF	60,220	-0.9885559	-0.9886458	0.000090	100.91
		183,735	-0.9985228	-0.98859474	-0.009928	
Discharge	Stationary	67,956	34.0236100	34.0232640	0.000346	94.86
		108,159	34.0238800	34.0171530	0.006727	
	MRF	67,956	34.0235060	34.0232490	0.000257	61.64
		108,159	34.0233770	34.0232180	0.000159	

Table 3.1 Grid sensitive study.

CHAPTER FOUR

RESULTS AND DISCUSSIONS

Three cases are simulated in the present study. The baseline case is the stationary case where the simulations are carried out using non-rotating fluid zones. The second case is simulated by assuming it is steady state but using the moving reference frame (MRF) approach, where the moving fluid zones are assigned a rotating speed of 100 rpm although the actual fluid zones do not rotate. The third case employs the transient flow approach using the moving mesh method with a rotating speed of 100 rpm and a time step of 0.001sec. All the above methods are employed in both the suction and discharge parts of the pump. This chapter discusses the results obtained from each of the above-mentioned simulations.

The static pressure and total pressure values of the suction section obtained from CFD calculation are not the actual pressures because the exit boundary condition has not been truly simulated. In this study, the outlet boundary condition of the suction section was set to be vacuum at -0.999999 atm. As explained in Section 3.2 the exit pressure does not maintain at this value because when the water enters the cylinders the exit pressure will gradually increase. Since the computation is done by the pressure difference, using the simplified outlet boundary condition set at a constant value will not affect the flow field calculation, although the calculated static pressure values may be different from the true values. To correct this pressure drift, all the pressure values are added with a constant value that is the value making the inlet total pressure equal to 1 atm. For example, if the inlet total pressure is computed as -0.999 atm, a constant

value of 1.999 atm is added to all the total and static pressure values. The corrected static pressure and total pressure are plotted in the presentation below.

4.1 Suction Section - Stationary Results (Case 1)

The stationary case serves as the baseline case to qualify the computational results without the complexity of rotating motion. The fundamental physics of flow behaviors, pressure distribution, and total pressure losses are examined to ensure the overall prediction of the flow field is reasonable.

Figure 4.1(a) and 4.1(b) shows the 3-D velocity vector distribution in the entire flow domain of the suction section. It can be observed from Figure 4.1 that the flow is well conducted and guided by the impeller vanes. The magnitude of the velocity is maximum at the outlets and minimum at the other four closed outlet walls. The lower-right four cylinders are closed, so the flow shows weak activity (almost stagnant) inside the cylinders.

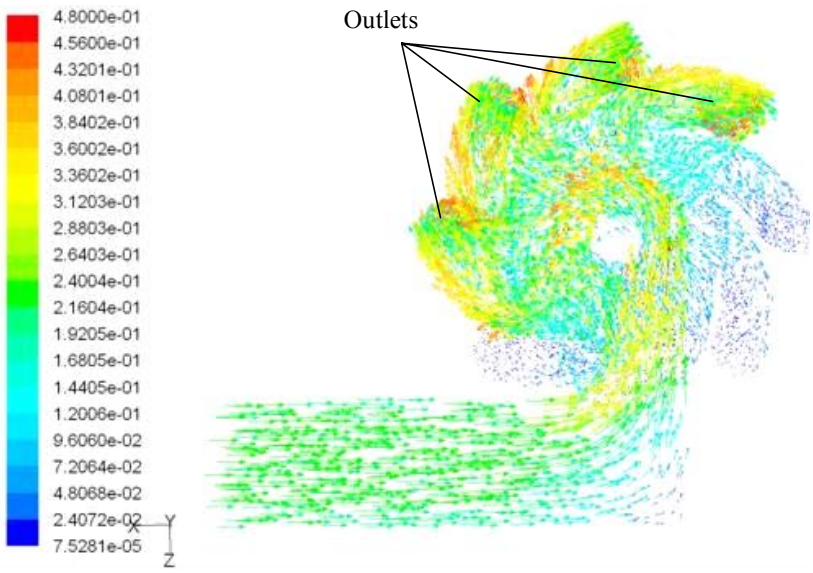

Figure 4.1(a) Case 1: Velocity vectors (m/s) colored by velocity magnitude in the entire 3-D Computational domain at the suction side looking in the direction of flow.

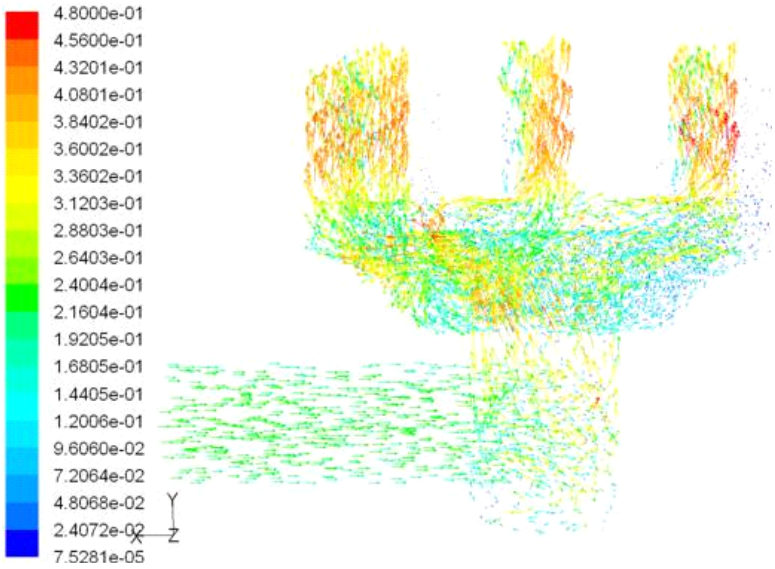

Figure 4.1(b) Case 1: Velocity vectors (m/s) colored by velocity magnitude in the entire 3-D computational domain at the suction side.

Figures 4.2 and 4.5 represent the surface contour plots of the total pressure looking at two opposite directions. Figure 4.2 shows the view following the flow direction from the flow inlet toward the rotating disk. Figure 4.5 shows the view against the flow direction. It can be observed that the total pressure decreases from the inlet to the outlet because of the friction losses. The

region of large total pressure losses occurs at the elbow and at the regions closer to the shaft due to recirculation shown in Figure 4.2. These losses extend along the whole length of the impeller, which is evident from the region outside of area "A" in Figure 4.5. More losses occur on the upper four cylinders, which is natural because they are open flow passages. The total pressure losses are minor in the closed cylinders, but there are some losses. Figures 4.3 and 4.4 are two cut-away planes showing that the high total pressure losses occur in the recirculation regions at the elbows and near the region where the leeward site of the flow (near the 9 o'clock location) meets the incoming flow. Due to flow inertia, most of the flow enters the shaft sleeve toward the right side of the shaft and leaves behind a large recirculation region on the left side (leeward site) of the shaft.

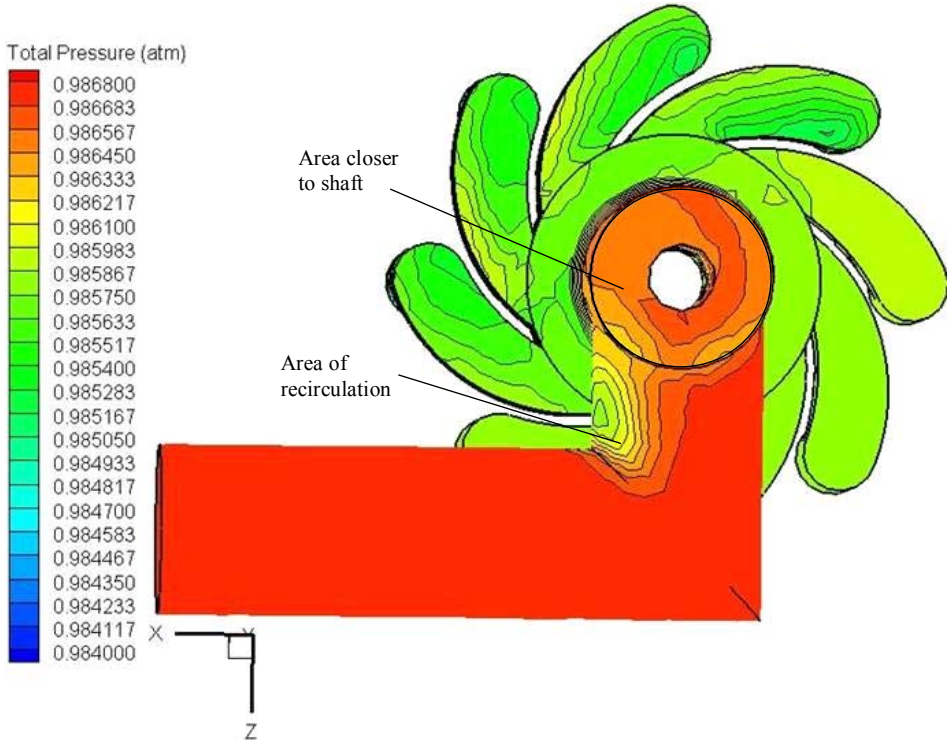

Figure 4.2 Stationary Case 1: Surface contour plot of the total pressure (atm) for the entire domain looking from the suction end toward the rotating.

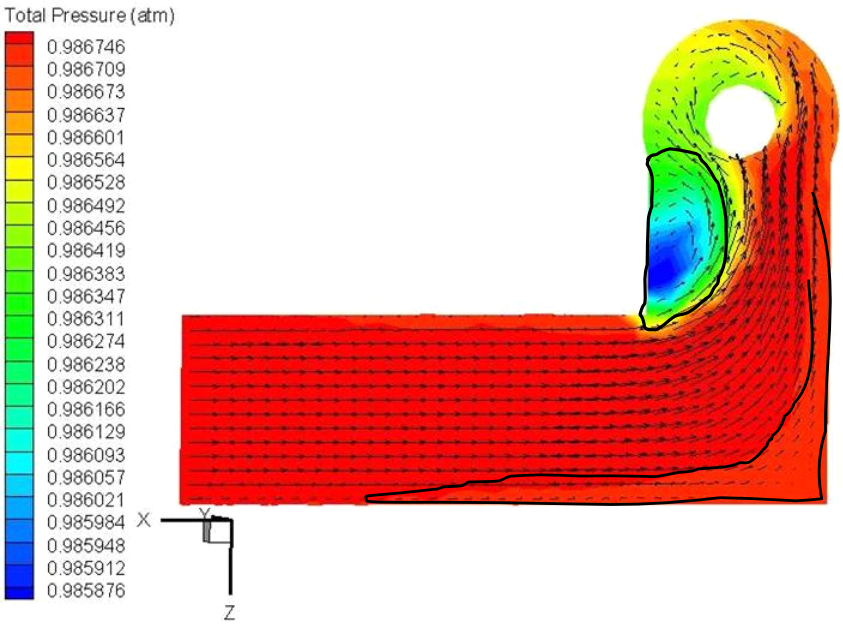

Figure 4.3 Stationary Case 1: Total pressure (atm, in color) contour plot at the midplane of the inlet pipe with the velocity vectors (m/s).

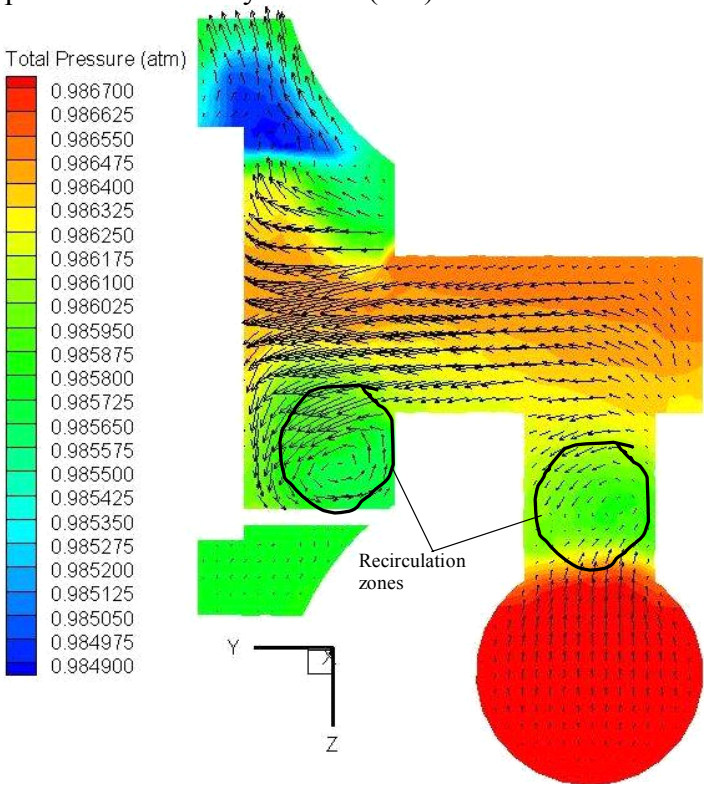

Figure 4.4 Stationary Case 1: A plane view of the total pressure contour plot (atm, color) with the velocity vectors (m/s) after entering the second elbow in a Y-Z plane off the midplane of the pipe.

Static pressure distribution in Figure 4.6 indicates that the flow is brought to stagnant with high static pressure near the outer 90-degree bend where the flow is separated from the wall and creates a low-pressure center near the inner 90-degree bend. Comparing the total pressure distribution in Figure 4.3 with the static pressure distribution in Figure 4.6 indicates that the total pressure losses downstream of the inner 90-degree bend is more pronounced than the minor losses near the outer 90-degree bend. Figure 4.7 shows a high-pressure area on the disk indicating a possible flow impingement on the disk.

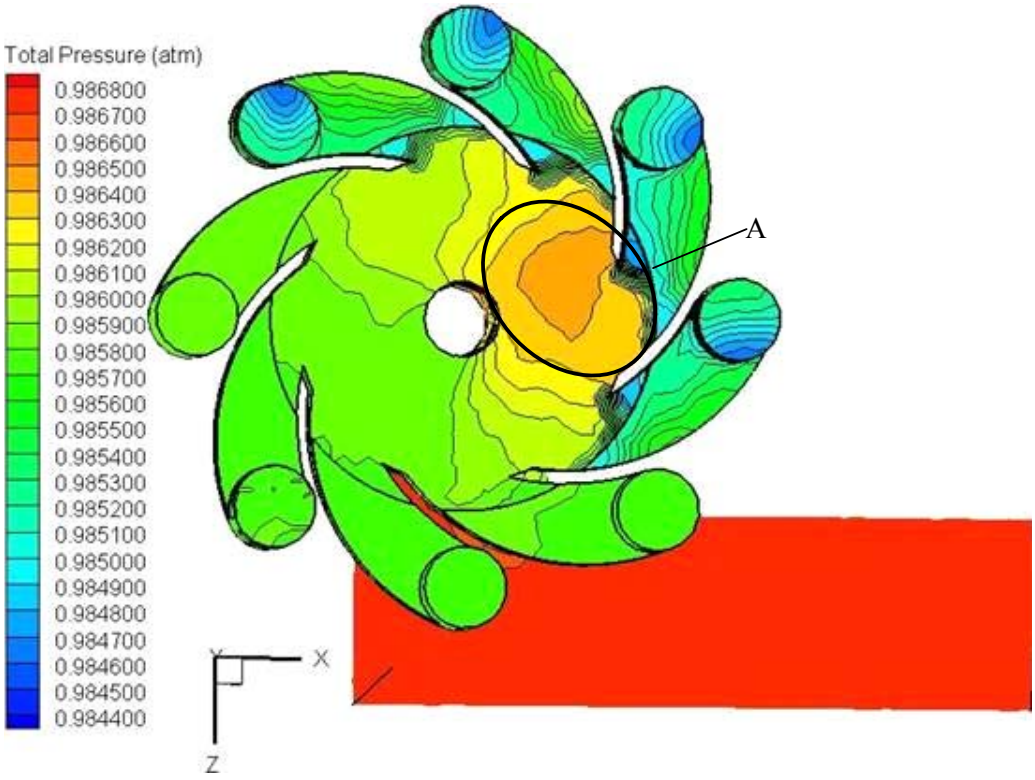

Figure 4.5 Stationary Case 1: Surface contour plot of the total pressure (atm, in color) looking from the disk toward the suction side and the flow inlet on an X-Z plane.

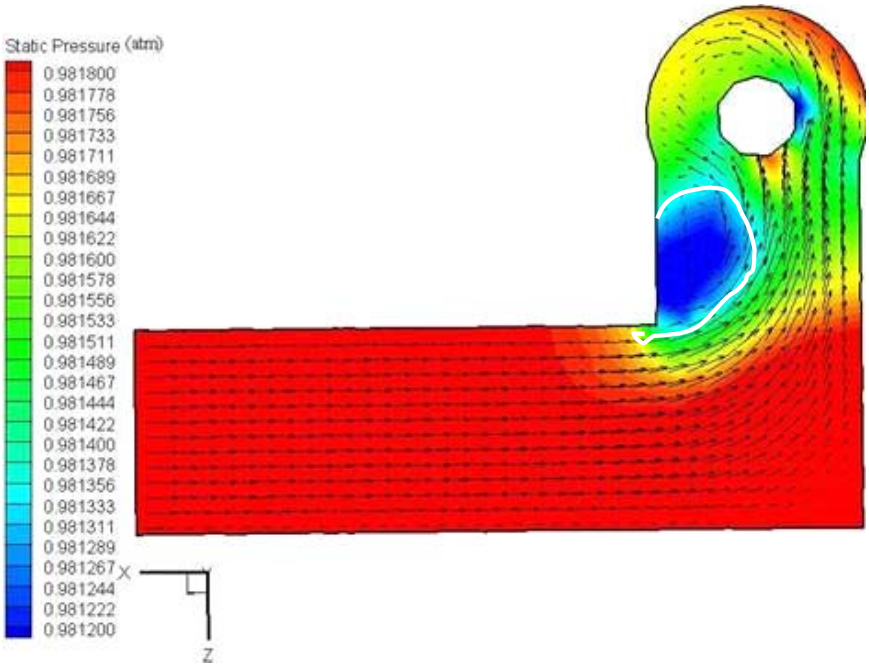

Figure 4.6 Stationary Case 1: Static pressure (atm, in color) contour plot with the velocity (m/s) vectors at the "L" shaped pipe.

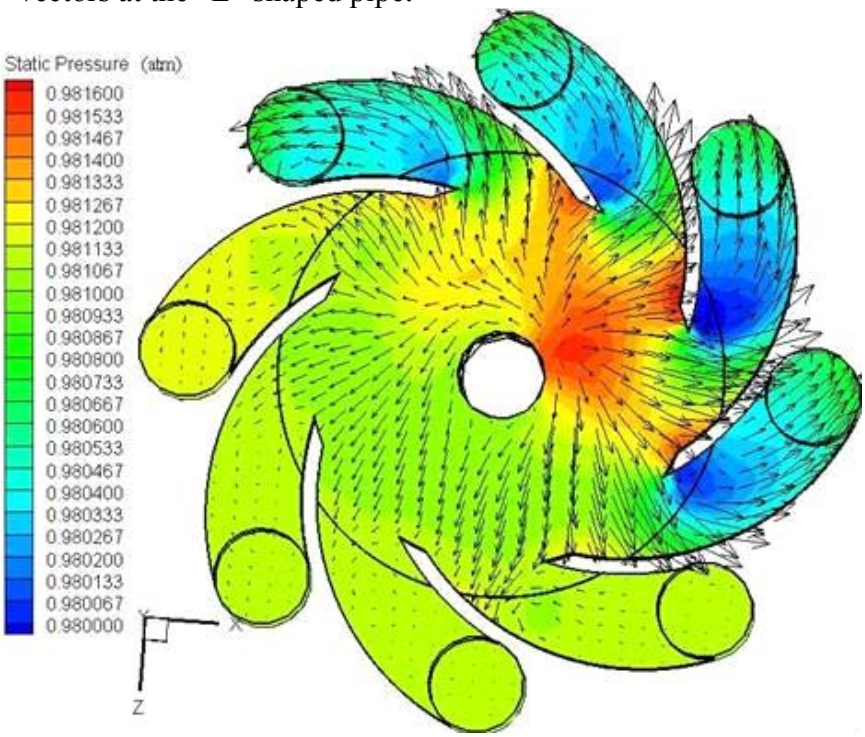

Figure 4.7 Stationary Case 1: Contour plot of the static pressure (atm) with the velocity (m/s) across a plane cut through the impeller. Look against the flow from the disk toward the suction section.

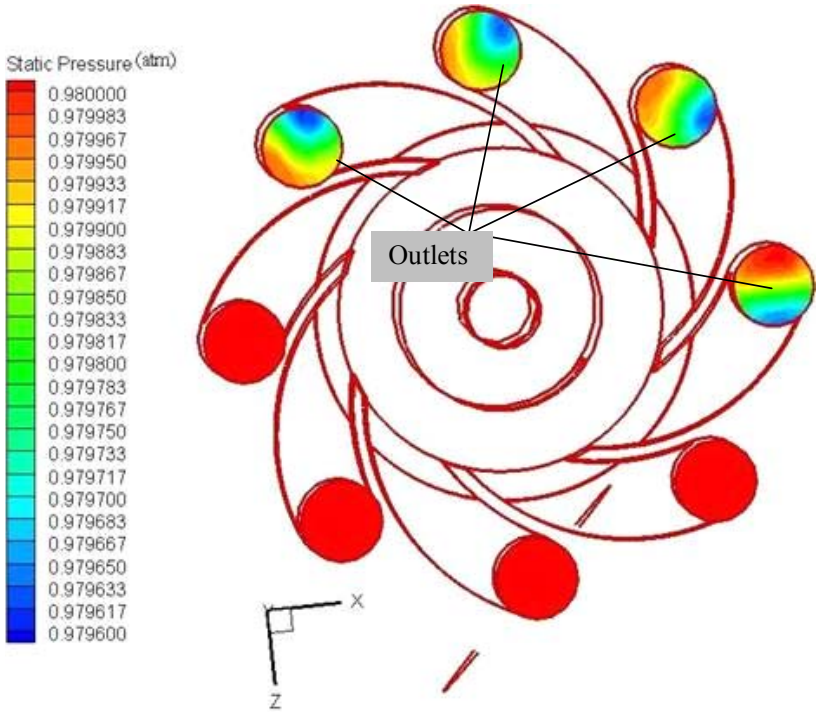

Figure 4.8 Stationary Case 1: Static pressure (atm) contour plot at the outlet.

4.2 Suction Section - Moving Reference Frame (MRF) Results (Case 2)

In this case, the flow volume is simulated with an operating pressure of 1 atm and a rotational speed of 100 rpm. Recall again that the mesh and the physical location do not rotate in this scheme. The assigned rotational speed creates an additional force and momentum, which simulate a snapshot of rotational motion. The computation is conducted at the steady-state condition. The inlet and the outlet boundary conditions remain the same as those of the stationary simulation in Case 1.

Figure 4.9 shows the 3-D velocity vectors of Case 2. Due to the imposed rotational momentum, flow is more active in the four lower-left closed cylinders than in Case 1. To show more clearly the flow fields, a composite figure of two cut-away planes are shown in Figure 4.10a. The frontal plane cuts through the mid plane of the inlet pipe and the rear plane cuts

through the interface between the impeller and cylinders. The velocity shown in the rear plane is the absolute velocity, so the tangential velocity component is shown almost evenly distributed at the entrance of all the cylinders including the closed walls. The tangential magnitude of the velocity increases from inlet to outlets due to the centrifugal force.

Figure 4.10 (a) also shows the total pressure distribution in color. There is an increase in the total pressure in the moving domain due to the addition of the rotating kinetic energy. A section plane cut through the impeller in Figure 4.10 (b) shows that as the radius increases, the total pressure increases due to more added rotating kinetic energy. The increase is more predominant across the outlets 1,2,3,4 than in the closed cylinders due to increased velocity-induced kinetic energy. The areas marked as a, b, c and d show the regions of significant pressure losses, which can be explained using Figure 4.11 (a). In this figure the flow is shown to take a detour and several extra turns, as exemplified by the complex velocity vectors when the flow enters the passage between impeller vanes towards cylinders with opened outlets in the region marked "A". Whereas when the flow enters the other impeller vane passages towards the closed cylinders, i.e., the region marked "B", the flow moves more orderly. The phenomenon of the total pressure losses can be further understood by examining Figure 4.11(b), which consists of multiple plane sections including plane 1 and plane 2. These are planes cut at the start and end of the impeller domain, and a vertical plane that is placed to bridge planes 1 and 2. It can be seen in Figure 4.11(b) that the total pressure losses occur through the length of the impeller vanes when the vanes forcefully guide the flow to turn to the directions toward the inlet of the cylinders. The region marked "C" in Figure 4.11 (b) shows the total pressure losses along the path vertical to the disk.

Figures 4.12 and 4.13 indicate a large static pressure increases radially outward in each of the cylinder indicating a non-uniform pressure distribution not seen in a conventional stationary cylinder assembly. This non-uniform pressure distribution would potentially affect the piston head's stress and cause some disk fluttering.

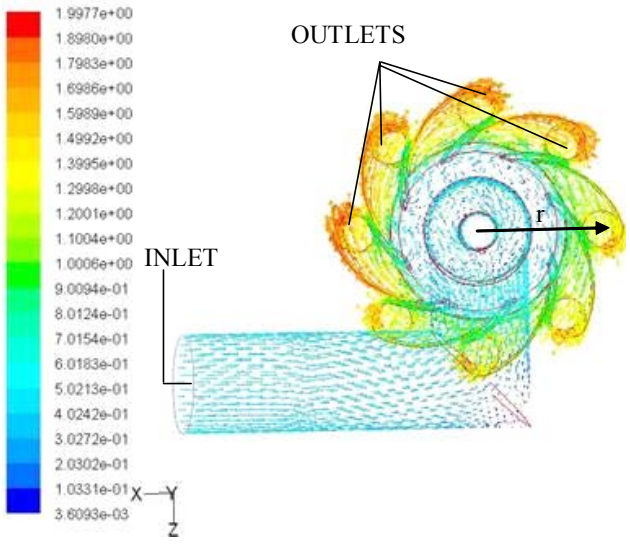

Figure 4.9 100 rpm, MRF Case2: 3-D velocity vectors (m/s) colored by velocity magnitude in the entire computational domain at the suction.

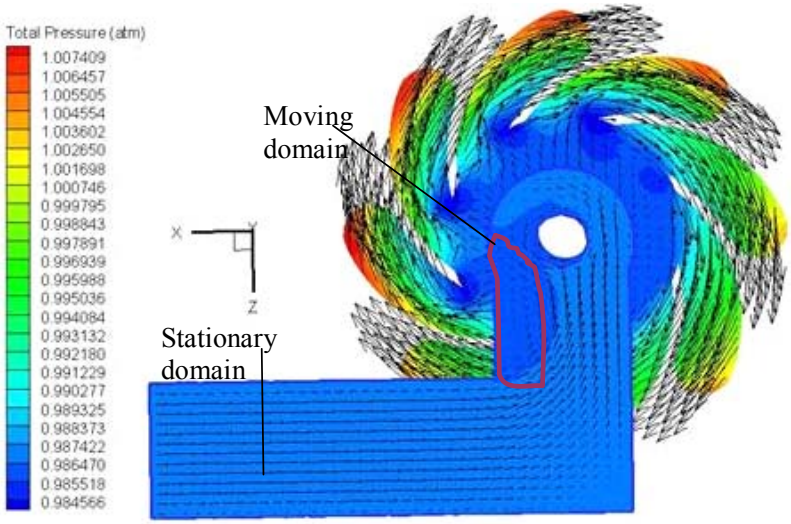

Figure 4.10a 100 rpm, MRF Case 2: Contour plot of the total pressure (atm) with the velocity vectors (m/s) on two plane sections.

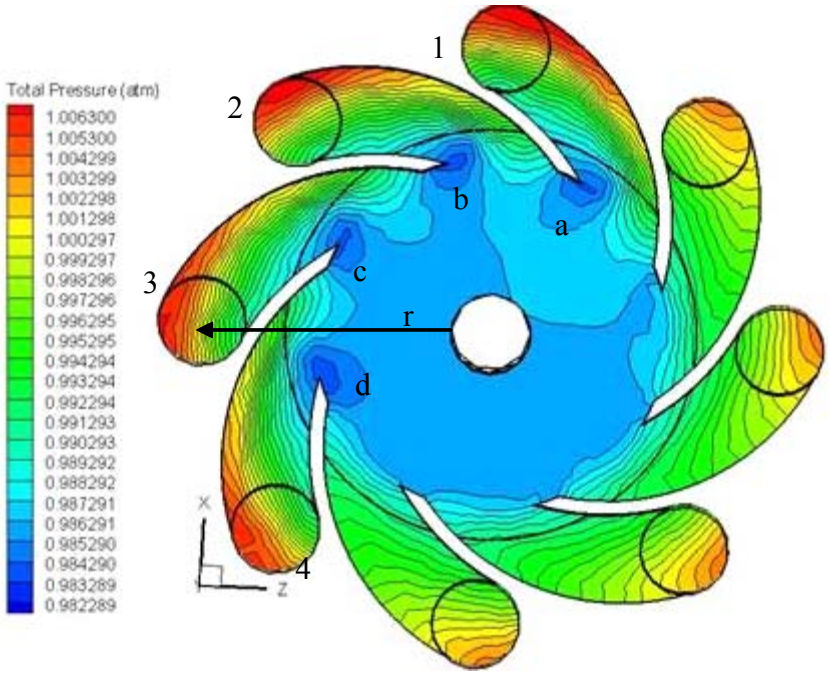

Figure 4.10b 100 rpm, MRF Case 2: Contour plot of the total pressure (atm) across a section plane of the impeller, looking against the flow direction.

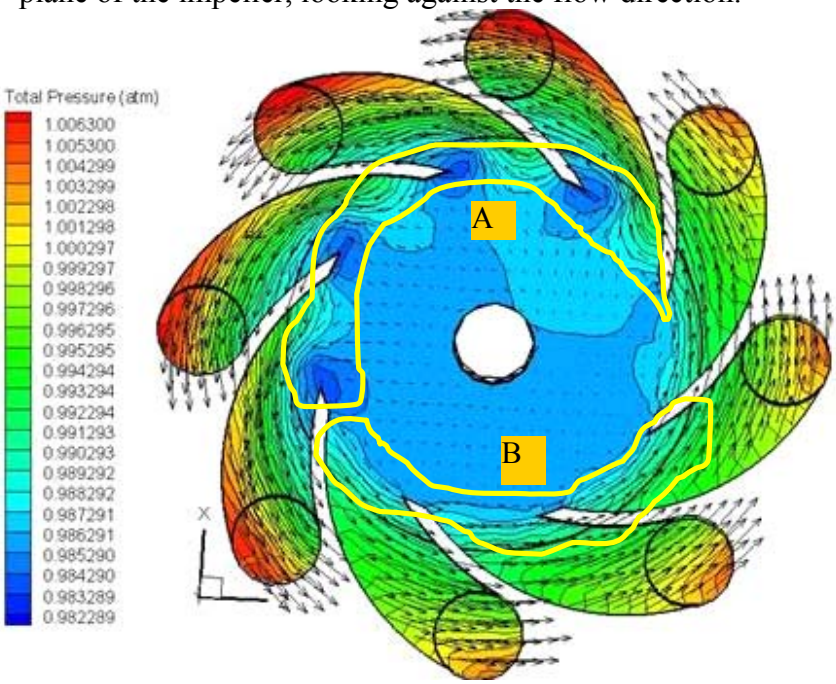

Figure 4.11a 100 rpm, MRF Case 2: Contour plot of the total pressure (atm) with the velocity vectors (m/s) across a section plane of the impeller, looking against the flow direction.

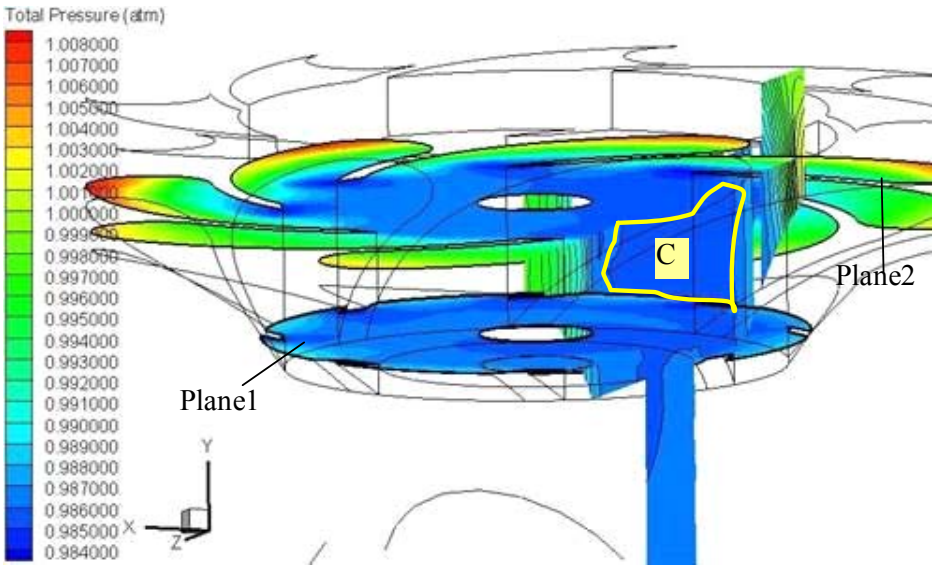

Figure 4.11b 100 rpm, MRF Case 2: Contour plot of the total pressure (atm) across different section-planes of the impeller to illustrate a flow path that generates large total pressure losses.

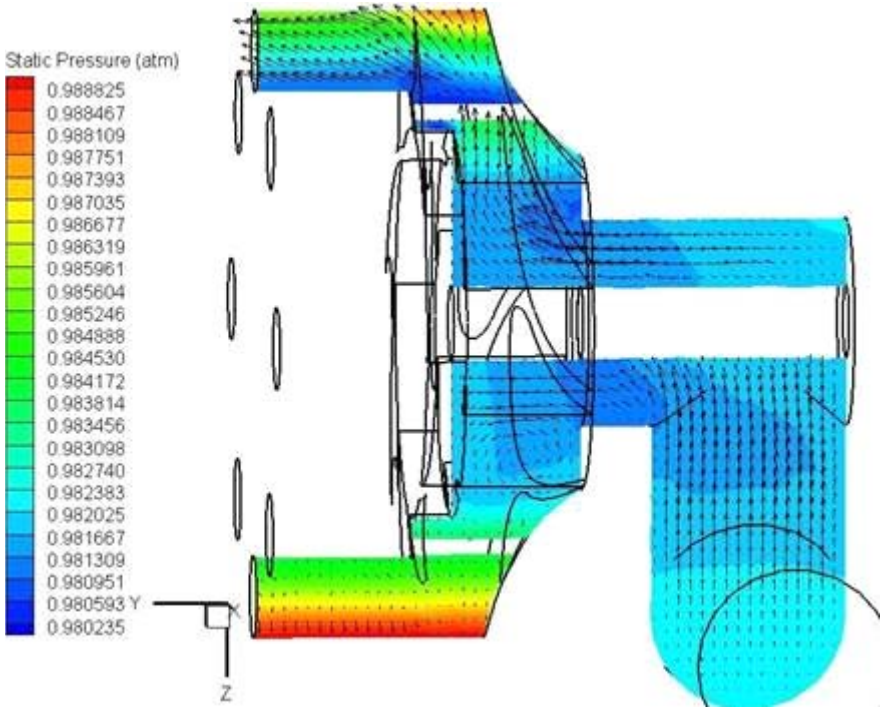

Figure 4.12 100 rpm, MRF Case 2: Contour plot of the static pressure (atm) with the velocity (m/s) across a plane X=0.

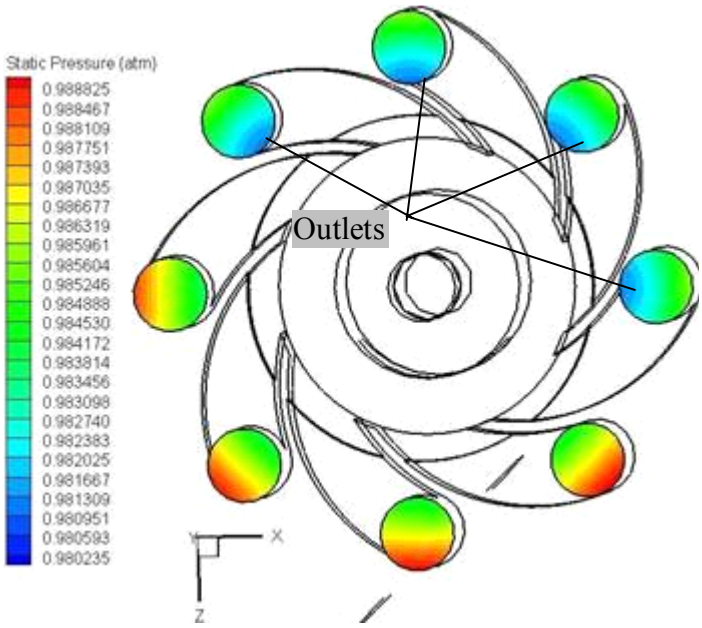

Figure 4.13 100 rpm, MRF Case 2: Contour plot of the static pressure (atm) at the outlet.

4.3 Suction Section - Sliding Mesh Transient Case (Case 3)

In this case the flow volume is simulated using an unsteady state approach. The time period is computed using $T = \theta/\Omega$, where "θ" is the sector angle in radians, and "Ω" is the rotor speed in radians/sec. Using the above expression, one cycle time period is calculated as 0.6 seconds for 100 rpm. The time step is taken as 0.001 seconds. Simulations are carried out using 600 time steps with 50 iterations per time step.

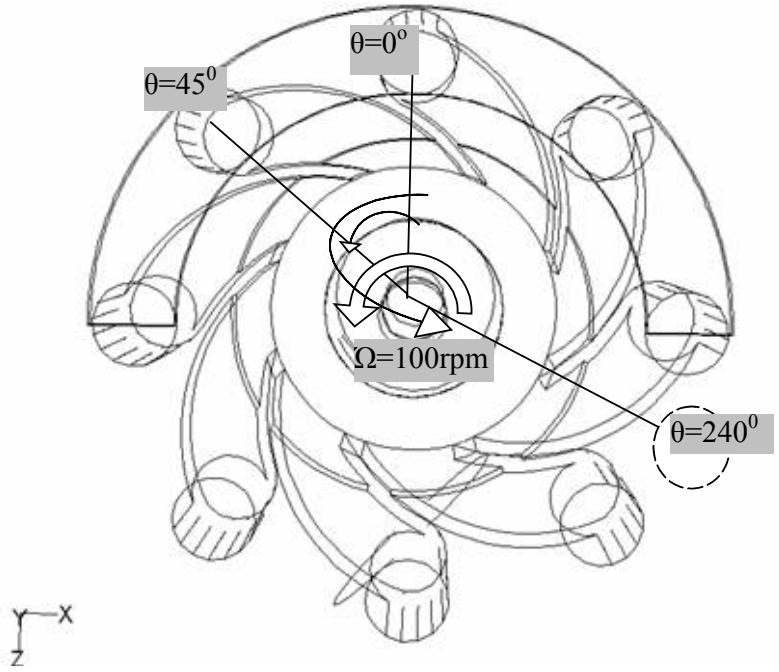

Figure 4.14 100 rpm, Transient Case 3: Transient model showing the sector angle and the direction of rotation looking against flow direction from the disk toward the flow inlet.

4.3.1 Suction Section - Transient results of the suction domain at time t = 0.55 seconds, θ = 240⁰ (Case 3)

The instantaneous snapshot of the flow phenomenon exhibited in the transient case is almost similar to the moving reference frame method. Recirculation losses are found at the elbow as shown in Figure 4.15. Figure 4.16 shows that the flow is dominant in the upper half region with open outlets than the lower half without outlets. The regions of relatively high total pressure losses follow the rotating motion of the open pistons (Figure 4.18 vs. Figure 4.11a). Similar to the moving reference frame case (Case 2), the loss is shown to extend through the whole length of the impeller (see region 3 in Figure 4.19).

At the exit surface of the "shadow domain," the effect of the lateral diffusion is minimal as evidenced from the velocity distribution at the exit in Figure 4.20. This negligible lateral

diffusion justifies the method of adopting "shadow domain" to simplify the dynamic boundary condition for the transient case as explained in Chapter 3.

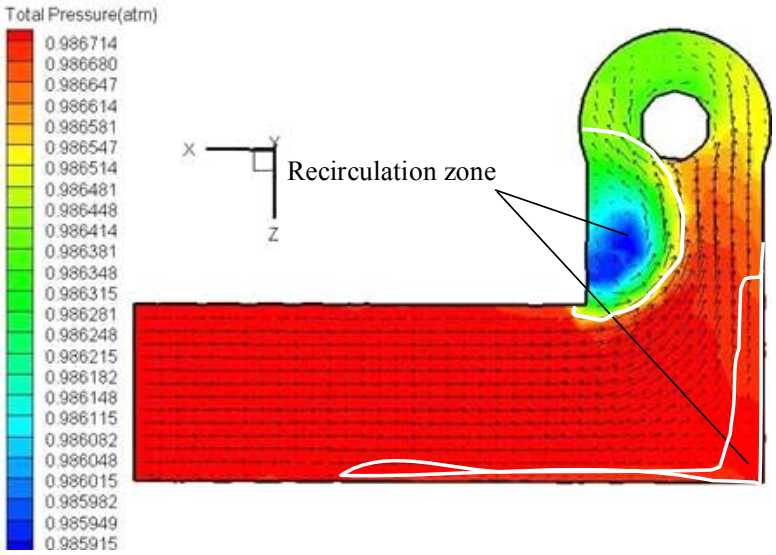

Figure 4.15 100 rpm, Transient Case 3: Transient contour plot of the total pressure (atm) with the velocity (m/s) vectors at the "L" shaped pipe at t = 0.55 seconds, $\theta = 240^0$.

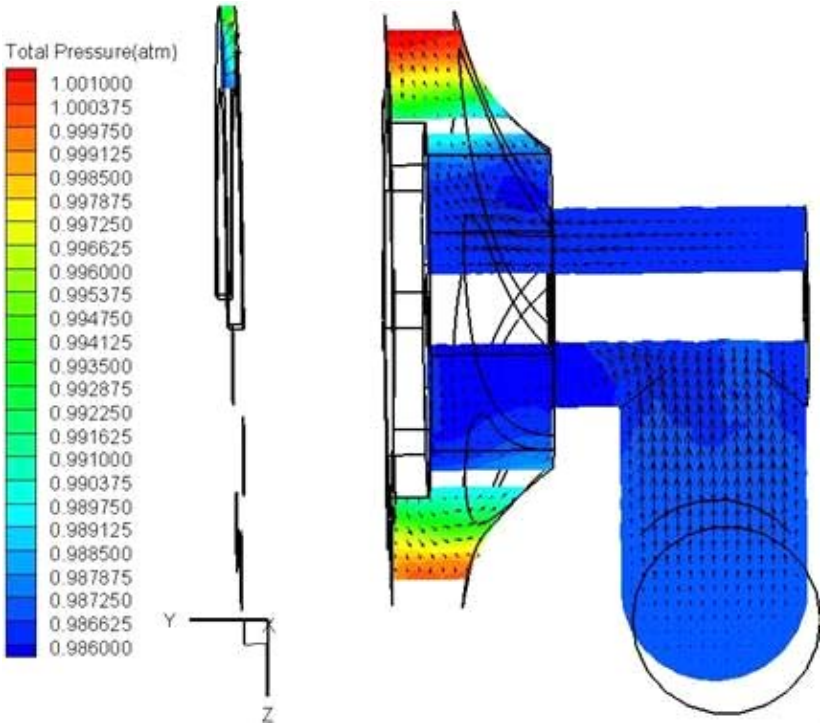

Figure 4.16 100 rpm, Transient Case 3: Transient contour plot of the total pressure (atm) with the velocity (m/s) vectors at the midplane of the rotating shaft (plane X=0) at t = 0.55 sec, $\theta = 240^0$.

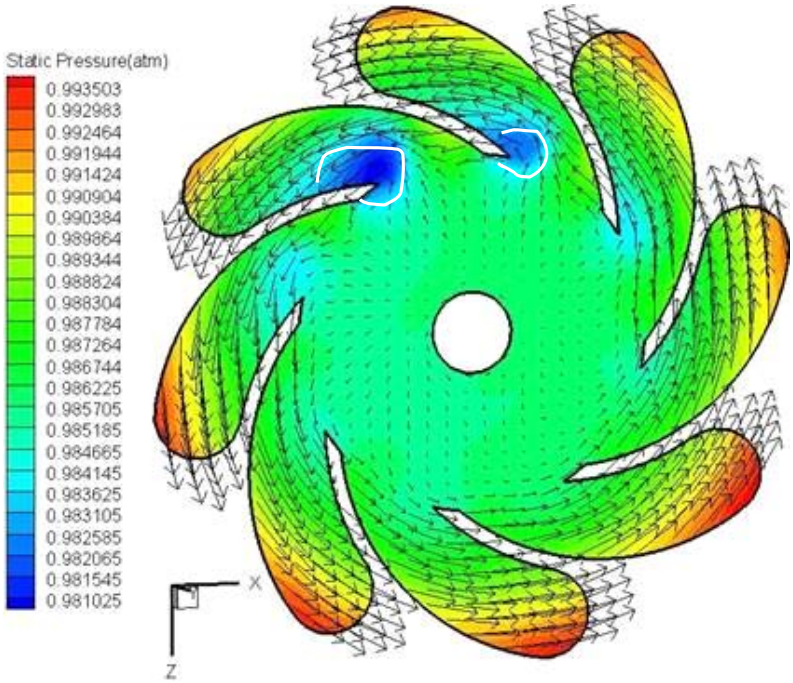

Figure 4.17 100 rpm, Transient Case 3: Transient contour plot of the static pressure (atm) with the velocity (m/s) vectors at a plane across the impeller at t = 0.55 seconds, $\theta = 240^0$.

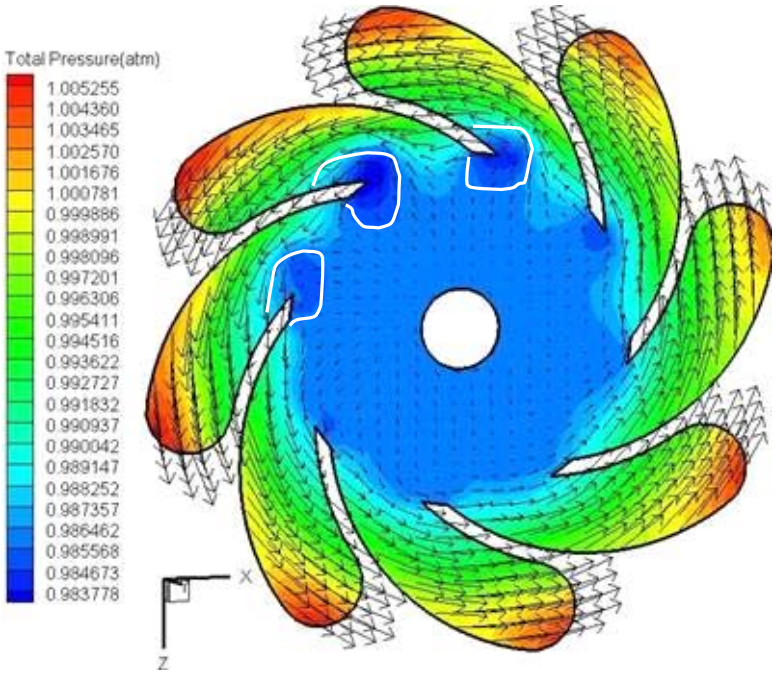

Figure 4.18 100 rpm, Transient Case 3: contour plot of the total pressure (atm) with the velocity (m/s) vectors at a plane across the impeller at t = 0.55 seconds, $\theta = 240^0$.

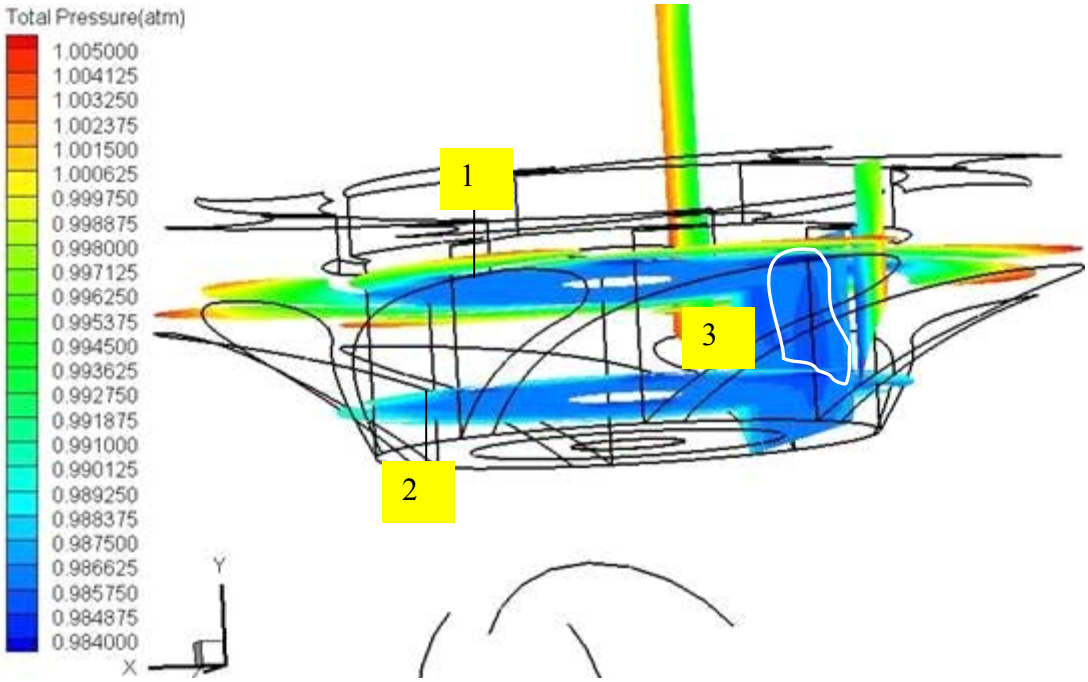

Figure 4.19 100 rpm, Transient Case 3: Transient contour plot of the total pressure (atm) at four different impeller planes at t = 0.55 seconds, $\theta = 240^0$.

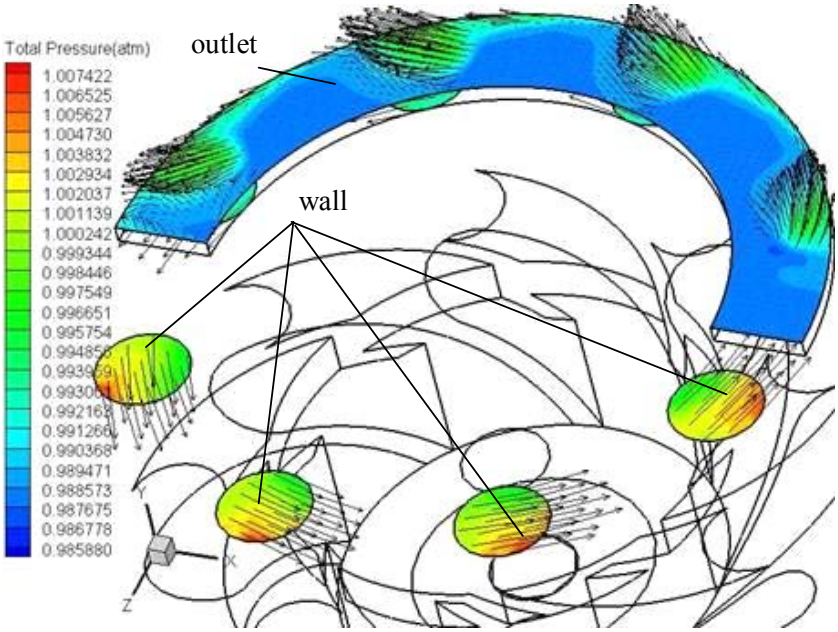

Figure 4.20 100 rpm, Transient Case 3: Transient contour plot of the total pressure (atm) with the velocity (m/s) vectors at the walls and outlet of the domain at t = 0.55 seconds, $\theta = 240^0$.

Comparison among the results of these three cases indicates:

(a) The results of the stationary part of the computational domain do not vary much from case to case.

(b) The moving reference frame scheme gives a reasonable approximation of the flow field in the rotational domain, but it seems to over predict the total pressure losses.

(c) The true transient case using the sliding mesh scheme is computational intensive and time consuming; however, it gives the most reasonable results.

4.3.2 Suction Section- Transient results of the suction domain at time=0.2 seconds, $\theta = 30^0$ and at t= 0.05 seconds, $\theta = 300^0$

From Figures 4.21 through 4.28, there is not much significant difference in the flow pattern between 30^o and 300^o. Take note that a difference can be observed only in the magnitude of the total pressure as seen from Figures 4.23 and 4.24. Also, the regions of total pressure loss are more significant in Figure 4.23 than in Figure 4.24. It could be concluded that the pressure loss is slightly more at $\theta = 30^0$ than at $\theta = 300^0$. The regions of low static pressure are more at $\theta = 30^0$ than at $\theta = 300^0$ as seen from "A" and "B" in Figures 4.27 and 4.28.

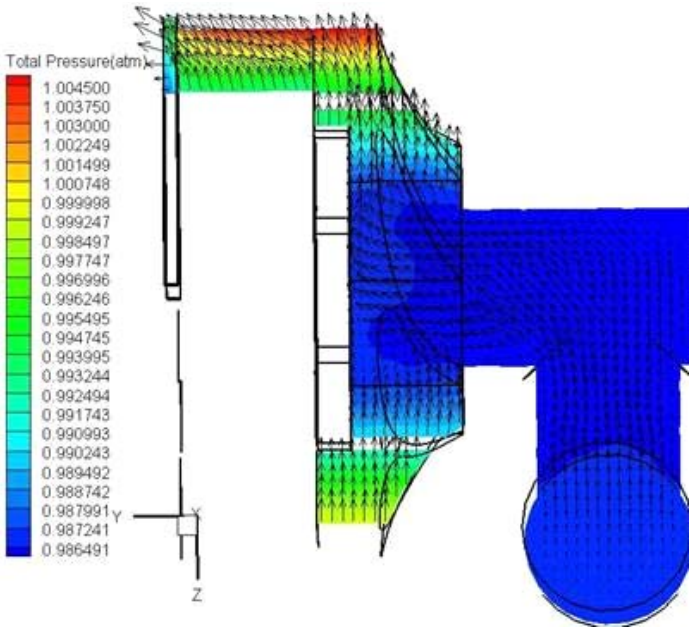

Figure 4.21 100 rpm, Transient Case 3: 100 rpm total pressure (atm) contour plot with the velocity (m/s) vectors at a midspan passing through the outlet at t = 0.2sec, $\theta = 30^0$.

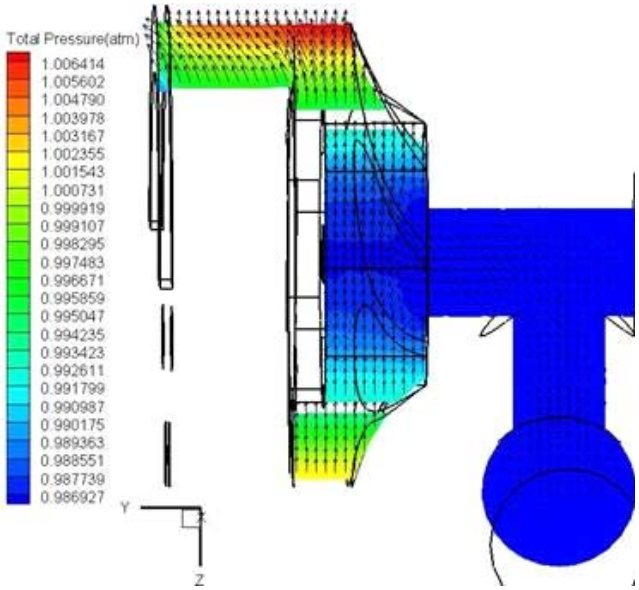

Figure 4.22 100rpm,Transient Case 3: 100 rpm total pressure (atm) contour plot with the velocity (m/s) vectors at a mid span passing through the outlet at t = 0.05sec, $\theta = 300^0$.

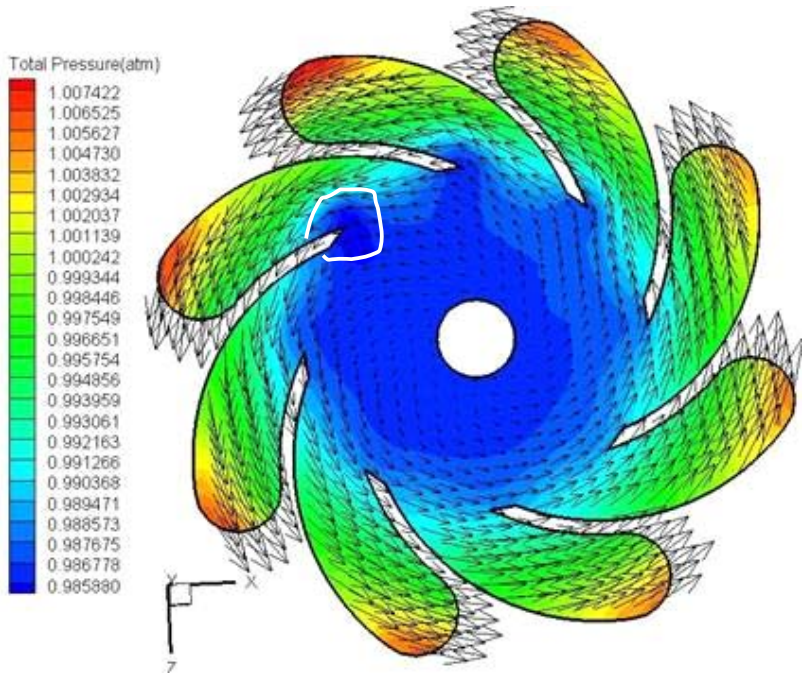

Figure 4.23 100 rpm, Transient Case 3: Total pressure (atm) contour plot with the velocity (m/s) vectors at a plane across the impeller t = 0.2sec, $\theta = 30^0$.

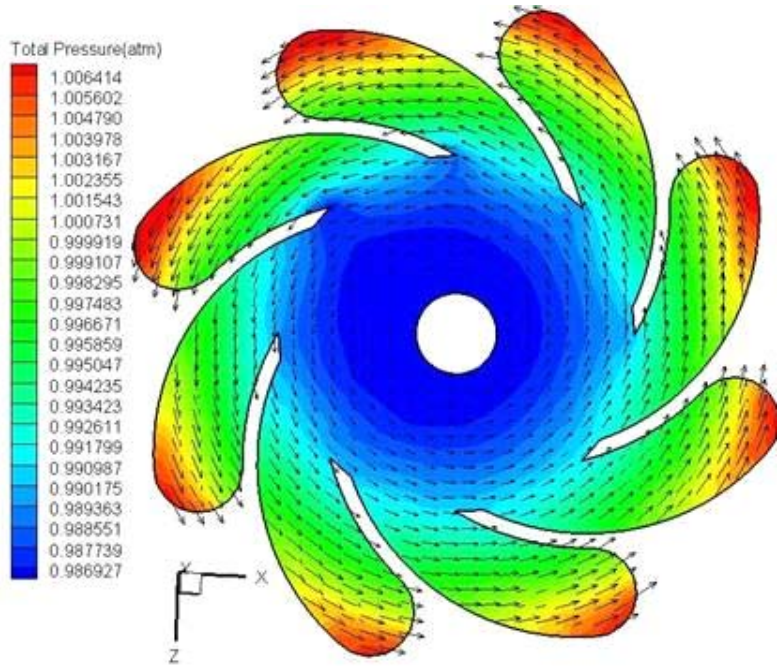

Figure 4.24 100 rpm, Transient Case 3: Total pressure (atm) contour plot with the velocity (m/s) vectors at a plane across the impeller t = 0.05sec, $\theta = 300^0$.

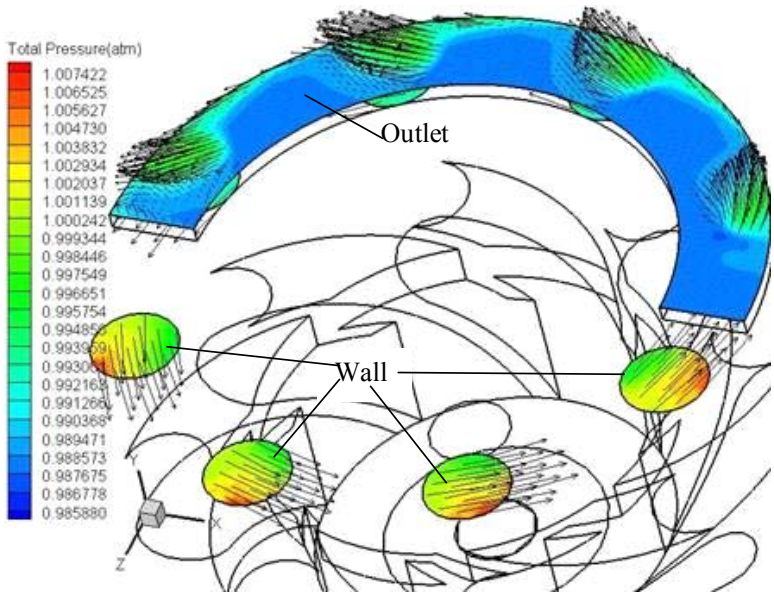

Figure 4.25 100 rpm, Transient Case 3: Total pressure (atm) contour plot with the velocity (m/s) vectors at the walls and outlet of the domain t = 0.2 sec, $\theta = 30^0$.

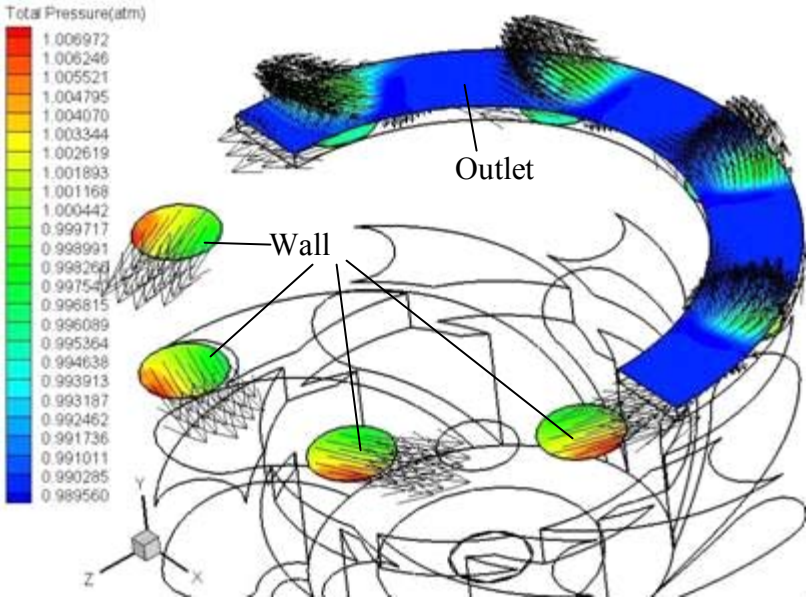

Figure 4.26 100 rpm, Transient Case 3: Total pressure (atm) contour plot with the velocity (m/s) vectors at the walls and outlet of the domain t = 0.05sec, $\theta = 300^0$.

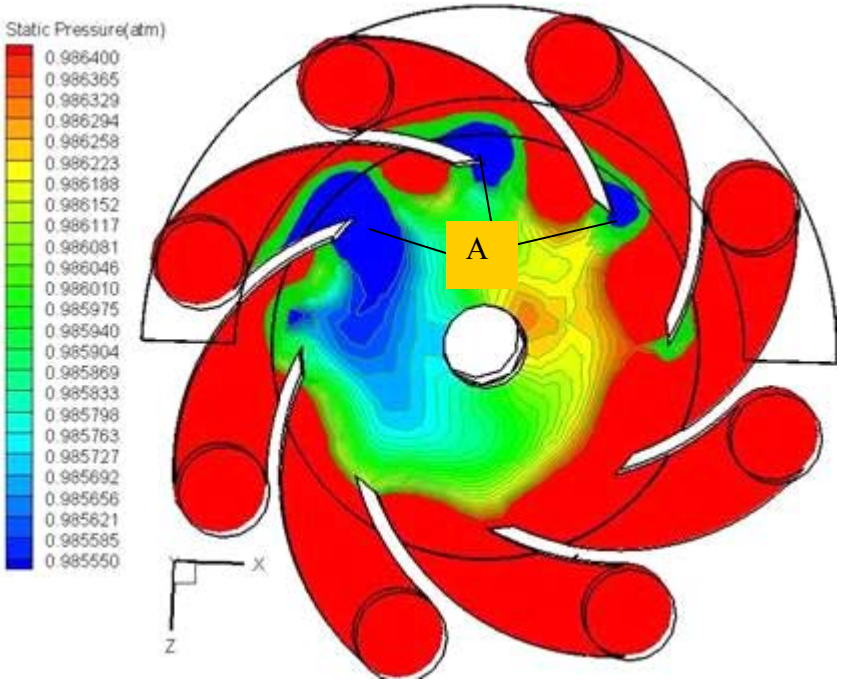

Figure 4.27 100 rpm, Transient Case 3: Static pressure (atm) contour plot across the midspan of the impeller at t = 0.2sec, $\theta = 30^0$.

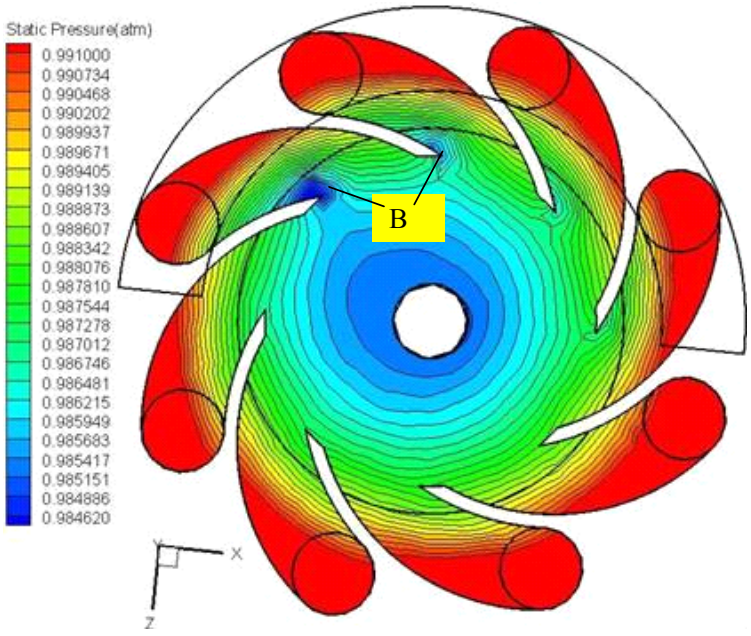

Figure 4.28 100 rpm, Transient Case 3: Static pressure (atm) contour plot across the midspan of the impeller at t = 0.05sec, $\theta = 300^0$.

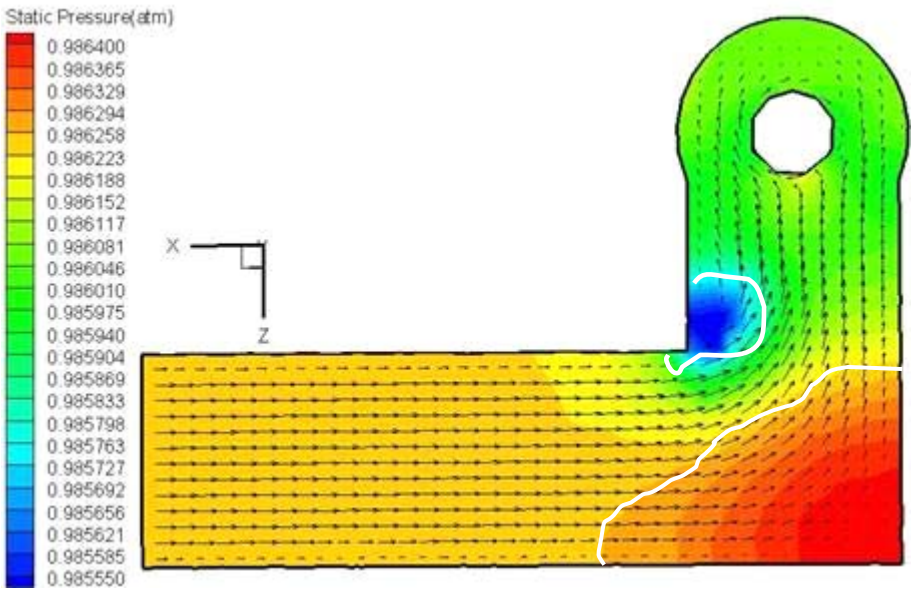

Figure 4.29 100 rpm, Transient Case 3: Contour plot of the static pressure (atm) with the velocity (m/s) vectors at the "L" shaped pipe at t = 0.2sec, $\theta = 30^0$.

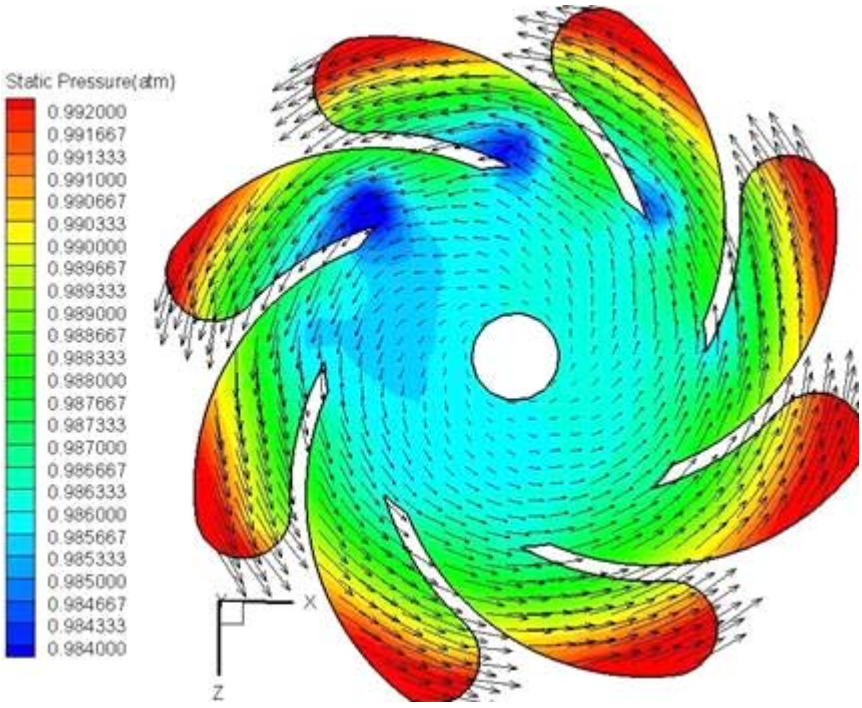

Figure 4.30 100 rpm, Transient Case 3: Static pressure (atm) contour plot with the velocity (m/s) vectors a plane across the impeller at t=0.2 sec, $\theta = 30^0$.

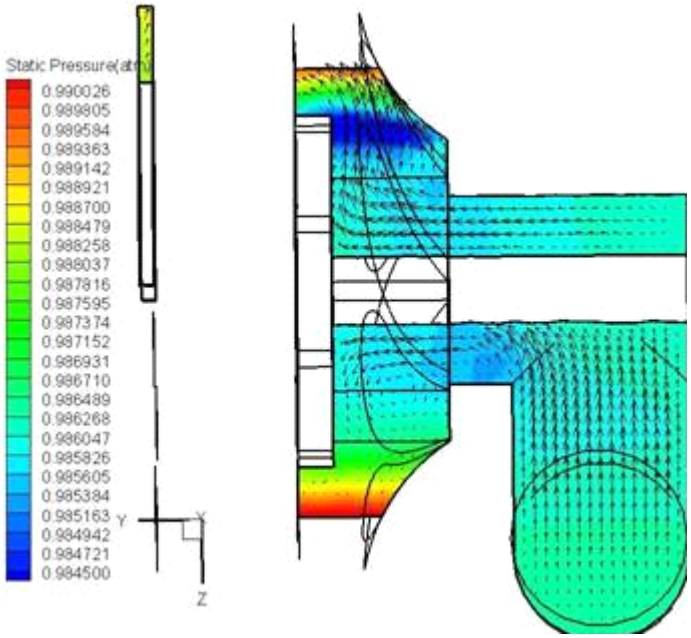

Figure 4.31 100 rpm, Transient Case 3: Static pressure (atm) contour plot with the velocity (m/s) vectors at plane X=0 at t = 0.2sec, $\theta = 30^0$.

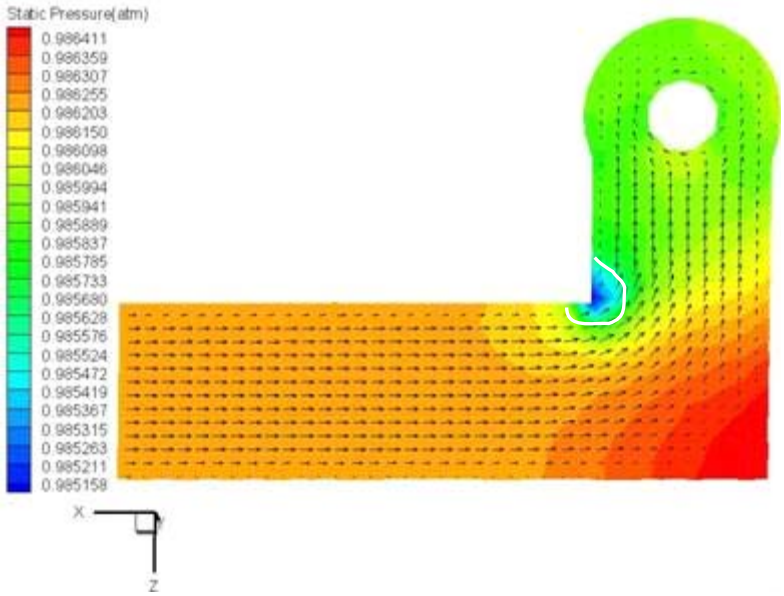

Figure 4.32 100 rpm, Transient Case 3:100 rpm static pressure (atm) contour plot with the velocity(m/s) vectors at the "L" shaped pipe at t=0.05sec,$\theta = 300^0$.

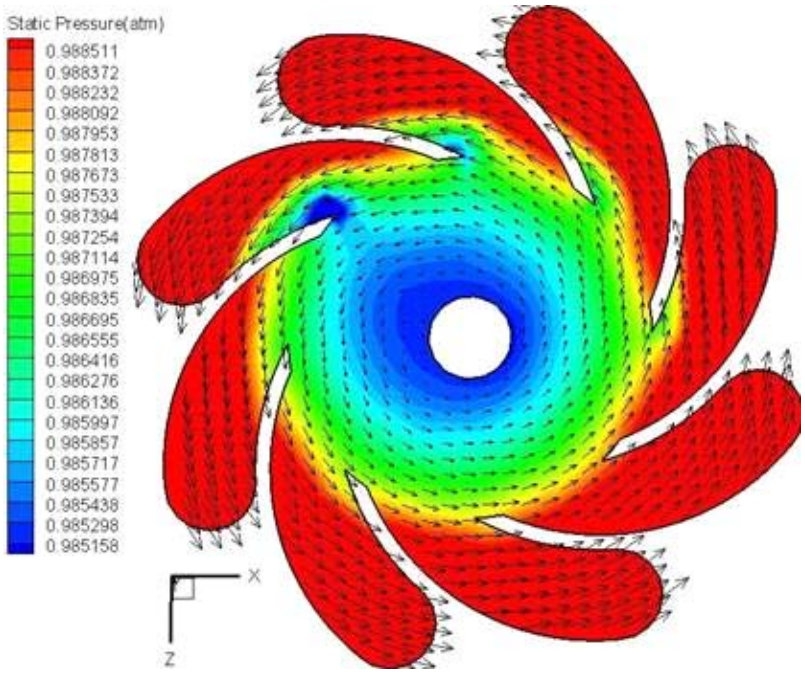

Figure 4.33 100 rpm, Transient Case 3:100 rpm static pressure (atm) contour plot with the velocity (m/s) vectors a plane across the impeller at t = 0.05 sec, $\theta = 300^0$.

Comparison of the above static pressure distributions between stationary, transient and moving reference frame cases shows that the stagnant regions near the outer 90-degree bend and around the separated region downstream of the inner 90-degree bend are smaller in the rotating frame cases than in the stationary case. The areas of the significant low pressure could create cavitation when rotating speed increases. Experiments are needed to help identify whether cavitation occurs. Care must be taken to minimize or remove cavitation.

4.4 Analysis of Total Pressure Losses and Static Pressure Distribution

The following table gives the total pressure obtained at the inlet and outlet, and the total pressure losses for all the cases. Since the total pressure differences are calculated, the pressure correction is not used in this table.

Case	Time (sec)	Cylinder Position (degrees)	Outlet (atm)	Ptot,1 (atm) at inlet	Ptot,2 (atm) at outlet	Rotating KE (atm)	1-(2-rotating KE) (atm)
Case 1	NA	NA	-0.999999	-0.9973215	-0.9990247	0	0.0017032
Case 2	NA	NA	-0.999999	-0.9885559	-0.9886458	0.008436	0.0085257
Case3	0.050	300	-0.999999	-1.0028836	-0.9967797	0.008436	0.0023319
	0.100	330	-0.999999	-1.0026396	-0.9968196	0.008436	0.0026158
	0.125	345	-0.999999	-1.0023293	-0.9964997	0.008436	0.0026062
	0.150	360	-0.999999	-1.0008750	-0.9954654	0.008436	0.0030261
	0.200	30	-0.999999	-1.0016124	-0.9963755	0.008436	0.0031989
	0.225	45	-0.999999	-1.0003600	-0.9954615	0.008436	0.0035373
	0.250	60	-0.999999	-1.0013839	-0.9965580	0.008436	0.0036099
	0.300	90	-0.999999	-0.9999113	-0.9954104	0.008436	0.0039349
	0.350	120	-0.999999	-1.0008951	-0.9963881	0.008436	0.0039288
	0.450	180	-0.999999	-0.9994023	-0.9954298	0.008436	0.0044632
	0.550	240	-0.999999	-1.0004073	-0.9965901	0.008436	0.0046185

Table 4.1 Total pressure losses at the suction section for different cases without pressure correction.

Table 4.1 shows the total pressure losses increase for the rotating cases when compared to the stationary case. The moving reference frame (MRF) case (Case 2) significantly over predicts the total pressure losses.

4.5 Stationary Case Discharge End (Case 1A)

The discharge section of the pump is simulated using the mass flow rate, 1.337 Kg/s, as the inlet condition and an elevated pressure, 500 psia, as the outlet boundary condition.

The velocity results from the stationary frame case (Case 1A) show that flow patterns (Figures 4.34 - 4.37) are highly three-dimensional and complex. There are many circulations and whirlpools that are sources for generating entropy and creating total pressure losses. For example, in regions marked “A” in Figures 4.34-4.37, showing regions of strong flow circulations. Deep blue regions in Figure 4.37 indicate large total pressure losses.

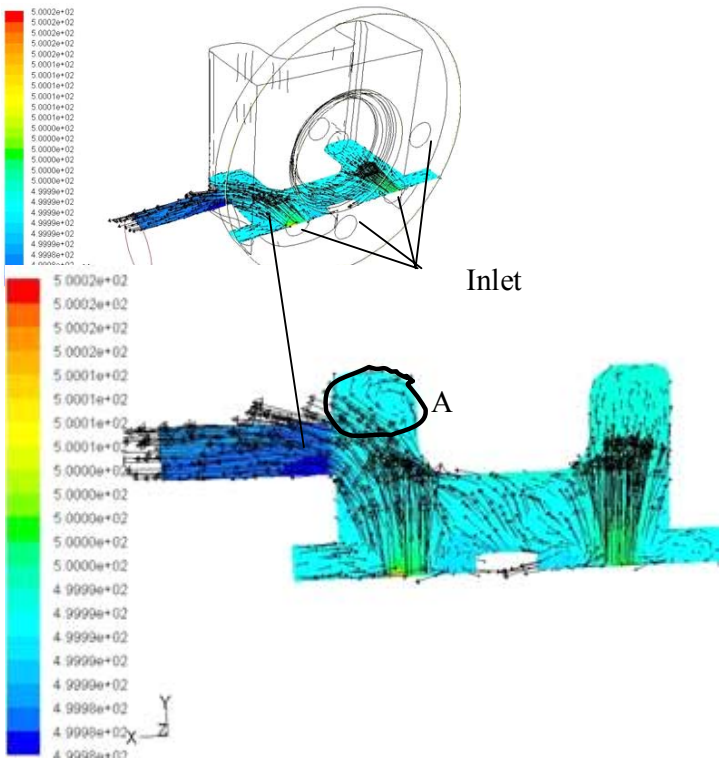

Figure 4.34 Stationary Case 1A: Total pressure (psi) contour plot with the velocity (m/s) vectors in the z-plane across the inlet.

The discharge section of the pump is simulated using the mass flow rate, 1.337 Kg/s, as the inlet condition and an elevated pressure, 500 psia, as the outlet boundary condition.

The velocity results from the stationary frame case (Case 1A) show that flow patterns (Figures 4.34 - 4.37) are highly three-dimensional and complex. There are many circulations and whirlpools that are sources for generating entropy and creating total pressure losses. For example, in regions marked "A" in Figures 4.34-4.37, showing regions of strong flow circulations. Deep blue regions in Figure 4.37 indicates large total pressure losses.

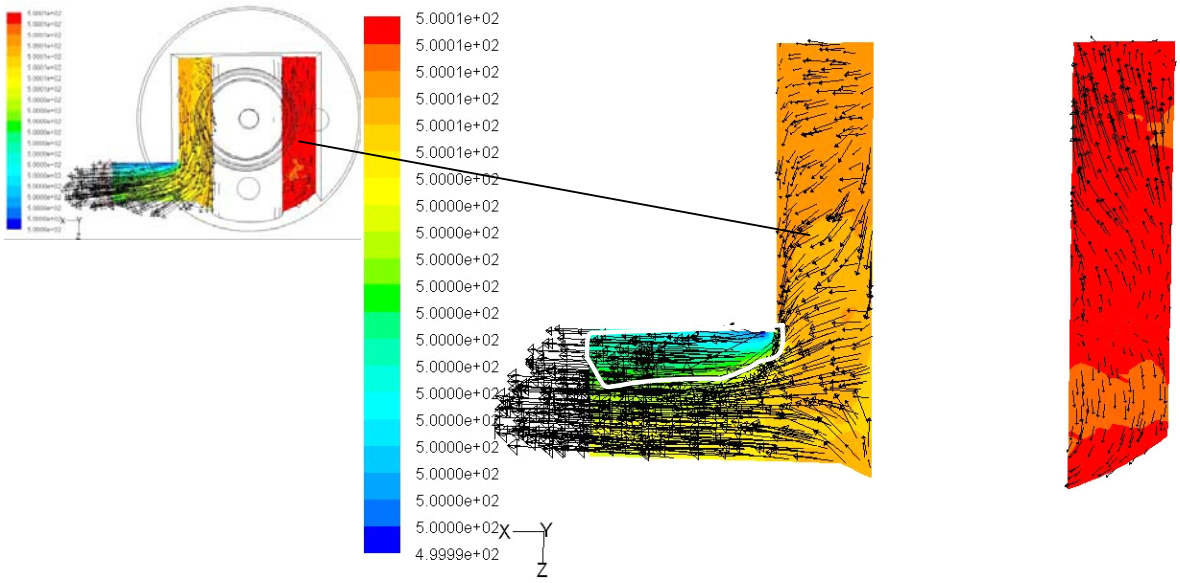

Figure 4.35 Stationary Case 1A: total pressure (psi) contour plot with the velocity (m/s) vectors in the mid-plane across the outlet.

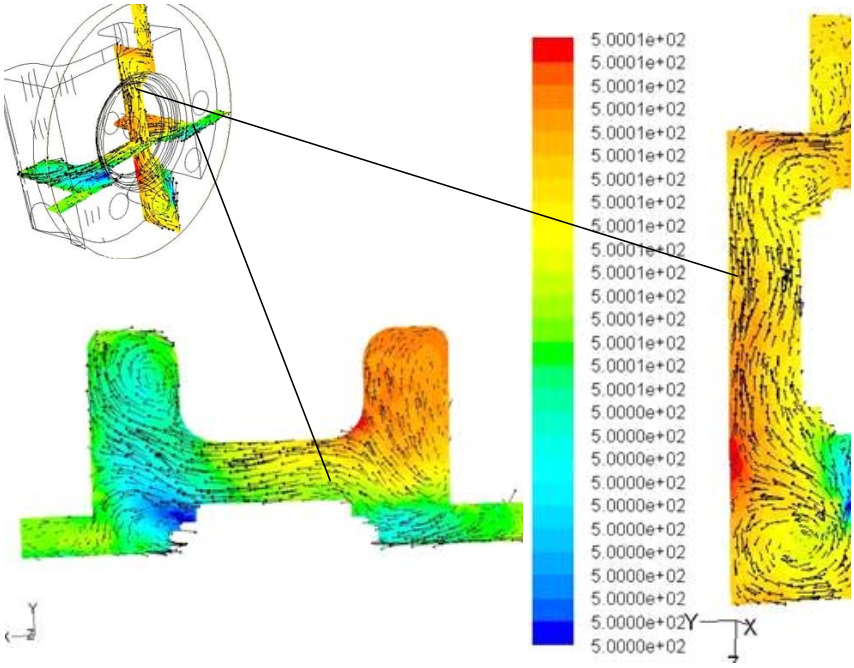

Figure 4.36 Stationary Case 1A: Total pressure (psi) contour plot with the velocity (m/s) vectors showing different re-circulation regions. .

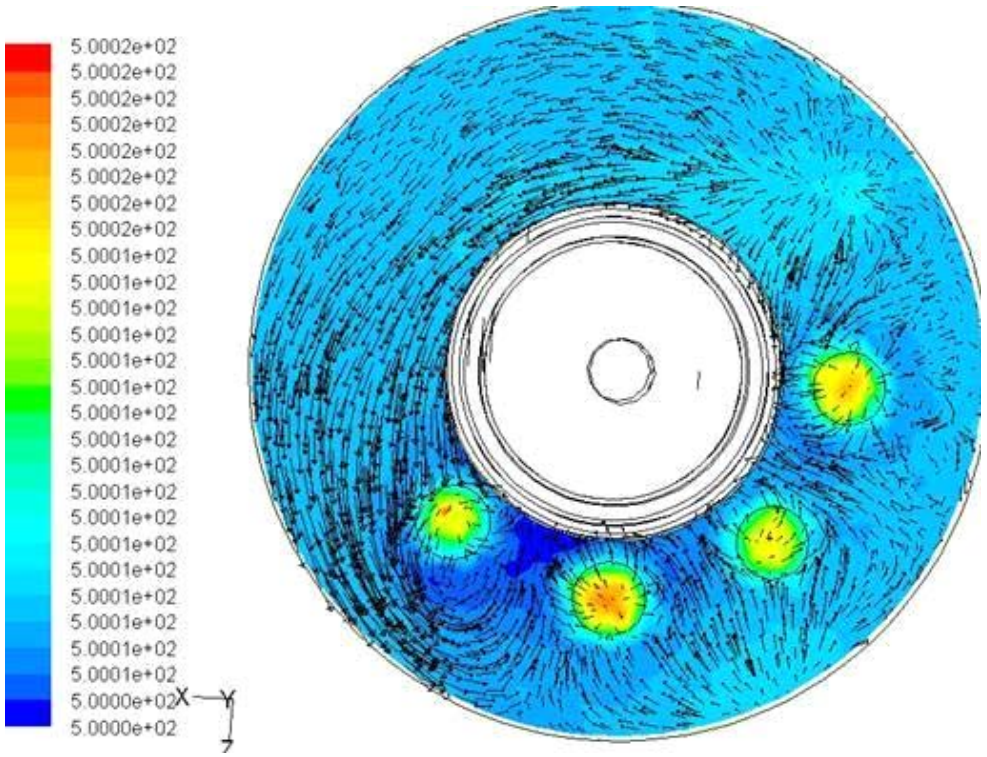

Figure 4.37 Stationary Case 1A: Total pressure (psi) contour plot with the velocity (m/s) vectors at the inlet interface.

4.6 Discharge Section- Moving Reference Frame (Case 2A)

Figures (4.38 - 4.43) show the flow pattern of the discharge section computed using the moving reference frame scheme. Figure 4.38 shows the horizontal view of the recirculation in the cavity of the discharge section. The vertical plane view in Figure 4.39 shows the inlet jet flow coming from the piston generates large swirl flows. Figure 4.40 shows recirculation regions in different vertical planes. As the flow enters from the inlets, it is observed that the flow in the upper half of the section (Figure 4.41) moves toward the opposite direction of the outlet due to the shear force of the pump. Later on, this stream of flow needs to return back towards the outlet. This kind of travel is not efficient and creates large losses as shown in the blue region in Figure 4.42. Figure 4.42 shows the losses generated by flow separation following the 90-degree elbow zone. Overall, the flow pattern in the discharge section is highly complex and 3-D. Considerable

aerodynamic improvements can be achieved. Similar to the suction section, the total pressure at the discharge section also increases with radius as shown in Figure 4.43. Most losses are occurring near the lower part of the plenum, which is where the flow is compressed inward as the jet flows.

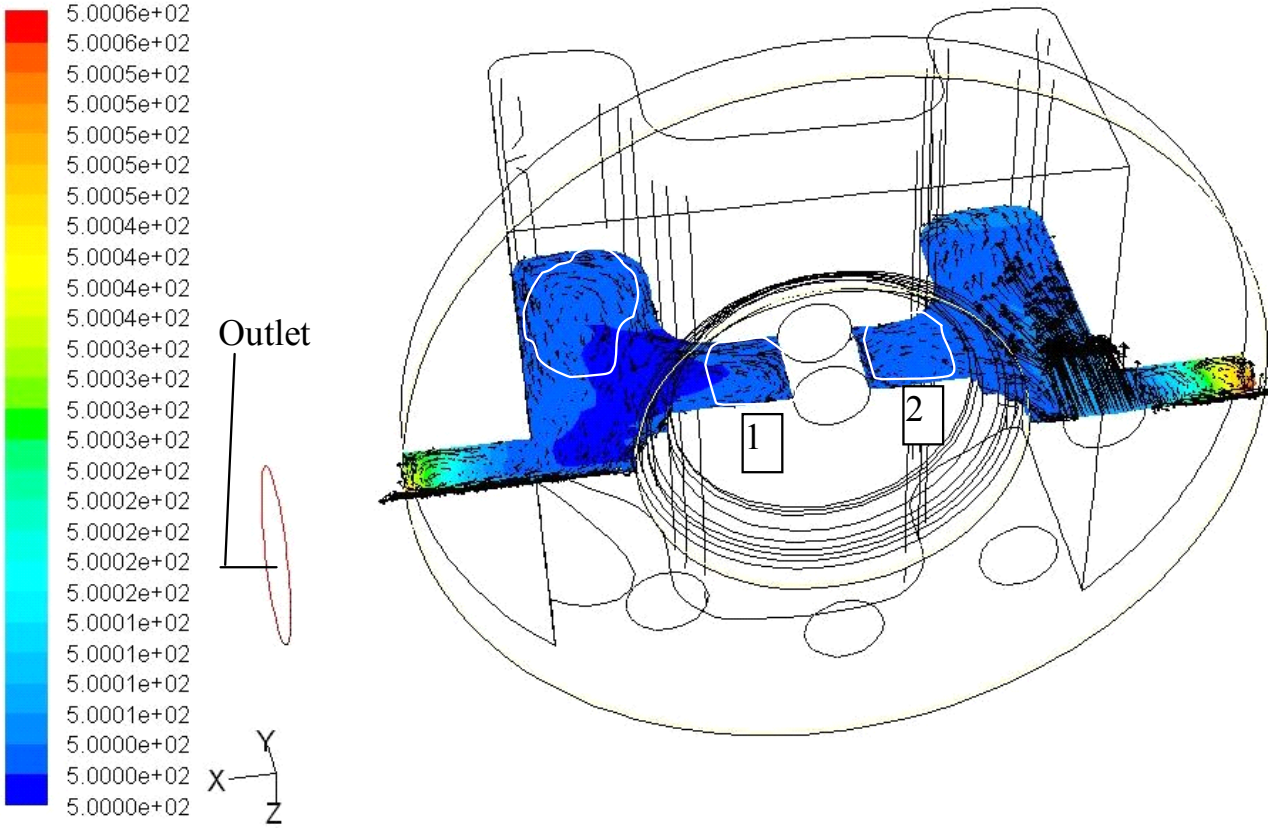

Figure 4.38 100 rpm, MRF Case 2A: Total pressure (psi) contour plot with the velocity (m/s) vectors in the z-plane.

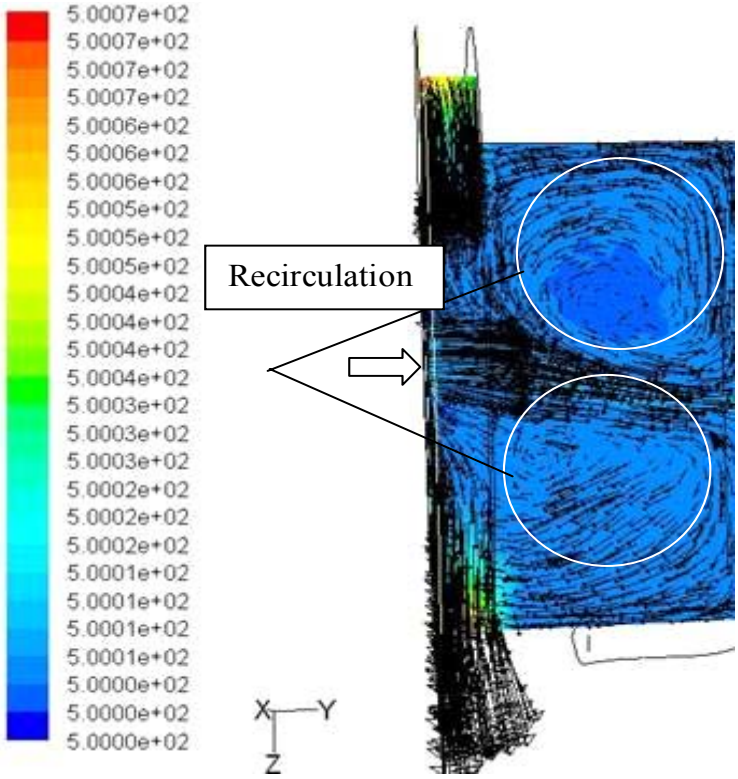

Figure 4.39 100 rpm, MRF Case 2A: Total pressure (psi) contour plot with the velocity (m/s) vectors in the x-plane.

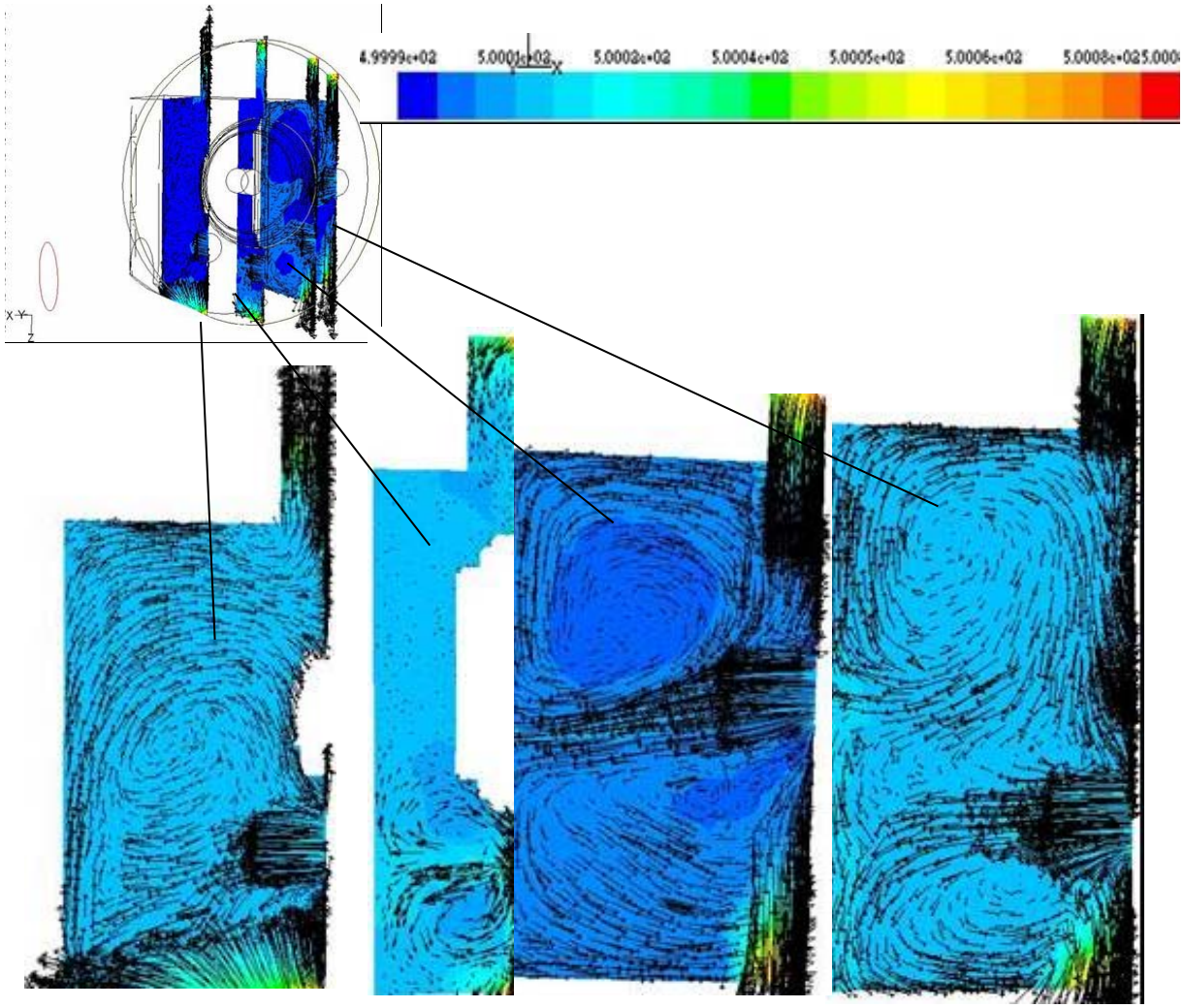

Figure 4.40 100 rpm, MRF Case 2A: Total pressure (psi) contour plot with the velocity (m/s) vectors in different "X" planes perpendicular to the disk.

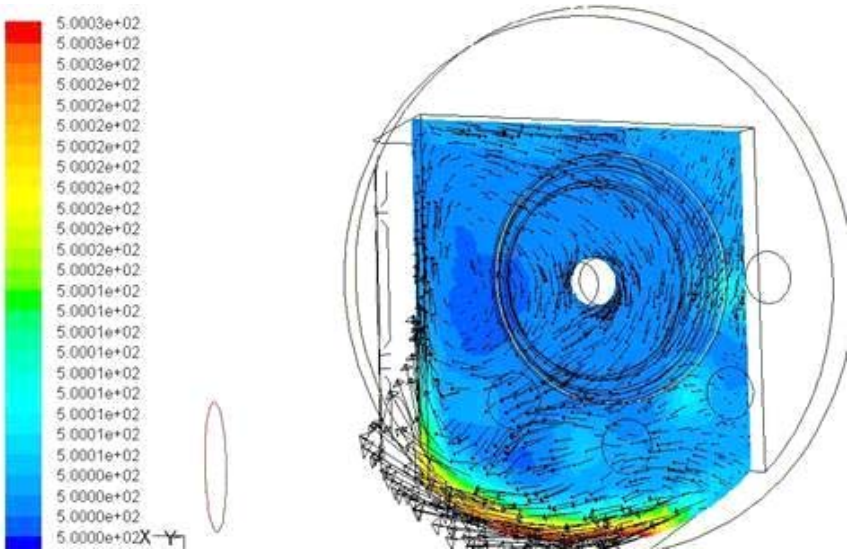

Figure 4.41 100 rpm, MRF Case 2A: Total pressure (psi) contour plot with the velocity (m/s) vectors across a plane after the moving frame.

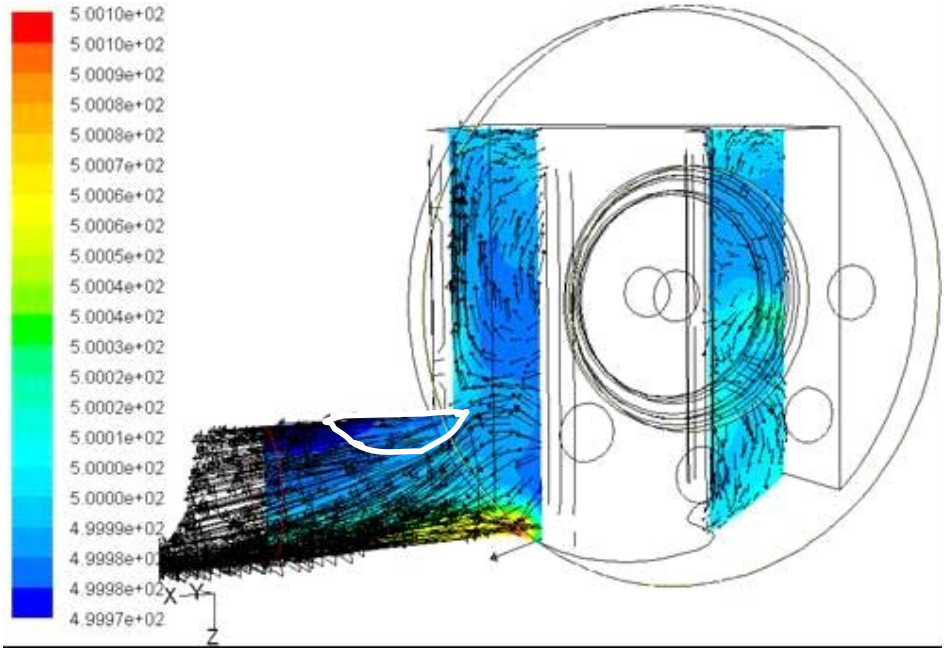

Figure 4.42 100 rpm, MRF Case 2A: Total pressure (psi) contour plot with the velocity (m/s) vectors across a mid plane of the outlet.

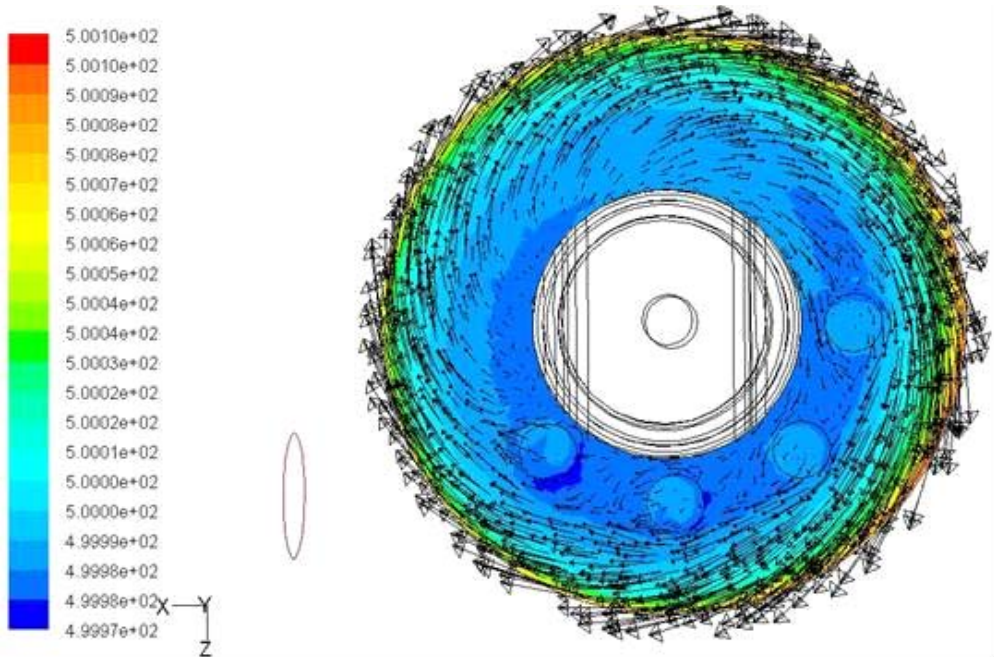

Figure 4.43 100 rpm, MRF Case 2A: Total pressure (psi) contour plot with the velocity (m/s) vectors across a plane parallel to the disk.

4.7 Discharge Section - Sliding Mesh Transient Case at Time t = 0.55 seconds, $\theta = 60^0$ (Case 3A)

The transient computation shows in Figure 4.44 the marked regions of maximum total pressure just after the flow enters the inlets, and the total pressure losses in the elbow. Figure 4.45 shows recirculation regions in the plane right after flow enters the inlet. Again, the overall flow is highly complex and 3-D, which creates a lot of entropy.

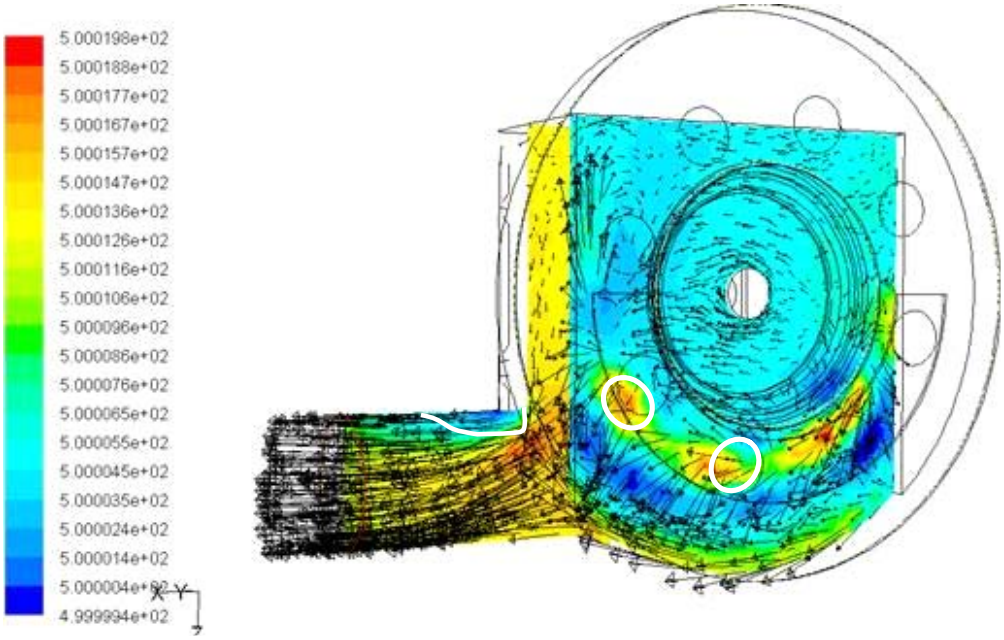

Figure 4.44 100 rpm, Transient Case 3A: Transient total pressure (psi) contour plot with the velocity (m/s) vectors at different planes parallel to the disk at t=0.55 sec, $\theta = 60^0$.

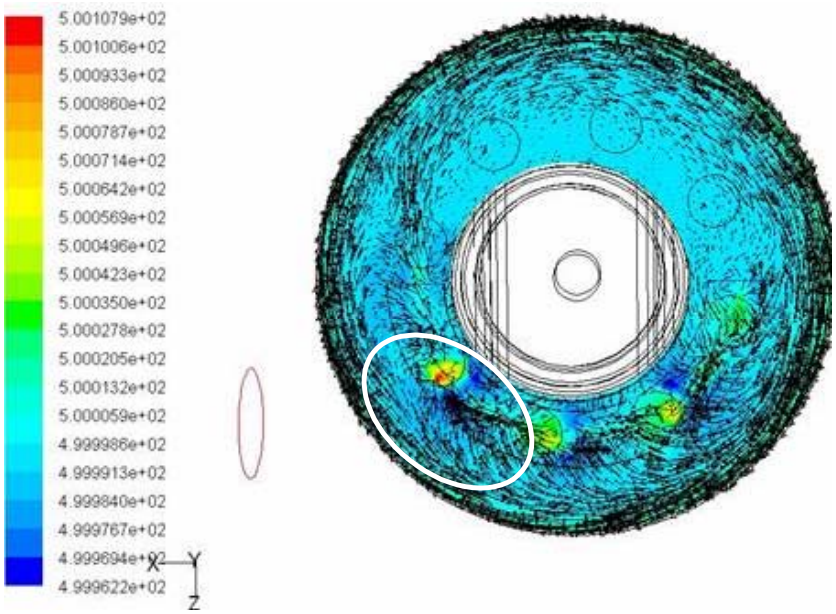

Figure 4.45 100 rpm, Transient Case 3A: Transient total pressure (psi) contour plot with the velocity (m/s) vectors in a plane adjacent to the rotating disk at t = 0.55sec, $\theta = 60^0$.

4.7.1 Discharge Section - Transient results of the at time t = 0.05 seconds, θ = 120^0 and t = 0.2 seconds, θ = 210^0

The transient computation shows regions of maximum total pressure "B" and minimum pressure "A" in Figure 4.46 just after the flow enters the discharge plenum at t = 0.05 sec (θ = 120^0). In Figure 4.48, these maximum and minimum total pressure regions are seen more pronounced as B1 and A1 at a later time at t = 0.2 sec (θ = 210^0). The total pressure losses consistently increase along the exit pipe as shown in Figures 4.47 and 4.49. Both the stationary case (Case1A) and the MRF case (Case 2B) significantly under-predict the total pressure losses by a factor of 5 as seen from Table 4.2.

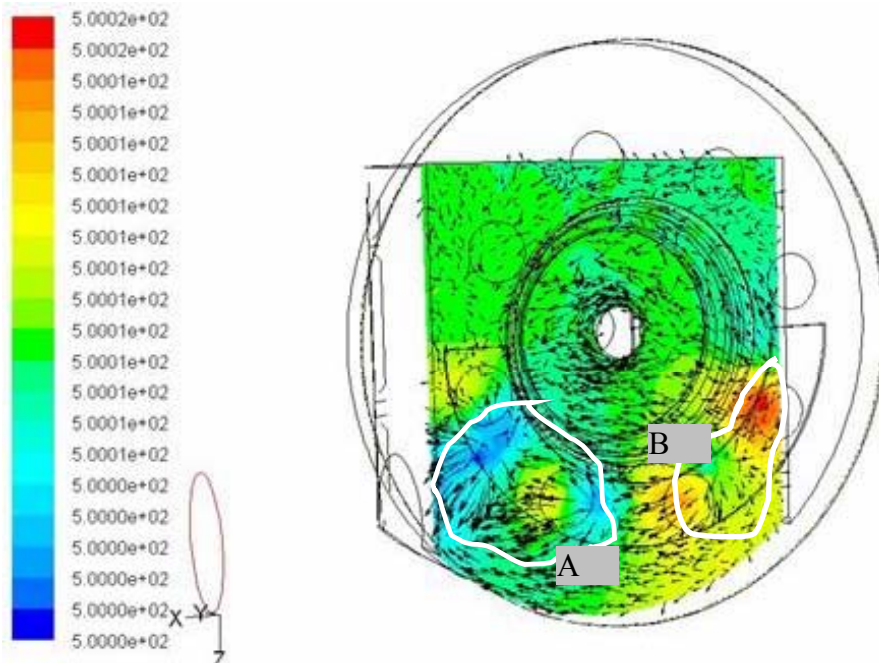

Figure 4.46 100 rpm, Transient Case 3A: Transient Contour plot of the total pressure (psi) with the velocity (m/s) vectors on a plane adjacent to the flow inlet at t = 0.05 sec, θ = 120^0.

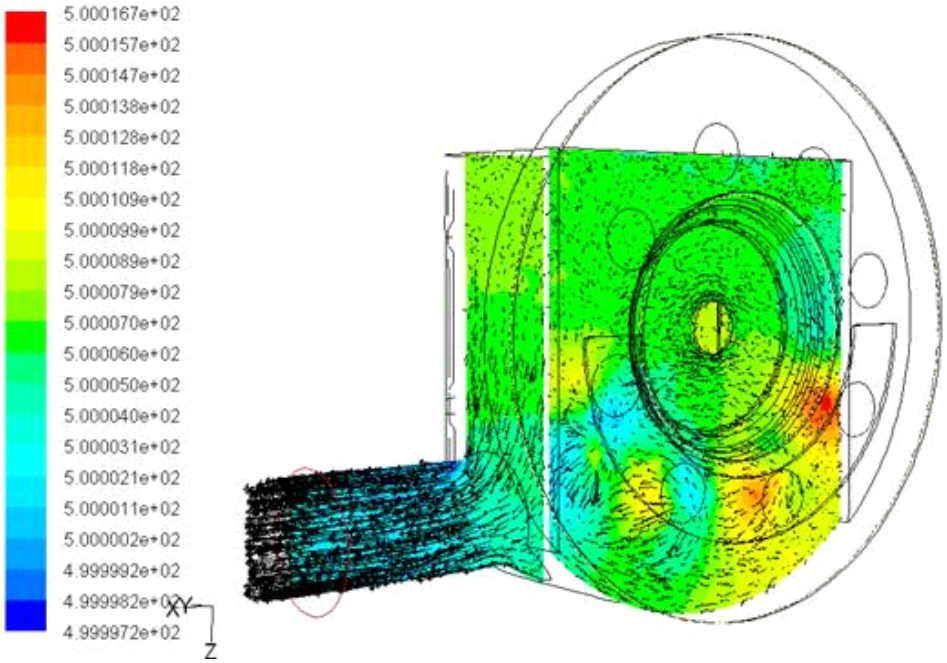

Figure 4.47 100 rpm, Transient Case 3A: Transient Contour plot of the total pressure (psi) with the velocity (m/s) vectors before and after the elbow at the outlet at t = 0.05 sec, θ = 120^0).

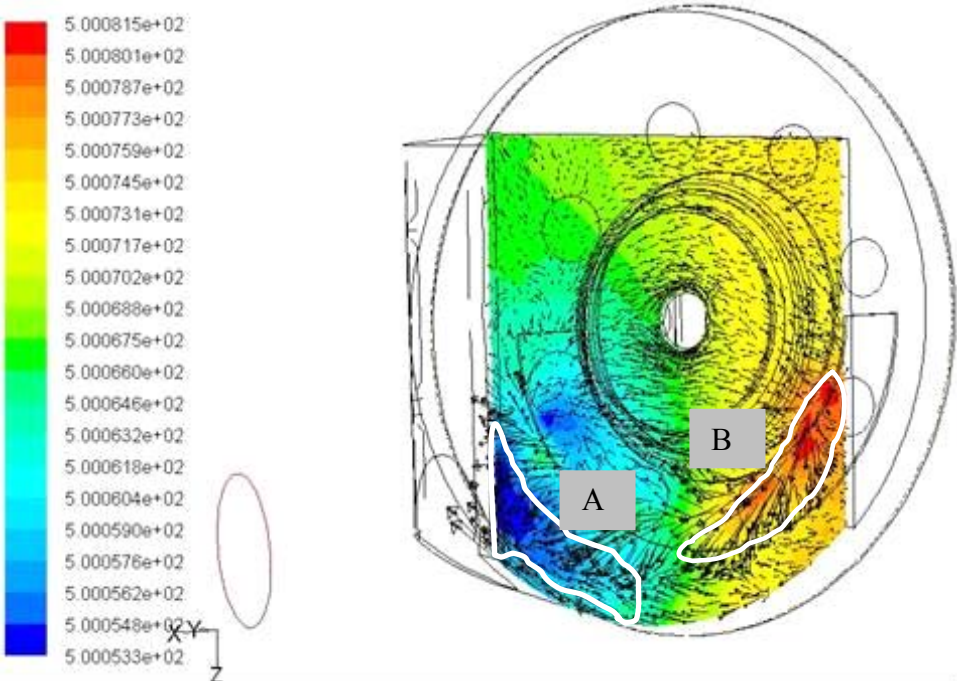

Figure 4.48 100rpm, Transient Case 3A: Transient Contour plot of the total pressure (psi) with the velocity (m/s) vectors after the inlet at t = 0.2 sec, θ = 210^0.

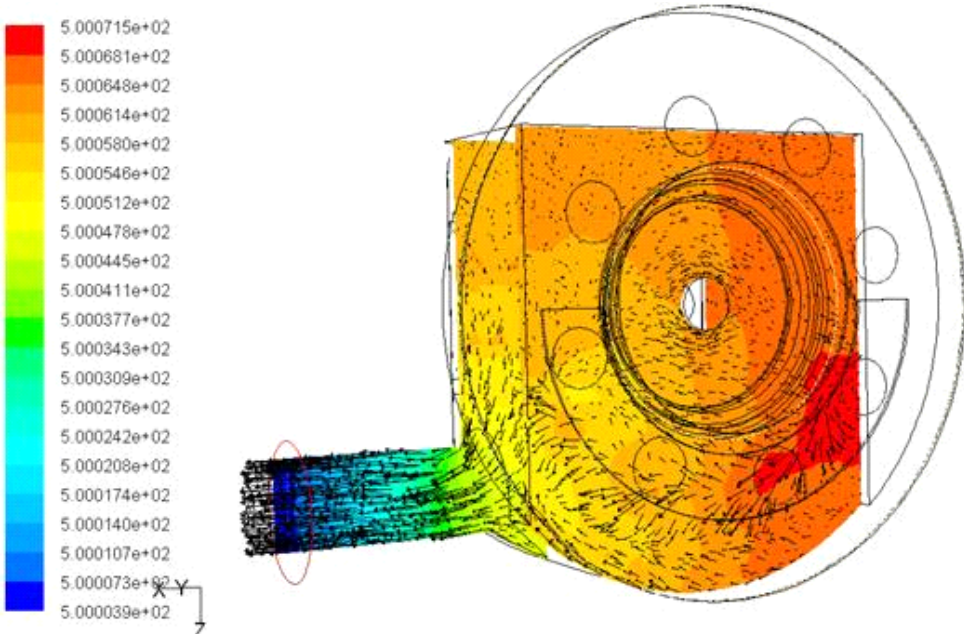

Figure 4.49 100 rpm, Transient Case 3A: Transient Contour plot of the total pressure (psi) with the velocity (m/s) vectors on two planes parallel to the disk at t = 0.2 sec, $\theta = 210^0$.

Case	Time (sec)	Cylinder Position (degrees)	Outlet (psi)	Outlet (atm)	Ptot,1 (atm) at inlet	Ptot,2 (atm) at outlet	Ptot,1-2 (atm)
Case 1	NA	NA	500	34.0230	34.0239	34.0232	0.0007
Case 2	NA	NA	500	34.0230	34.0234	34.0232	0.0001
Case3	0.050	120	500	34.0230	34.0374	34.0233	0.0141
	0.100	150	500	34.0230	34.0360	34.0232	0.0128
	0.125	165	500	34.0230	34.0370	34.0232	0.0137
	0.150	180	500	34.0230	34.0343	34.0232	0.0111
	0.200	210	500	34.0230	34.0411	34.0232	0.0178
	0.225	225	500	34.0230	34.0338	34.0232	0.0106
	0.250	240	500	34.0230	34.0364	34.0232	0.0132
	0.300	270	500	34.0230	34.0343	34.0232	0.0111
	0.350	300	500	34.0230	34.0371	34.0232	0.0138
	0.450	360	500	34.0230	34.0344	34.0232	0.0112
	0.550	60	500	34.0230	34.0364	34.0232	0.0132

Table 4.2 Total pressure losses at the discharge end for different cases.

4.8 Loss in Efficiency of the TurboPiston Pump (TPP)

Frictional losses created by fluid mechanics are only considered in this study without considering the other mechanical losses such as seals and rotating shafts. The total fluid mechanical losses in the TPP are calculated by adding the total pressure losses from the suction domain, the piston-cylinder sections, and the discharge domain. The total pressure losses in the cylinders are calculated using engineering calculations as explained in detail in appendix-C. Table 4.3 lists the total pressure losses of each section and the calculated loss in efficiency of the TurboPiston pump. The results show the total fluid mechanical losses are minimal (~0.02%), which is underpredicted. Finer meshes are needed to improve the total pressure losses calculation.

Case	Time (sec)	Cylinder Position (degrees)	Pl,Suction (atm)	Pl,Cylinder (atm)	Pl,Discharge (atm)	Pt,loss (atm)	del Pt (atm)	η loss (%) = (Pt,loss/del Pt)
Stat	N/A	N/A	0.0017032	0.0008497	0.0008535	0.0034064	33	0.0103
MRF	N/A	N/A	0.0085257	0.0008497	0.0076760	0.0170514	33	0.0517
Trans	0.050	300	0.0023319	0.0008497	0.0014822	0.0046638	33	0.0141
	0.100	330	0.0026158	0.0008497	0.0017661	0.0052315	33	0.0159
	0.125	345	0.0026062	0.0008497	0.0017565	0.0052124	33	0.0158
	0.150	360	0.0030261	0.0008497	0.0021764	0.0060522	33	0.0183
	0.200	30	0.0031989	0.0008497	0.0023492	0.0063978	33	0.0194
	0.225	45	0.0035373	0.0008497	0.0026876	0.0070746	33	0.0214
	0.250	60	0.0036099	0.0008497	0.0027602	0.0072197	33	0.0219
	0.300	90	0.0039349	0.0008497	0.0030852	0.0078697	33	0.0238
	0.350	120	0.0039288	0.0008497	0.0030791	0.0078575	33	0.0238
	0.450	180	0.0044632	0.0008497	0.0036136	0.0089264	33	0.0270
	0.55	240	0.0046185	0.0008497	0.0037689	0.0092371	33	0.0280

Table 4.3 Loss in efficiency of the TurboPiston pump

CHAPTER FIVE

CONCLUSIONS

A 3-D computational model has been constructed for the newly invented TurboPiston pump. The commercial CFD code, FLUENT, was used to solve the complete 3-D Navier-Stokes equations to obtain the flow field and the total pressure losses. The standard k-ε turbulence model was used. Three different cases are simulated: the stationary case, the moving reference case at 100 rpm, and the transient case using the moving frame/sliding mesh scheme at 100 rpm. The results are summarized below.

5.1 Stationary Case

The stationary case is used for the purpose of examining the CFD model setup and ensuring the 3-D model is adequately constructed and the fundamental physics of flow behavior, pressure distribution, and total pressure loses are reasonable. The results show that the flow is well conducted and guided by the impeller vanes. Large total pressure losses occur downstream of the inner 90-degree bend and near the regions closer to the rotating shaft due to recirculations. A minor loss occurs near the outer 90-degree bend.

The flow pattern in the stationary simulation of the discharge section is found to be highly complex and three-dimensional. There are many circulations and whirlpools, which are all sources for generating entropy and creating total pressure losses.

5.2 Moving Reference Frame Case

In this case, the computation was conducted at a steady-state condition. The rotational speed was assigned to the disk although the meshes are not actually rotating. The assigned rotational speed creates an additional force and momentum that simulate a snapshot of rotational motion. Due to imposed rotational momentum, flow is more active in the four lower-left closed cylinders than in the stationary case. Because of centrifugal force, tangential magnitude of the velocity increases from inlet to outlets. In addition, there is an increase in the total pressure in the moving domain due to the addition of rotational kinetic energy. This non-uniform pressure distribution across the cylinder due to rotational motion could potentially affect piston head stress and might cause some disk fluttering. Total pressure losses are more in the moving reference frame (MRF) case than the other two cases.

In the discharge section simulation, flow does not move in an efficient way and causes additional total pressure losses.

5.3 Transient Case

The transient analysis is more accurate in simulating the time-dependent pump motion, although it is more computationally demanding and time consuming. The instantaneous snapshots of the flow phenomenon in the transient case show the results are similar to those of the moving reference frame method. Total pressure losses vary with different positions of the rotation angle and from moment to moment.

In the entrance duct, the stagnant region near the outer 90-degree bend and the separated region downstream of the inner 90-degree bend are smaller in the rotating cases than in the

stationary case. Areas of significantly low static pressure occur in the flow passages through the impeller and downstream of the inner 90-degree bend of the entrance duct. Since cavitation may occur in these areas of low static pressure, experiments are needed to help identify whether or not cavitation occurs. Redesign of the entrance duct and the impeller vanes could minimize or alleviate the cavitation problem.

The total pressure losses in the stationary and the moving reference frame cases significantly under predict the pressure losses by a factor five.

A comparative study of the three cases shows that results of the stationary part of the computational domain do not vary much from case to case. The moving reference frame scheme gives a reasonable approximation of the flow field, but it seems to over predict total pressure losses.

5.4 Grid Sensitive Study

A grid sensitivity study indicates the mesh numbers set in this study are not sufficient to resolve the total pressure losses. However, due to the nature of this study as a first step toward providing a preliminary view of the complex flow inside a new pump, the results of the coarse mesh are acceptable to the present study. Finer mesh simulations will be used in future studies.

5.5 Efficiency

The loss in the efficiency has been calculated by considering only fluid mechanical frictional losses. Other mechanical losses are not included. The results show the total fluid mechanical losses are minimal (~0.02%). Finer meshes are needed to improve the total pressure losses calculation.

5.6 Future Work

The following future work is recommended:

- Use finer meshes with smaller near-wall meshes (low first mesh Y+ value)
- Incorporate the cylinder dynamics into the computational domain
- Redesign the entrance duct elbow and the impeller vane geometry to reduce the total pressure losses
- Redesign the discharge section flow path to reduce the total pressure losses.

REFERENCES

1. Wachel,J.C., Szenasi, F.R., Denison, S.C., 1985 "Analysis of Vibration and Failure Problems in Reciprocating Triplex Pumps for Oil Pipelines," *Energy Sources and Technology Conference and Exhibition* 85-Pet 10.

2. Wachel , J.C., Titson J.D., Price S.M., 1989 "The Effect of Pulsations on Cavitation in Reciprocating Pump Systems," *Energy Sources and Technology Conference and Exhibition* 89-Pet 10.

3. Warren E. Wilson., *Positive Displacement Pumps and Fluid Motors,* Pitman Publising Corporation, January 1950, ASIN-B0007E6VGQ.

4. Igor J.Karassik, *Pump Hand Book,* McGrawHill, 1985, ISBN 007033325.

5. John D.Anderson Jr., *Computational Fluid Dynamics,* McGrawHill, 1995, ISBN0-07-113210-4.

6. Bruce R. Munson, Donald F.Young, Theodore H. Okiishi, *Fundamentals of Fluid Mechanics*, John Wiley and Sons, 2001, ISBN 9814-12-667-5.

7. FLUENT 6.1 User's Guide, February 2003.

8. Patankar S.V., *Numerical Heat Transfer and Fluid Flow*, McGraw Hill, 1980.

APPENDIX A

CALCULATION OF VOLUME FLOW RATE FOR THE TURBOPISTON PUMP

This section documents calculation of the volume rate related to Turbo PistonPump (TPP):

1. Volume flow rate under selected RPMs, piston diameters and strokes.
2. Plot for speed versus volume flow rate

Assumptions:

Temperature = Room temperature = 80^0F

Service fluid = Water

Incompressible flow

1. Calculation of volume flow rates

$$V_O = [\Pi \times d^2/4] \times [\text{displacement} \times \Omega \times n] \quad \text{(A1)}$$

Where,

V_O is the volume flow rate

d is the diameter of the piston cylinder = 2.75 inches

Ω is the rotational speed of the shaft (RPM) [$N = 2\pi\Omega/60$ (rad/s)]

n is the number of cylinders = 8

displacement or the stroke length of the piston = 1.03 inches

Rotating Speed (rpm)	Volume Flow Rate (cfm)	Volume flow Rate (USGPM)	Volume Flow Rate (m^3/s)	Mass flow rate (kg/s)
0	0	0	0	0
100	2.83	21.1848	0.0013	1.29
500	14.16	105.9240	0.0067	6.68
1000	28.32	211.8481	0.0134	13.37
1500	42.48	317.7721	0.0201	20.06
2000	56.64	423.6962	0.0267	26.65

Table A1 Example of calculated volume flow rate based on the piston diameter and the stroke

Unit conversion:

1 gal = 3.785412 L = 3.785412 x 10^{-3} m^3 = 231 in^3 =0.13368 ft^3

1cfs = 448.97 USGPM

1US GPM =0.1336 cfm =2.228 x 10^{-3} cfs

2. Sample Calculation:

For a 1000 rpm case, volume flow rate

V_O = $[\Pi \times d^2 /4] \times [\text{displacement} \times \Omega \times n]$

d = 2.75in/12 = 0.2291ft

Displacement = 1.03in/12 = 0.0858ft

Ω is the rotational speed of the shaft = 1000 rpm=1000/60 = 16.66 rps

n = 8

Using the above values,

V_O = (Π /4) x (0.229) x (0.229) x (0.0858) x 8 x (16.6)

V_O = 0.4719995 cfs

2. Plot for speed vs. volume flow rate

Using the values from Table A-1, a graph is plotted between angular speed of the shaft and volume flow rate of the pump. The graph is a linear graph which shows that as the speed of the shaft increases the flow rate also increases.

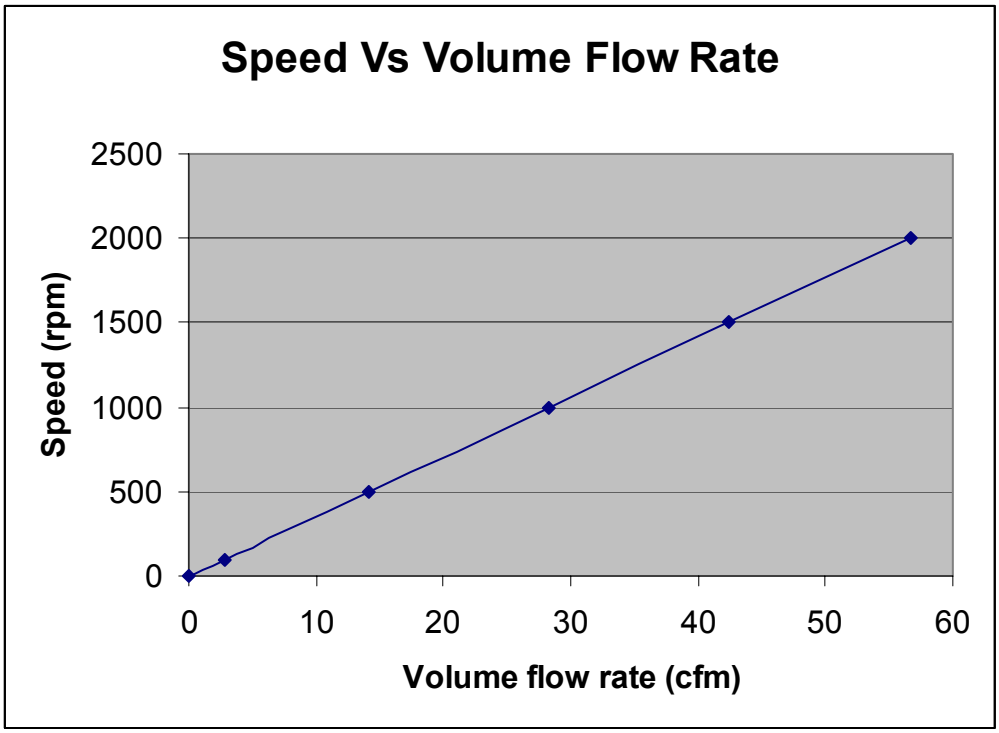

Figure A1 Plot of speed (rpm) vs. volume flow rate (cfm)

APPENDIX B

CALCULATIONS OF VOLUME FLOW RATE, TRANSPORT DISTANCE, AND POWER OF THE TURBOPISTON PUMP

This short report documents calculations of three characteristics related to TurboPiston Pump (TPP):

1. Volume flow rate under selected RPMs and piston diameters and strokes.
2. The height of water column that can be raised by 1000 psi output.
3. The distance the water can be transported under 1000 psi
4. The power required by transporting 1601.9 cfs water at 1000 psi.

Assumptions:

Temperature = Room temperature = 80^0F.

Service fluid = Water

Incompressible flow.

Pipe material = concrete

2. Calculation of volume flow rates

$$V_O = [\pi \times d^2/4] \times [\text{displacement} \times \Omega \times n] \quad \text{(B1)}$$

Where,

V_O is the volume flow rate

d is the diameter of the piston cylinder

Ω is the rotational speed of the shaft (RPM) [$N = 2\pi\Omega/60$ (rad/s)]

n is the number of cylinders = 8

Piston dia (in)	Stroke length. (in)	Given Volume flow rate(cfs)		Volume flow rate(cfs)- Power Eng Inc.		Given Volume flow rate(USGPM)-		Volume flow rate(USGPM)- Power Eng Inc.	
		@900 (rpm)	@1800 (rpm)	@900 (rpm)	@1800 (rpm)	@900 (rpm)	@1800 (rpm)	@900 (rpm)	@1800 (rpm)
44.25	15.00	1,601.9	3,204	1,610	3,221	719,205	1,438,499	722,863	1,445,726
92.25	31.25	14,504.8	29,008	14,582	29,164	6,512,220	13,023,721	6,545,170	13,090,340

Table B1 Example of calculated volume flow rate based on the piston diameter and the stroke

Unit conversion:

1 gal = 3.785412 L = 3.785412 x 10^{-3} m^3 = 231 in^3 =0.13368 ft^3

1cfs = 448.97 USGPM

1US GPM =0.1336 cfm =2.228 x 10^{-3} cfs

Sample Calculation:

V_O = $[\pi \times d^2/4] \times [\text{displacement} \times \Omega \times n]$

d = 44.25in/12 = 3.6875ft

Displacement = 15in/12 = 1.25ft

Ω is the rotational speed of the shaft = 900 rpm=900/60 = 15 rps

n = 8

Using the above values V_O = (3.1416/4) x (3.6875) x (3.6875) x (1.25) x 8 x (15)

= 1,601.90 cfs

Note: The results are approximately 0.5% lower than the values calculated by Power Engineering.

3. Calculation of the height of water column that can be raised by 1000psi at the pump exit

Given, Pressure = 1000 psig, γ = 62.2 lbf/ft^3

The equivalent water column height that the pump with a discharge pressure of 1000 psi can raise, in the absence of friction, is:

h = 1000 (lb/in^2) × 144 (in^2/ft^2) /62.22 (lbf/ft^3)

h = 2,314 ft (water column height that can be raised by 1000 psig pressure).

4. Calculation of the horizontal distance to which the water can be transported at 1,610 cfs with a pressure head of 1000 psig in a 12-feet diameter conduit.

Applying Bernoulli equation and considering friction losses and minor losses

$$\frac{P_1}{\gamma}+\frac{V_1^2}{2g}+z_1=\frac{P_2}{\gamma}+\frac{V_2^2}{2g}+z_2+\frac{fLV^2}{2gD}+\text{minor losses} \quad \text{(B2)}$$

Assuming a horizontal pipe without elevation change (Z_1=Z_2) and constant conduit diameter. In this condition, $V_1 = V_2$ due to mass conservation. The above equation can be simplified as,

$$\frac{P_1-P_2}{\gamma}=\frac{fLV^2}{2gD}+\text{minor losses} \quad \text{(B3)}$$

Need to determine the friction coefficient using the Moody Diagram.

a) Calculating the Reynolds number of 1610 cfs water flowing in a 12-ft diameter conduit

$$Re = Ud/\nu \quad \text{(B4)}$$

Given volume flow rate = 1610 cfs

The diameter of the pipe D = 12ft = 3.6576m

Calculation for velocity

Area × velocity = volume flow rate

$\Pi \times (12^2(ft)/4)\times V = 1610$ cfs

V = 14.23 ft/s = 4.33m/s

The kinematic viscosity $\nu = 1.004 \times 10^{-6}$ m^2/s

Substituting all the above into (4) the Re = 1.57×10^7

c) Calculating the friction coefficient in the 12-ft conduit

Assuming the pipe is made of concrete

Surface roughness "ε" = 0.01 ft

Given the diameter of the pipe "D" = 12ft

From the above "ε/D" = 0.00083

Looking into the Moody charts, the friction factor "f" for ε/D = 0.00083 and Re = 1.57 x 10^7 is

f = 0.019

ρ = 1.934 slugs/ft^3

V = velocity of the fluid in the conduit = 14.23ft/s

g = 32.174ft/s^2

D = diameter of the pipe = 12ft

(c) Calculation of the minor losses

1. Exit and entrance losses
2. Sudden expansion and contraction losses
3. Elbow losses

Total Minor losses = $\sum k \frac{V^2}{2g}$

For

Exit loss $k = k_e = 1.0$

Entrance loss $k = k_{en} = 1.0$

Elbow losses $k = k_{elb} = 0.3 \times 20 = 6$ (20 elbows)

Sudden expansion $k = k_s = 1.0$

Sudden contraction losses $k = k_{sc} = 0.8$

Substituting all the above data in (5)

The total minor losses

$= [V^2/2 \times g] \times [1.0+1.0+6+1.0+0.8]$

$= [14.23^2(\text{ft/s})/2\times 32.174(\text{ft/s}^2)]\times [9.8]$

$= 30.839\text{ft}$

Substituting all the above values in (3) i.e.

$$\frac{1000\times 144(\text{lb/ft}^2)}{62.22(\text{lb/ft}^3)} + 0 = \frac{0.019\times \text{L}\times(14.23\text{ft})^2}{2\times 32.174(\text{ft/s}^2)\times 12(\text{ft})} + 30.839(\text{ft})$$

2,314.36(ft)-30.839(ft) = 0.00498249(ft) ×L

L = 458,310.87(ft), 1ft = 0.0001893939miles

L = 86.8(miles)

4. Calculating the pump power required to deliver 1,000 psig with 1,610 ft^3/s water

For the axial piston pump the power is given by

Power = Volume flow rate × pressure difference (B5)

Substituting the values in the above equation the power is given as

Power = 1610 (ft^3/s) × 1000 (lbf/in^2) ×144 (in^2/ft^2)

= 231,840,000 (lbf-ft/s) = 421,527 (hp) = 314,332 (KW)

Assuming 90% efficiency

Power = 257,600,000(lbf-ft/s) =468,363 (hp) = 349,258 (KW)

Assuming 70% efficiency

Power = 331,200,000(lbf-ft/s) = 602,181 (hp) = 449,046(KW)

APPENDIX C

CALCULATIONS OF FRICTION LOSSES IN THE CYLINDER

This section documents calculations of the pressure losses in the cylinder of the TurboPiston Pump (TPP)

Assumptions:

Temperature = Room temperature = 80

Service fluid = Water

Incompressible flow

Pipe material = Commercial steel or Wrought Iron

1. Calculation of velocity

$$V_O = [\pi d^2/4] \times [\text{displacement} \times \Omega \times n] \quad \text{(C1)}$$

Where,

From Table A-1, the volume flow rate for 100 rpm case is 0.0013 m^3/s = 0.047167ft^3/s

d is the diameter of the piston cylinder = 1.5 inches = 0.125 ft

Ω is the rotational speed of the shaft (RPM) = 100 rpm

Displacement is 1.03 inches

n is the number of cylinders = 8

Area × velocity = volume flow rate

$\pi (0.125^2(ft)/4) \times V = 0.047167/4$ cfs (Since we are computing for a single cylinder)

V = 0.960875 ft/s = 0.292875 m/s

The kinematic viscosity $\nu = 1.004 \times 10^{-6}$ m^2/s

$$Re = V \times d/\nu \quad \text{(C2)}$$

Substituting all the above into (2) the $Re = 1.1125 \times 10^8$

2. Calculating the friction coefficient in the 0.125-ft cylinder

Assuming the pipe is made of commercial steel

Surface roughness "ε" = 0.00015 ft

Given the diameter of the pipe "d" = 0.125 ft

From the above "ε/d" = 0.0012

Looking into the Moody charts, friction factor "f" for ε/D = 0.0012 and

Re = 1.1125 x 10^8 is

f = 0.0205

g = 32.174ft/s^2

d = diameter of the pipe = 0.125ft

3. Calculating the minor losses

Minor losses

$$\sum k \frac{V^2}{2g} \qquad \text{(C3)}$$

For,

Valve loss k = 1.0

The total minor losses

= [V^2/2×g] × [2]

= [0.960875^2 (ft/s)/2×32.174(ft/s^2)] × [2]

= 0.028696 ft

$$\frac{P_1 - P_2}{\gamma} = \frac{fLV^2}{2gd} + \text{minor losses} \qquad \text{(C4)}$$

Substituting the values of

γ = 62.2 lbf/ft^3

d= 0.125ft

L= 0.08583333ft

g = 32.174ft/s^2

V = 0.960875ft/s

Substituting all the above values in (4) i.e.

$$\frac{P_1 - P_2}{62.22(\text{lbf/ft}^3)} = \frac{0.0205 \times 0.08583333(\text{ft}) \times (0.960875\text{ft})^2}{2 \times 32.174(\text{ft/s}^2) \times 0.125(\text{ft})} + 0.028696(\text{ft}) \qquad \text{(C5)}$$

$$\frac{P_1 - P_2}{62.22(\text{lbf/ft}^3)} = 0.002019754316(\text{ft}) + 0.028696(\text{ft}) \qquad \text{(C6)}$$

P_1-P_2 = 1.798062319 lbf/ft^2

P_1-P_2 = 0.0008496601atm

But the above pressure loss is for one cylinder. It has to be multiplied by four to get the total pressure loss in the cylindrical domain.

The total pressure loss will be equal to 0.0033986404atm.

APPENDIX D

CONSTRUCTION OF COMPUTATIONAL FLOW VOLUME THROUGH THE IMPELLER

This section documents the step-by-step construction of the computational flow volume through the impeller-using GAMBIT.

Step1: The vertices of the vane profile are taken from AutoCAD and the face of the profile is created in GAMBIT.

Step2: Eight vane surfaces are created using the created face as the master element with the "COPY" and "ROTATE" commands. The following figure shows the 2-D footprint of the impeller.

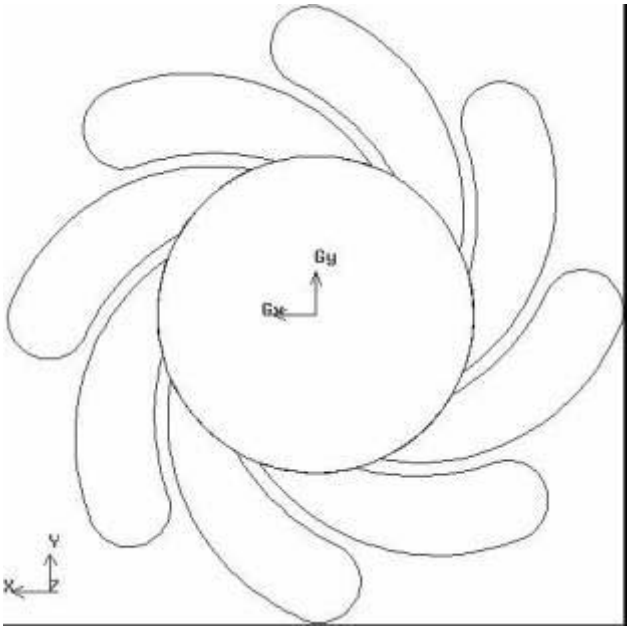

Figure D1 The 2-D footprint of the impeller

Step 3: The 2-D profile of the impeller hub domain is created using the vertices data from AutoCAD. The 2-D face is then revolved about an axis to form a 3-D volume of the shell.

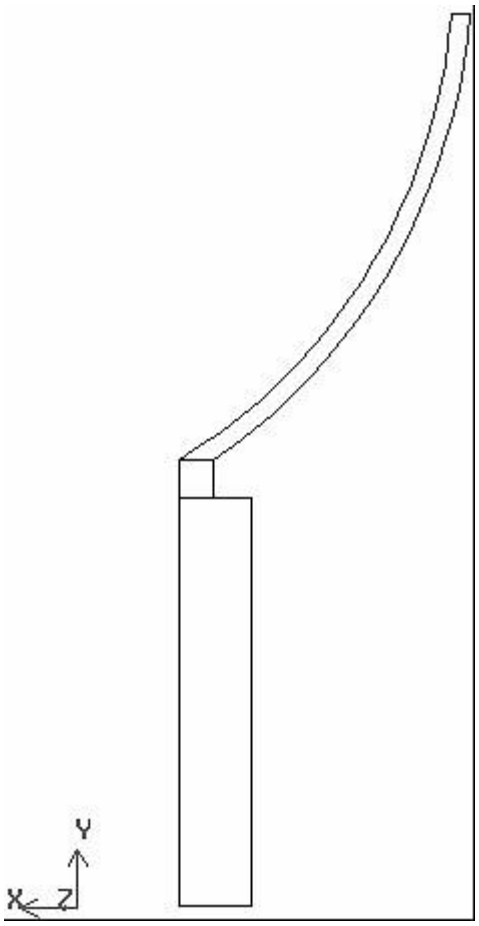

Figure D2 The 2-D model of the impeller shell.

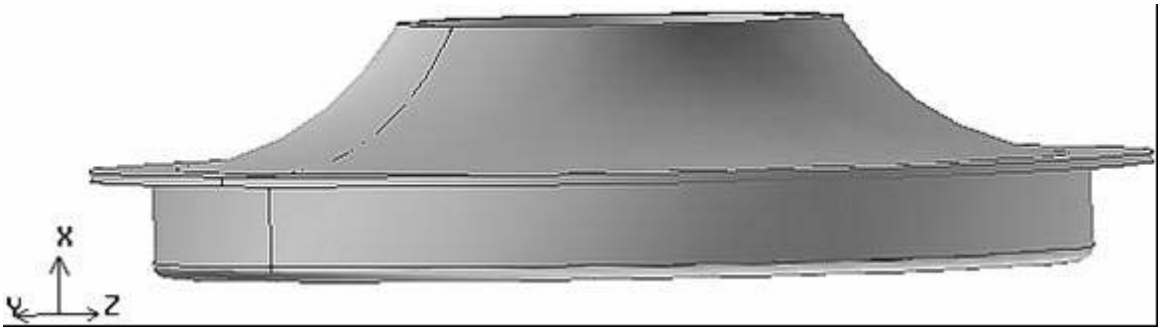

Figure D3 The 3-D model of the impeller shell.

Step 4: The vane profile created is aligned with the impeller shell volume, and is extruded beyond the height of the shell, thus creating eight volumes. All the eight volumes are now shortened to the actual computational length using the “split” command.

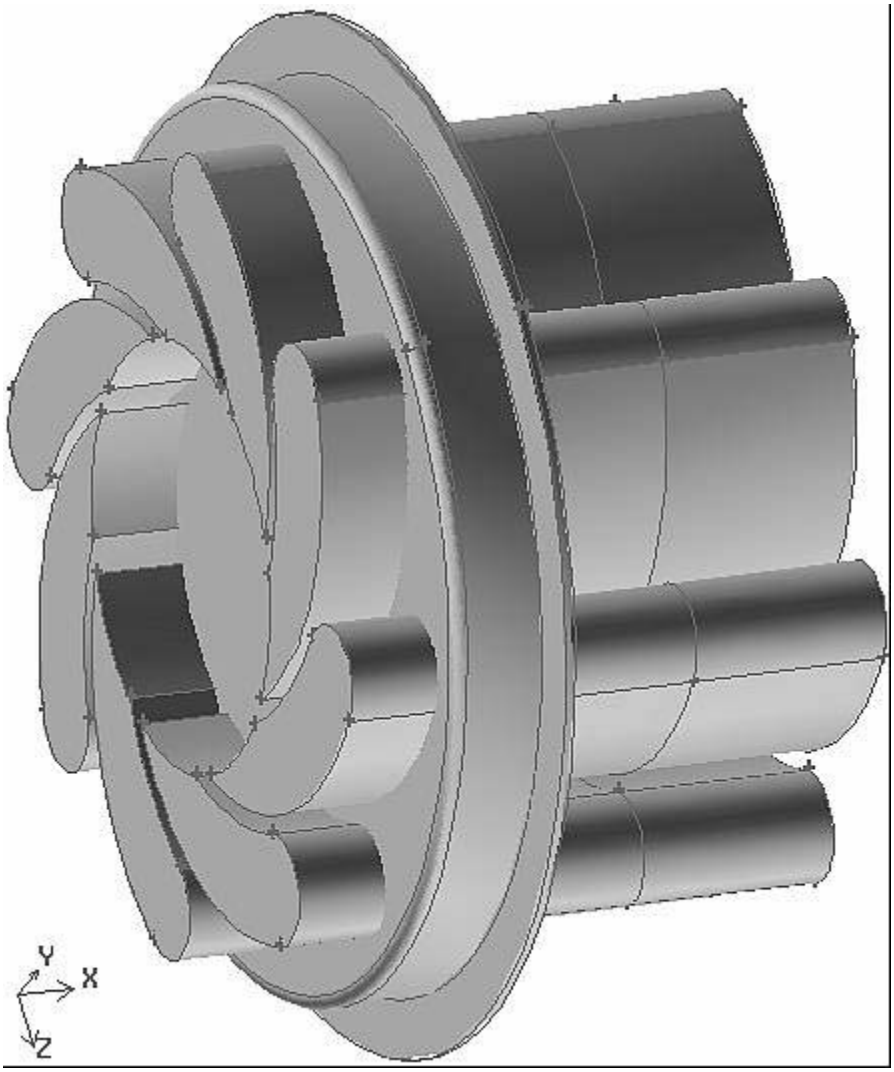

Figure D4 The 3-D model showing the vane geometry extruded beyond the impeller hub

Step 5: The shell volume thickness is removed from the height of the eight vanes and the following figure shows the 3-D model of the flow volume through the impeller.

Figure D5 The model of the computational flow domain of the impeller

APPENDIX E

SETTING UP THE TRANSIENT CASE IN FLUENT CASE

Three cases are studied in this thesis, this section documents the step-by-step establishment of setting the case in FLUENT.

Step 1: Grid

a. The required mesh file from GAMBIT is read in the FLUENT 6.2.16 3D version.

File → Read → Case

b. Check the grid

Grid → Check

FLUENT will perform various checks on the mesh and report the progress in the console window. It checks to ensure that the minimum volume reported is a positive number.

c. Scale the grid

Grid → Scale

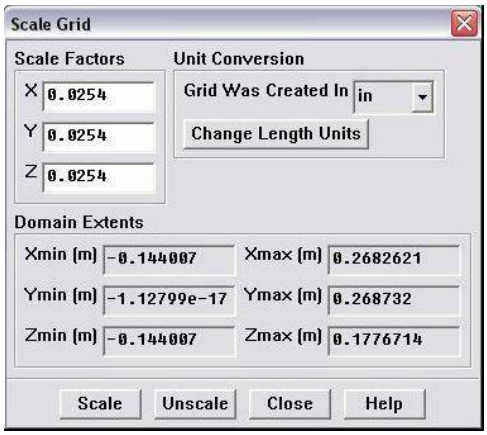

Under the unit conversion, select inches from the dropdown list

Step 2: Models

a. Select the coupled or segregated solver.

Define → Models → Solver

The "segregated solver" an the "unsteady" condition are selected

b. Enable the standard k-ε turbulence model

Define → Models → Viscous

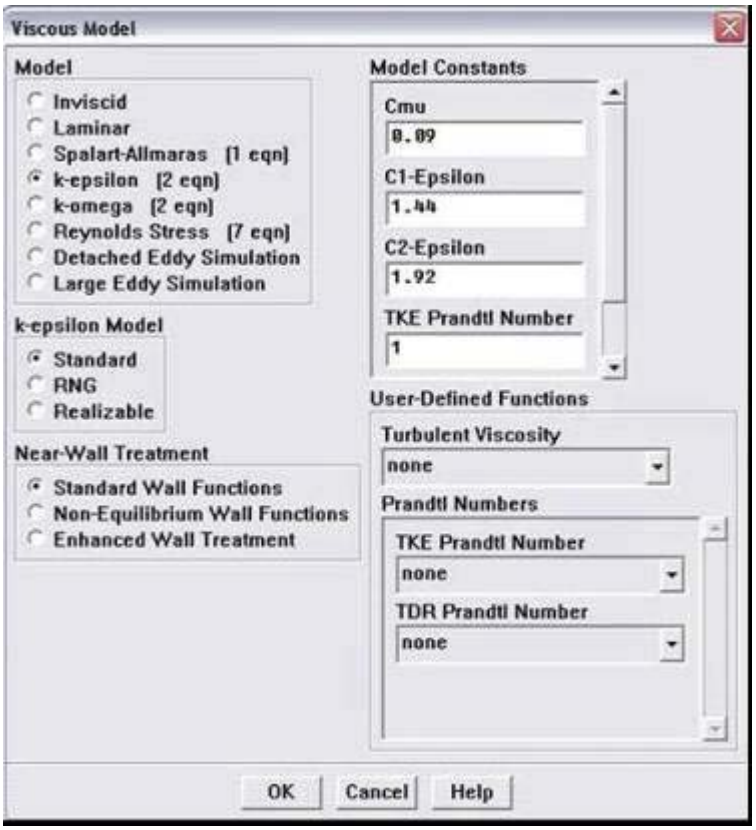

Step 3: Materials

a. Select "water" as the fluid material and retain the default values for all other properties

Step 4: Operating Conditions

a. Set the operating pressure to `1atm`

Define → Operating Conditions

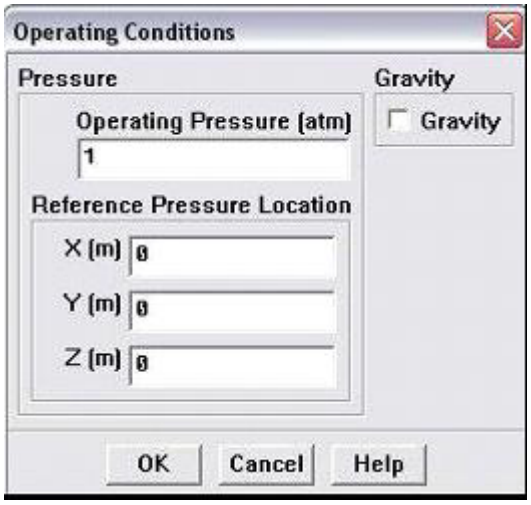

Step 5: Boundary Conditions

a. Set the conditions for the boundary (mass flow inlet).

Define → Boundary Conditions

b. Set the conditions for the boundary as the "pressure outlet" and select "Radial Pressure Equilibrium

c. Set the conditions for the zones

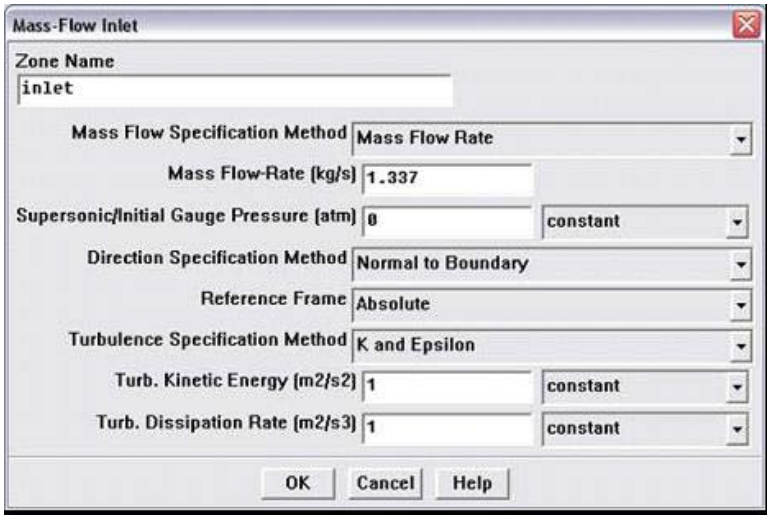

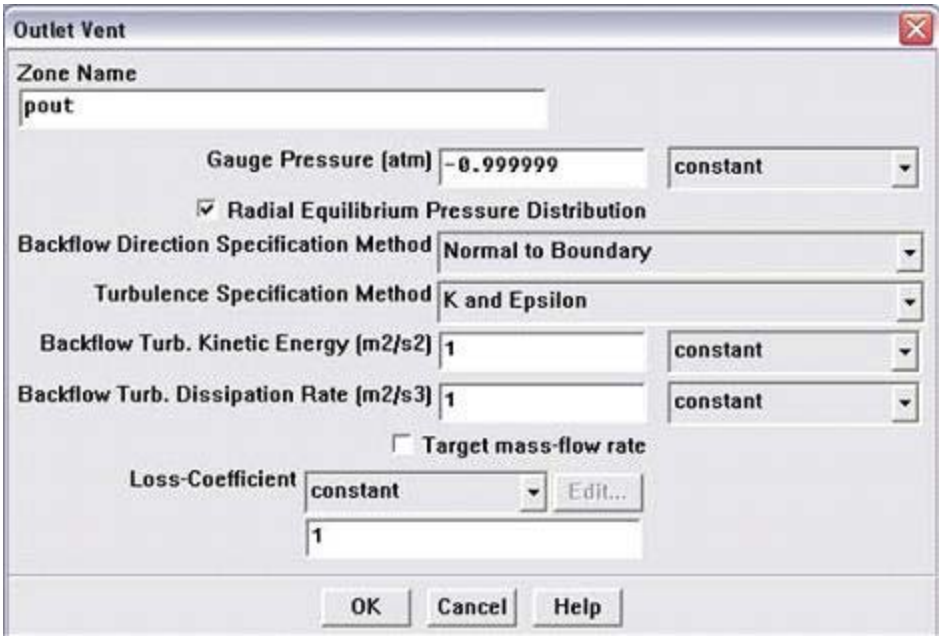

Under the motion type for the moving zone select "moving mesh" from the dropdown menu and "stationary" for the stationary zone.

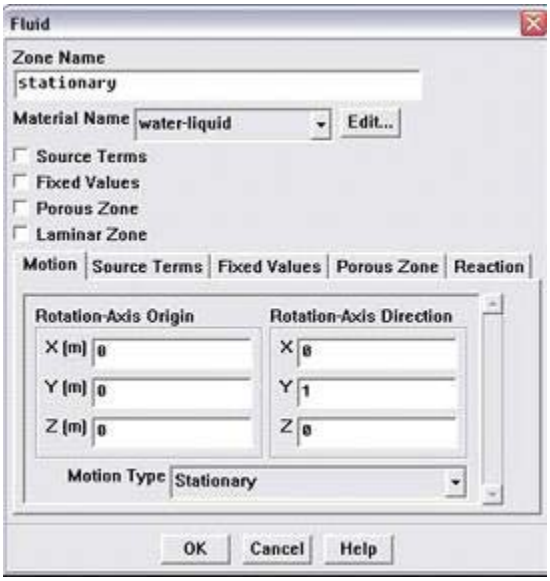

d. Setting the conditions for shaft

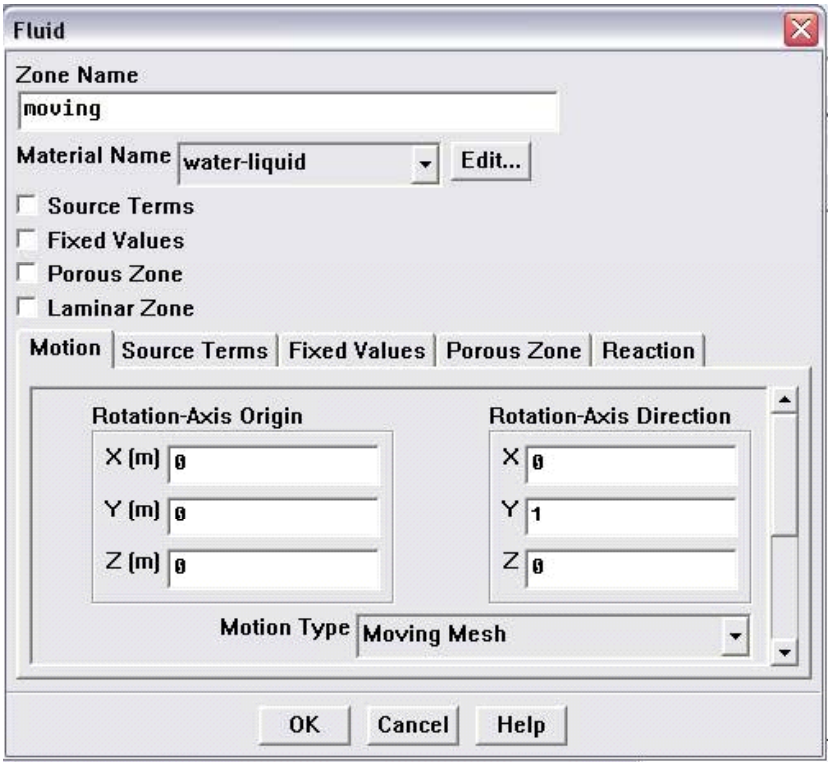

The shaft is assigned as moving wall and the rotational speed 100 rpm is assigned.

Step 6: Setting Grid Interfaces

Define → Grid Interfaces

The interfaces for stationary and rotary zones are defined.

Define → Mesh Motion

The time step and the number of time steps are initialized here.

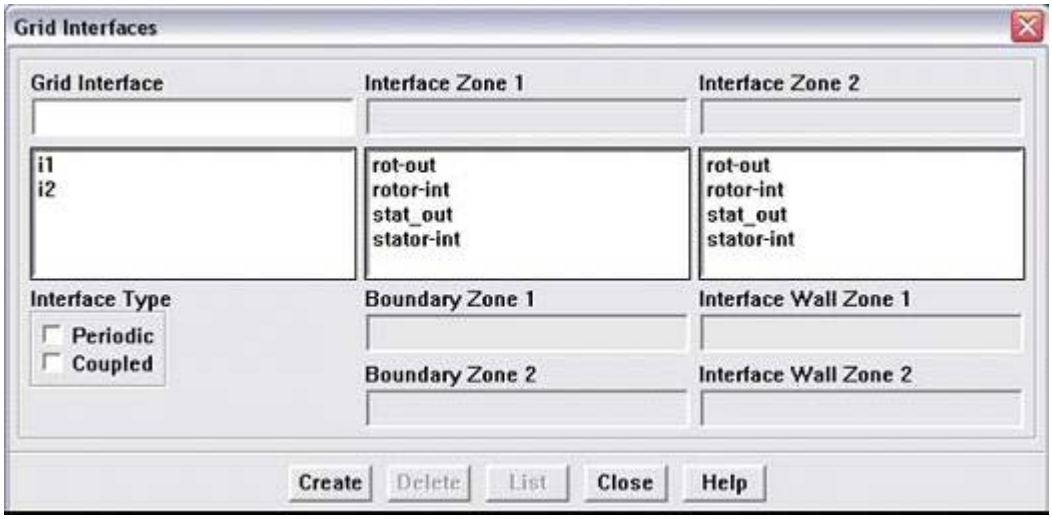

Step 7: Solution

Solve → Controls → Solution

a. The under relaxation factors are set here and the second order upwind method is selected.

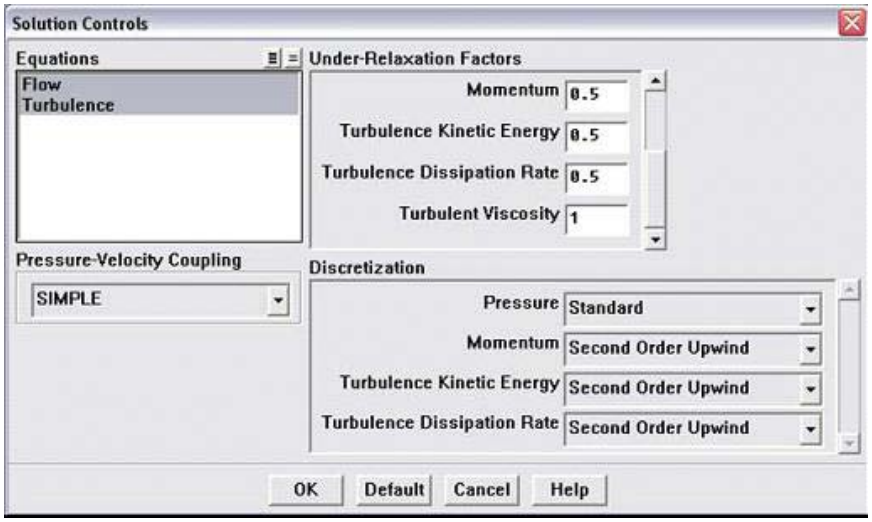

Solve → Initialize → Initialize

b. Initialize the solution for unsteady flow.

c. Solve → Iterate

The solution is iterated. Set the time step and the numbers of steps and iterations per time step.

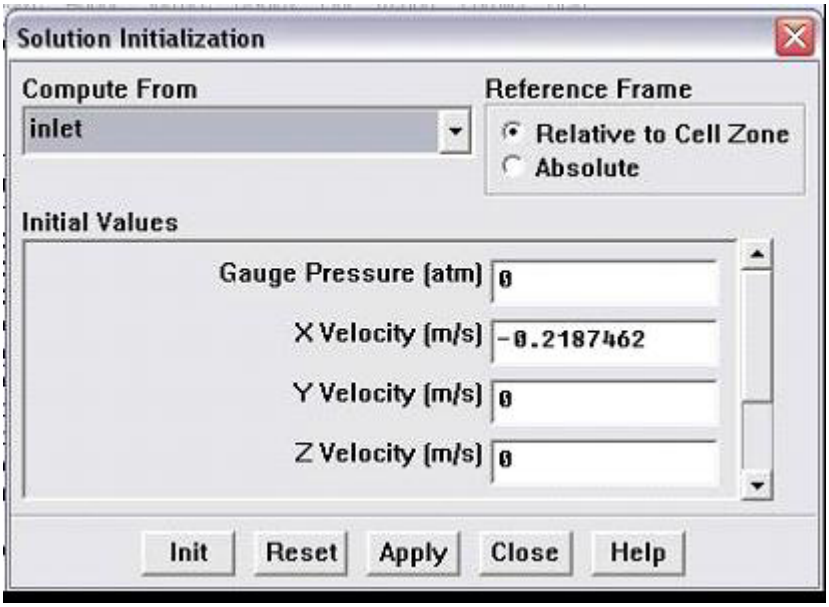

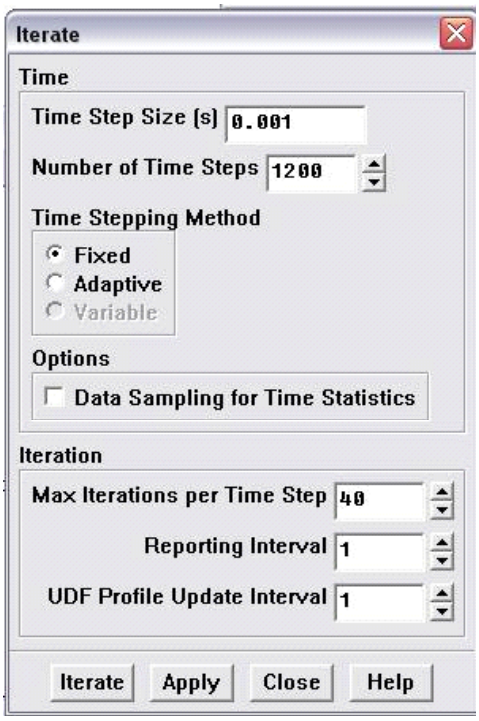

APPENDIX F

University of New Orleans Press Release (December 16, 2005)

Innovative Pump Could Solve Floodwater Problems in New Orleans

NEW ORLEANS, LA The University of New Orleans in partnership with Power Engineering, Inc. announces the development of an innovative new pump that could be the final solution to resolving emergency floodwater problems in the Greater New Orleans area.

The disaster caused by Hurricane Katrina has brought the New Orleans hurricane protection problem to national and international attention. While most of the discussion has focused on building stronger and higher levees, University of New Orleans (UNO) engineers are working on resolving water pumping problems and increasing flood protection by implementing an innovative new pump.

It has been more than 90 years since A. Baldwin Wood invented the revolutionary 12foot screw pump in 1913. The Wood Screw Pump has resolved New Orleans's drainage problems and uniquely contributed to the health and wealth of New Orleans' environmental and commercial foundations. The Wood pumps were, however, designed for drainage but not for saving the city from fast and massive flooding. The Wood Screw Pump is characterized by high volume and low pressure for lifting a large amount of water 20 or 30 feet over the levee and dumping it into canals connected to Lake Pontchartrain.

The existing centrifugal pumps can offer a bit more pressure but not much more than 300 feet before their efficiencies drop significantly to below 50%. The disadvantage of the Wood pumps and the centrifugal pumps is that they must be located near the dump sites and therefore, canals become necessary to be stretched into the inner city from Lake Pontchartrain. The breaches of the 17th Street and London Avenue canal levees have led to an avoidable tragedy if those canals were not there. Another type of traditional pump, the piston pump, can deliver very high pressure; unfortunately, its volume flow rate is unacceptably low (less than 5% of the centrifugal pump at an equivalent size). Hence, the only solution to the limitations of the current pumps is to invent a high pressure and high volume pump that can pump water several miles directly into the Mississippi River or to Lake Pontchartrain without going through the canals.

The Energy Conversion and Conservation Center (ECCC) of University of New Orleans is currently collaborating with the New Orleans based Power Engineering, Inc.to make this happen.

A revolutionary new pump "TurboPiston Pump" (TPP) has been invented by Patrick Rousset, PE, the President of the Power Engineering, Inc. and a mechanical engineer who graduated from UNO in 1982. This new pump combines the merits of each existing type of pumps (ie. centrifugal pump, reciprocating piston pump, and rotary screw pump) while discarding the problems relating to each.

The TPP consists of two opposing rotating disks (see Figure 1) with the suction side disk being mounted with a slightly inclined angle, so these two disks are separated with a wedge of volume. Eight pistons are built on the inclined suction disk and eight corresponding cylinders are built on the vertical discharging disk. Each chamber has both suction and a discharge valve associated with it and rotating as an integral part of each rotor. The rotating motion will drive a continuous piston motion of compressing and expanding as the pistons and cylinders combine on the circumference of a circle and glide in and out of each other. The rotating motion harnesses the feature of a high volume flow rate of the centrifugal pump (Turbo-motion), the piston motion achieves the positive displacement feature of high compression ratio of a piston pump, and the wedge volume simulates the energy saving feature of the extended surface of a rotary screw pump. Therefore the TPP and economic to maintain because it has only two moving parts, whereas a traditional reciprocating pump has 50 to 100 moving parts. In addition, a normal reciprocating pump requires a charge pump upstream to assure proper chamber filling to avoid cavitation, which can damage the pump or render the pump useless. The TPP requires no upstream charge pump since the rotary motion acts as its own charge pump. Due to its high rotating speed, the common problem of a pulsating discharge from a piston pump is minimized, and the discharge of TPP is comparable to the centrifugal pump. TPP displaces a fixed quantity of fluid per revolution thereby fine control of the flow rate is as simple as controlling the speed of the unit at a linearly proportional rate.

Present New Orleans pumps can move average 335,650 gallons of water per minute and discharge at 30 pounds of pressure per square inch (30 psi). With a similar 12 ft diameter cross-sectional area running at 900 rpm, the TPP can pump 722,860 gallons of water per minute and discharge at 1000 psi pressure, which can lift a water column **2,300 feet high** or transport water horizontally for **sixty miles**. This allows the floodwaters to be moved away in closed piping systems protected from overflow or breaching. A single TPP pump, can pump flood water from anywhere in the Greater New Orleans directly into the Mississippi River or into the Lake Pontchartrain or into the Gulf of Mexico 40 miles away. Although hundreds of TPP pumps are needed to keep up with the floodwater volume, the cost will be significantly cheaper than building hundreds of miles of category-five levees with the subsequent maintenance costs after each major storm. Even with the possibility of building the category-five levees, a reliable pumping system is definitely required to keep Greater New Orleans dry under any conditions. The TurboPiston Pump system is one of the best solutions to this need.

A smaller TPP has been built and tested at 900 rpm. The TPP is ready for implementation and be expanded to higher pressure and rpm. While the Power Engineering, Inc. is engaged in

marketing and implementing the TPP technology, the engineers at Energy Conversion and Conservation Center at UNO is working on improving the current design to make TPP more reliable, more efficient, and produce more pressure and flow. ECCC engineers will support Power Engineering to resolve installation and operation problems as well as any new product test. ECCC engineers are expanding the applications of TPP to other areas such as gas/oil industries, municipal waster water treatments, slurry transport for high-pressure biomass and coal feeding, and for high flow rate metering. ECCC is also developing a sister version of the TPP to apply the same working principle to a "TurboPiston Compressor" (TPC). UNO and Power Engineering are jointly developing and implementing this new pump technology that could be the ultimate solution to resolving emergency flood water problems in the Greater New Orleans areas.

Acknowledgement: The funding for UNO's R&D on this project has been partially supported by the Murphy Oil and the Governor's Energy Initiative through the Clean Power and Energy Research Consortium (CPERC) and administered by the Louisiana Board of Regents.

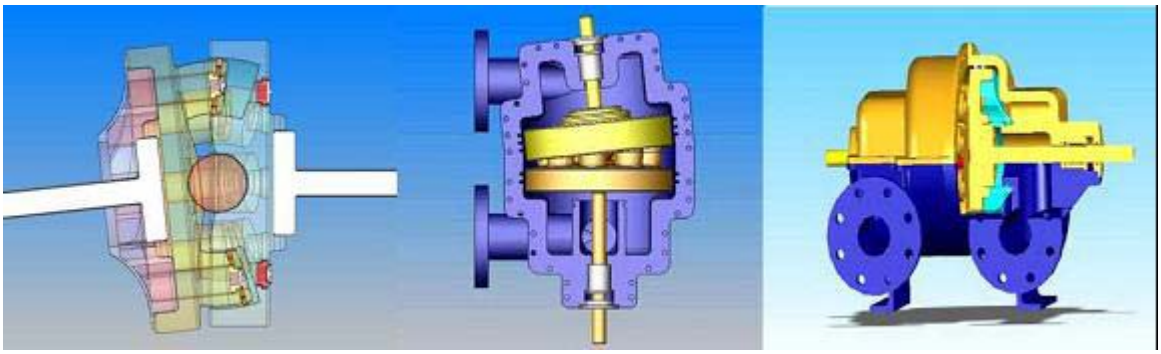

Administrative Contact:Sharon White Gruber (504-606-8134)

Technical Contacts:

Ting Wang, Director
Energy Conversion and Conservation Center
137 CERM
University of New Orleans
New Orleans, LA 70148-2220
504-280-7183, 504-280-5539 (Fax)
twang@uno.edu, www.uno.edu/eccc

Patrick W. Rousset, PE, President
Power Engineering, Inc.
603 French Street
New Orleans, LA 70124
504-957-8800
225-627-4066
prousset@powerengineeringinc.com

VITA

Kiranmayi Sristy was born in India in 1981. She graduated from Jyothi Vidyalaya High School, Hyderabad, India in 1996. She completed her Bachelors of Technology from Mahatma Gandhi Institute of Technology, India in 2002 and enrolled for a Masters program into the University of New Orleans in 2003.